DOI:10.14753/SE.2016.1824

Prothrombotic Effects of Manufactured Nanoparticles

Ph.D. Dissertation

Dr. Péter Bihari

Semmelweis University
Doctoral School of Basic Medicine

Supervisors:	Dr. Béla Merkely, D.Sc.
	Dr. Fritz Krombach, D.Sc.
Opponents:	Dr. Zsuzsanna Bereczky, Ph.D.
	Dr. János Szebeni, D.Sc.
Chairman of Committee:	Dr. Péter Ferdinandy, D.Sc.
Members:	Dr. Erzsébet Komorowicz, Ph.D.
	Dr. József Kaszaki, Ph.D.

Budapest
2015

DOI:10.14753/SE.2016.1824

Table of contents

I. ABBREVIATIONS **5**

II. INTRODUCTION **6**

1. Overview 6

2. Nanoparticles 7

a) Definitions *7*

b) Types of nanoparticles *8*

c) Properties *9*

d) Applications *11*

e) Interactions with biological molecules *13*

f) Interactions with cells *15*

g) Exposure routes, biodistribution, and fate *17*

3. Thrombus formation 20

4. Nanoparticles and thrombus formation 29

a) Thrombus formation on foreign surfaces *29*

b) Epidemiology of particulate matter-associated diseases *30*

c) Particulate matter and thrombus formation *32*

d) Manufactured nanoparticles and thrombus formation *35*

III. AIMS **37**

IV. MATERIALS AND METHODS **39**

1. Materials 39

a) Nanoparticles *39*

b) Reagents *40*

c) Mouse serum *40*

d) Antibodies and fluorescent beads for flow cytometry *40*

2. Characterisation of nanoparticles 41

a) Size distribution and zeta potential measurement *41*

b) Transmission electron microscopy *42*

c) Endotoxin measurement *42*

3. Optimisation of the nanoparticle dispersion method 42

DOI:10.14753/SE.2016.1824

a) Effect of different ultrasound energies *43*
b) Various sequences of preparation steps *43*
c) Mediums and dispersion stabilisers *43*
d) Different types of nanoparticles *43*
e) Evaluation of the stability of nanoparticle dispersions *44*
4. Dispersion of nanoparticles 44
5. Blood collection for *in vitro* studies 44
6. Optimisation of the platelet-granulocyte complex measurement 45
a) Experimental analysis of coincidence *45*
b) Mathematical description of coincidence *47*
7. Measurement of platelet activation *in vitro* 49
a) Incubation of whole blood with nanoparticles *49*
b) Flow cytometry *50*
c) Aggregometry *51*
8. Detection of *in vivo* thrombus formation 51
a) Animals *51*
b) Ferric chloride-induced thrombosis in small mesenteric arteries *51*
c) Light/dye-induced thrombosis in the cremasteric microcirculation *53*
9. Statistics 55

V. RESULTS 57

1. Physical characterisation of nanoparticles and optimisation of the dispersion method 57
a) Measurement of polystyrene beads *57*
b) Ultrasound energy *58*
c) Sequence of preparation steps *59*
d) Albumin and nanoparticle concentration *62*
e) Stability *65*
f) Different types of nanoparticles *66*
g) Zeta potential *70*
h) Transmission electron microscopy *70*
2. Optimisation of platelet-granulocyte complex measurement 74
a) Flow cytometric analysis of platelet-granulocyte coincidence *74*

DOI:10.14753/SE.2016.1824

b) Mathematical description of platelet-granulocyte complexes *79*

3. Effect of nanoparticles on platelet activation *in vitro* 80

a) Platelet P-selectin expression *80*

b) Platelet-granulocyte complexes *81*

c) Platelet aggregometry *83*

4. Effect of nanoparticles on thrombus formation *in vivo* 84

a) Mouse blood counts *84*

b) Mesenteric thrombosis *84*

c) Cremasteric thrombosis *86*

VI. DISCUSSION 88

1. Optimisation of the nanoparticle dispersion method 88

2. Optimisation of platelet-granulocyte complex measurement 94

3. Prothrombotic effects of nanoparticles 97

VII. CONCLUSIONS 103

VIII. SUMMARY 105

IX. ÖSSZEFOGLALÁS 106

X. REFERENCES 107

XI. PUBLICATIONS 126

XII. ACKNOWLEDGEMENTS 129

DOI:10.14753/SE.2016.1824

I. Abbreviations

ADP	adenosindiphosphate
BSA	bovine serum albumin
DEP	diesel exhaust particles
EDTA	ethylenediaminetetraacetic acid
FITC	fluorescein isothiocyanate
HSA	human serum albumin
LPS	lipopolysaccharide
MSA	mouse serum albumin
MWNT	multi-walled carbon nanotubes
PBS	phosphate-buffered saline
PdI	polydispersity index
PM	particulate matter
PPP	platelet-poor plasma
PRP	platelet-rich plasma
PSGL-1	P-selectin glycoprotein ligand-1
ROS	reactive oxygen species
SWNT	single-walled carbon nanotubes
TF	tissue factor
TFPI	tissue factor pathway inhibitor
vWF	von Willebrand factor

DOI:10.14753/SE.2016.1824

II. Introduction

1. Overview

Nanoparticles are particles with length scales under 100 nanometres (Lewinski et al. 2008). Nanoparticles always existed in our ambient nature, but they have received a substantial boost of interest in the last 50 years with the emergence of nanotechnology. Since then, nanotechnology has grown into a prominent industry and hundreds of different variants of nanomaterials and nanotech-based products are now commercially available (Maynard and Rejeski 2009).

The classification of nanoparticles as a new entity is justified by their physicochemical properties, which are different from the bulk material and the atoms and molecules from which they are built up. Although the unique physicochemical properties of manufactured nanoparticles enable the improvement of novel applications, they might also cause unusual types of interactions with biological materials and toxic effects not yet experienced.

Nanoparticles can come in contact with the human body through inhalation, ingestion, dermal deposition, but also through injection for medical applications. Nanoparticles, having entered the body, can translocate into the systemic blood circulation, reach various remote organs, and may affect their function. The significance of this phenomenon is underlined by previous epidemiological studies identifying ambient nano-sized particles as a major contributor to adverse cardio-respiratory effects of air pollution, where impact on haemostasis has been found to play an important role. (Oberdorster et al. 2005a, Oberdorster et al. 2005b)

Haemostasis is an important physiological function of the human body, maintaining integrity of blood vessels. Disruption of the vascular integrity, resulting in contact of human blood with any surfaces other then the inner wall of the vessels, induces thrombus formation to stop bleeding (Ruggeri 2002). A well-known consequence is unwanted thrombus formation on the surface of implanted foreign materials in the circulation (Gorbet and Sefton 2004). Although nanoparticles are small, they represent a very high cumulative surface that might also influence haemostasis.

The increasing utilisation of nanomaterials in technological and medical applications warrants an assessment of the risk of these manufactured materials on human health.

DOI:10.14753/SE.2016.1824

The fact that nanoparticles represent a potentially thrombogenic large cumulative surface, and knowledge of the prothrombotic effects of ambient nanoparticles, raises the question of whether manufactured nanoparticles also influence thrombus formation. Although circulating nanoparticles also reach the microcirculation, prothrombotic effects of manufactured nanoparticles in the microvasculature have not yet been examined. The aim of my dissertation was, therefore, to investigate the effects of manufactured nanoparticles on platelet activation and on thrombus formation in small arteries and in the microcirculation.

2. Nanoparticles

a) Definitions

Nanotechnology is a relatively new discipline where some of the definitions are still immature. The most often used definitions are listed below:

Nano is derived from the Greek word for dwarf and meaning extremely small. In physics, it means 10^{-9}.

Nanoparticles are just defined by size. There are, however different definitions in use. All of them share the criteria that nanoparticles should be smaller than 100 nm, but differ regarding how many dimensions should be considered (Oberdorster et al. 2005a, Lewinski et al. 2008). In this dissertation, the following more generalised definition is used:
Nanoparticles are particles with lengths that range from 1 to 100 nanometres in two or three dimensions (Lewinski et al. 2008).
Most of the nanoparticles are spherical particles, but the above definition is suitable also for particles that are in one dimension bigger than 100 nm such as fibres, tubes, or rods. The best examples of such high aspect ratio nanoparticles are carbon nanotubes, which have a diameter of a few nanometres and a length of several micrometres.

DOI:10.14753/SE.2016.1824

Nanotechnology is the engineering and manufacturing of material at the atomic and molecular scale.

Manufactured nanoparticles are nanoparticles made by nanotechnology.

b) Types of nanoparticles

Nanoparticles can be categorized as ambient or manufactured nanoparticles (Table 1). Ambient nanoparticles are nano-sized particles found in our environment that are generated by natural processes such as fires, volcanoes, sea spray, or erosion. In addition, they can originate from anthropogenic sources such as traffic or industry. In publications about air pollution, ambient nanoparticles are described as a fraction of particulate matter (PM). Particulate matter is categorized by size, where PM_{10} are particles under 10 µm, $PM_{2.5}$ are particles under 2.5 µm, and $PM_{0.1}$, also referred to as ultrafine particles, are nanoparticles present in the ambient air (Oberdorster et al. 2005a, Borm et al. 2006).

Although biological macromolecules are traditionally not considered as nanoparticles, many such molecules match the size criteria of nanoparticles. Thus, protein complexes (e.g. ribosome, transferrin), lipoproteins or viruses might be regarded as biological nanoparticles. Such biological particles are also recommended for the production of hybrid bio-nanoparticles (Douglas and Young 2006, Uchida et al. 2007).

In contrast to ambient nanoparticles, manufactured nanoparticles are produced intentionally by nanotechnology. They can be subcategorized according to their material (Table 1) (Oberdorster et al. 2005a, Borm et al. 2006).

DOI:10.14753/SE.2016.1824

Table 1. *Type of nanoparticles*

Source	Subtype	Examples
Ambient	natural processes (fires, volcanoes, sea spray, erosion)	ultrafine particles, or $PM_{0.1}$
	industrial processes (traffic, industry)	
	biological nanoparticles	ribosome, lipoproteins, viruses
manufactured	carbon nanoparticles	carbon black, single-walled carbon nanotubes (SWNT), multi-walled carbon nanotubes (MWNT), fullerenes
	quantum dots	cadmium selenide, cadmium sulfide, indium arsenide, indium phosphide
	metal, metal oxide nanoparticles	titanium dioxide, zinc oxide, gold, silver, iron oxide, silicium oxide
	organic nanoparticles	liposome, gelatine
	hybrid bio-nanoparticles	nanoparticles in protein cage

c) Properties

Nanoscale material is an intermediate between atomic and bulk material. Some of the special features of nanomaterials are due to the high surface area-volume ratio (Fig. 1). When particles are very small, most of the atoms are on the surface of the particle, resulting in a large active surface area with a high chemical reactivity. Another consequence of the high surface area-volume ratio is that the van der Waals forces between the relatively large surface areas are high enough to move the small mass nanoparticles together, resulting in the formation of agglomerates (Borm et al. 2006). The building of agglomerates is further exaggerated in biological fluids exerting high ionic strength and physiological pH (Nel et al. 2009).

DOI:10.14753/SE.2016.1824

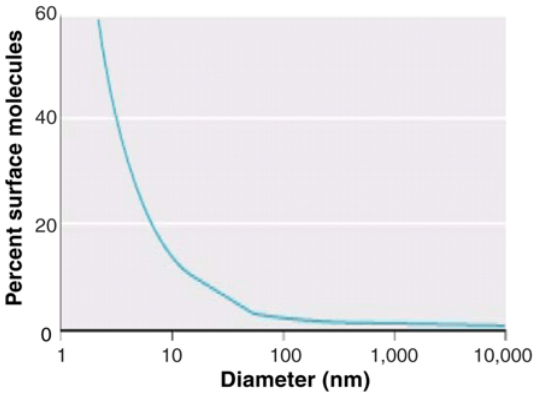

Fig. 1. *Inverse relationship between particle size and the percent of surface molecules (Nel et al. 2006).*

Moreover, materials on the nanoscale can exert properties that are independent of the high surface area (Burda et al. 2005). An example is the quantum size effect of semiconductor nanocrystals, i.e. variations in electric and optical properties at a size that is comparable or smaller then the length scale of electron motion in bulk material (Bohr radius). Although the bulk material of quantum dots (cadmium selenide, cadmium sulphide, indium arsenide, and indium phosphide) do not exert fluorescent properties, nanocrystals of these semiconductors (quantum dots) have a very strong and narrow fluorescent signal band upon excitation and the wavelength of emission depends on the particle size (Biju et al. 2008). In metallic nanoparticles, surface plasmon resonance can be induced, whereby free electrons respond collectively by oscillating in resonance with the light wave, resulting in light absorption (Burda et al. 2005). Properties of ferromagnetic or ferrimagnetic materials also change at around the size of 10-20 nm, resulting in a single magnetic domain that shows superparamagnetic behaviour (Lu et al. 2007). Carbon in nanotube form gains outstanding mechanical properties with extremely high tensile strength (Kis and Zettl 2008). Carbon nanotubes also have peculiar electronic characteristics. Their electronic conductivity depends on the tube diameter and the wrapping angle (a measure of the helicity of the tube lattice), with only slight differences in these parameters causing a shift from metallic to semiconducting properties (Wilder et al. 1998). These examples, although not exhaustive, demonstrate why nanoparticles open up many possibilities for innovations in technology.

d) Applications

Based on these unique properties, nanomaterials are already widely used in a diverse array of applications including chemistry, environmental engineering, food, clothes, personal care products, energy production and storage, optics, information technology, and construction materials (Maynard et al. 2006, Maynard and Rejeski 2009). There are also many biomedical applications of nanoparticles (Salata 2004). Different types of nanoparticle constructs are under development, where drugs are delivered by a nanoparticle directly to a target cell, lowering unwanted side effects on other cells (Davis et al. 2008). Several such drug-containing nanoparticles are already in medical use mainly for cancer therapy (Zhang et al. 2008). Labelled magnetic nanoparticles are applied for the visualisation of atherosclerotic plaques or tumours by magnetic resonance imaging. These magnetic nanoparticles can also be heated by alternating magnetic fields, and thus they can be utilised to kill cancer cells (magnetic hyperthermia treatment) (Ito et al. 2005, Lu et al. 2007). Nanotechnology is also used in tissue engineering to produce biomaterials with nanostructured surfaces that can be better incorporated into living tissue, such as in bone implants (Salata 2004). Other biomedical applications of nanoparticles include fluorescent labelling, biodetection of pathogens, probing of DNA structures, purification of biological molecules, or phagokinetic studies (Salata 2004) (Table 2).

Table 2. *Examples of nanoparticle applications already available on the market (normal text), or under development (in italics).*

Nanoparticle	**General applications**	**Medical application**
Carbon nanotubes	- construction materials e.g. in sport equipments or in wind turbine blades - antifouling paints for ships - batteries for electronic devices - *purification of drinking water* (De Volder et al. 2013)	- bone implants (Salata 2004) - *drug delivery* - *near infrared hyperthermia therapy* - *gene therapy* - *tissue engineering* *(He et al. 2013)*

DOI:10.14753/SE.2016.1824

Nanoparticle	General applications	Medical application
Metal, metal-oxide nanoparticles	- transparent sunscreens (contains TiO_2 or ZnO nanoparticles) - self-cleaning windows (Borm et al. 2006) - surface enhanced Raman spectroscopy (Burda et al. 2005) - many food products contain TiO_2 nanoparticles (Weir et al. 2012)	- *nanoparticle-based therapeutics in preclinical development (Zhang et al. 2008)*
Magnetic nanoparticles	- *high density data storage* - *magnetically separable catalysts* - *magnetic separation of biomolecules (Lu et al. 2007)*	- contrast agent for magnetic resonance imaging (superparamagnetic iron oxide nanoparticles) (Ittrich et al. 2013) - magnetic hyperthermia treatment (Ito et al. 2005) - *magnetic drug delivery (Lu et al. 2007)*
Quantum dots	- different applications of bioimaging (Chen and Liang 2014) - *quantum dot-LED display* - *solar cells with quantum dots (Hardman 2006)*	- *photodynamic therapy and* - *radiotherapy of cancer with quantum dots (Juzenas et al. 2008)*

DOI:10.14753/SE.2016.1824

Nanoparticle	General applications	Medical application
Liposomes, albumin based nanoparticles	Textile processing with liposomes (Barani and Montazer 2008)	Several clinically approved nanoparticle-based therapeutics, e.g. drugs for therapy of cancer, HIV infection, multiple sclerosis, fungal infections, and vaccines (Zhang et al. 2008)

e) Interactions with biological molecules

Nanoparticles in organisms come into contact with biological molecules, and these interactions affect their fate and effects in the body (Lynch and Dawson 2008). Due to the relatively high surface area versus the small mass, the van der Waals forces cause biological molecules to adhere to the particles. Interestingly, the number and types of biomolecule that adhere to the curved nanoparticle surface differ in many cases from those which adhere to flat surfaces of the same material (Lynch et al. 2009).

Nanoparticles in a biological fluid (e.g., plasma) are covered by proteins. This organized protein structure that surrounds the nanoparticles is called the protein corona (Fig. 2).

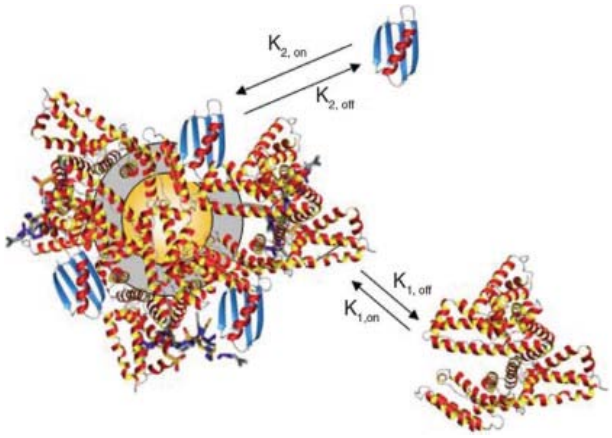

Fig. 2. *Nanoparticle protein corona. Adhesion of proteins to nanoparticles is determined by different equilibrium constants (Lynch and Dawson 2008).*

The composition of the protein corona depends on the proteins surrounding the nanoparticles, and on the size and surface properties of the nanoparticles (Lundqvist et al. 2008). Additionally, the composition of the protein corona is in continuous exchange with the proteins of the environment. First, nanoparticles are covered with proteins that are abundant in the solution; later, proteins in lower concentration but with higher affinity occupy the nanoparticle surface. Accordingly, it has been shown that nanoparticles in plasma first bind albumin and fibrinogen molecules, and then bind proteins that are present in lower concentrations in plasma but have higher affinity toward nanoparticles, such as apolipoproteins (Cedervall et al. 2007b, Lynch and Dawson 2008). In the nanoparticle corona almost all of the plasma proteins can be found at different amounts according to the particle surface properties: i.e. albumin, fibrinogen, immunoglobulins, proteins of the complement system, apolipoproteins, as well as coagulation cascade and acute phase proteins (Lundqvist et al. 2008). As a consequence of binding, the conformation and function of adhered proteins can change. This can lead to the exposure of new epitopes or alter protein function (Nel et al. 2009). Nanoparticles can also induce protein fibrillation, i.e. certain proteins aggregate into long, thin fibrils called amyloid structures (Colvin and Kulinowski 2007, Linse et al. 2007). It is generally perceived that the properties of nanoparticles determine the composition of the protein corona. In turn, the composition of the protein corona determines the behaviour of nanoparticles in biological systems. The protein corona can influence the interaction with receptors, cellular uptake, organ distribution, cell and organ functions, and excretion. It has been demonstrated that inhibition of protein adhesion by coating nanoparticles with amphiphilic polyethylene glycol molecules leads to decreased cellular uptake, longer circulation, and altered biodistribution (Praetner et al. 2010, Jokerst et al. 2011).

Nanoparticles also interact with membrane phospholipids. Adhesion depends on the charge of nanoparticles (Verma and Stellacci 2010). It has been shown that nanoparticles of negative charge induce local gelation in otherwise fluid bilayers; nanoparticles of positive charge induce otherwise gelled membranes to fluidize locally. It has been hypothesised that charged nanoparticles alter the tilt angle of the phospho-choline head group, which is an electric dipole of phosphate and choline. The

reorganisation of the phosphocholine head group changes the fluidity of membranes. (Wang et al. 2008)

Nucleic acids bind to nanoparticles as well. Cationic nanoparticles or nanoparticles bearing cationic ligands provide highly efficient DNA binding via electrostatic interaction. This kind of interaction can be utilised for electrostatic assembly of nanoparticles along DNA molecules (Saha et al. 2011). High affinity binding of single-stranded DNA to SWNT has been used for quantitative detection of SWNT in aqueous samples (Mota et al. 2013).

f) Interactions with cells

Nanoparticles are able to undergo diverse interactions with cells. Nanoparticles can adhere to cell surfaces, translocate into cells, and influence cellular functions through interactions with cell components (Zhao et al. 2011).

As described above (section II/2/e), nanoparticles can adhere to proteins and lipid macromolecules, which are the main components of cell membranes.

Cells can internalise nanoparticles by different mechanisms. Larger or aggregated nanoparticles are taken up by phagocytosis by specialized cells such as macrophages, monocytes, and neutrophils or by macropinocytosis by other cell types. Smaller particles can be endocytosed through the formation of endocytic vesicles of different sizes by clathrin-mediated (~120 nm), caveolae-mediated (~60 nm), or clathrin/caveolin independent (~90 nm) mechanisms (Conner and Schmid 2003, Dobrovolskaia and McNeil 2007, Verma and Stellacci 2010) (Fig 3). Moreover, some nanoparticles are able to penetrate cell membranes without any active process of the cell (Verma and Stellacci 2010).

DOI:10.14753/SE.2016.1824

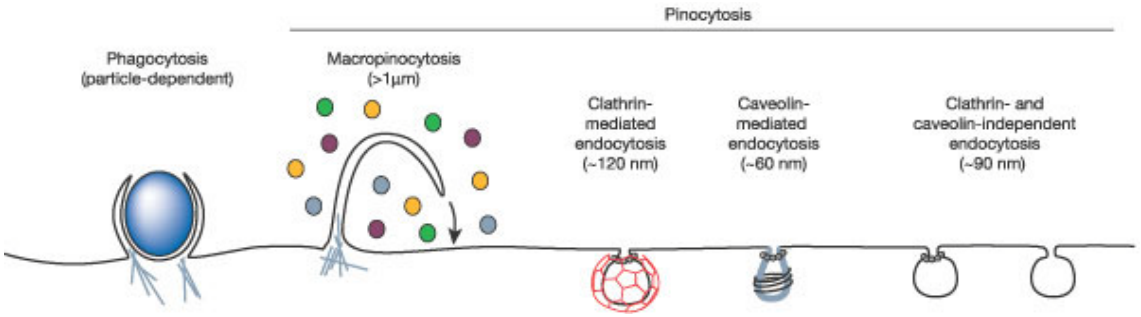

Fig 3. *Endocytosis mechanism depends on the size of nanoparticles (Conner and Schmid 2003).*

Nanoparticles taken up by an active internalisation process of the cell are enclosed in endosomes and thus separated from the cytosol. There are, however, several mechanisms that lead to the escape of nanoparticles from the endosomes. Internalisation of nanoparticles with high aspect ratio such as MWNT, which are relatively long and stiff, can lead to disruption of the phagosome (frustrated phagocytosis). Macrophages, in an attempt to destroy the carbon nanotubes, release harmful oxygen radicals, and hydrolytic enzymes which are deposited in the surrounding medium, leading to chronic inflammation (Poland et al. 2008). Amine-modified nanoparticles were also described as being able to escape from the lysosomes to the cytoplasm. This phenomenon can be explained by the proton sponge hypothesis that states that unsaturated amines on the material surface are capable of sequestering protons. The lysosomal proton pump, which is responsible for acidification, tries to acidize the lysosome, keeping the pump going, and leading to the retention of one Cl^- anion and one water molecule for each proton that enters the lysosome. Ultimately, this process causes lysosomal swelling and rupture, leading to particle deposition in the cytoplasm (Dobrovolskaia and McNeil 2007, Xia et al. 2008).

Oxidative stress is thought to play an important role in the mechanisms of nanoparticle-induced cytotoxicity. Nanoparticles can generate reactive oxygen species (ROS) through redox chemistry or interfere with the ROS production of the cell. The excited energy state in a semiconductor nanoparticle leads to the generation of superoxide radicals, e.g. titanium dioxide nanoparticles produce ROS upon ultraviolet light exposure. Transition metals on the nanomaterial surface (e.g. metal impurities in nanotubes) can generate superoxide anions through Fenton chemistry. Nanoparticles can

also alter phagocytosis leading to intracellular (proton sponge hypothesis) or extracellular release of ROS (frustrated phagocytosis). Furthermore, nanoparticles can lodge in mitochondria and interfere with the electron transport chain leading to the production of superoxide anions (Nel et al. 2006, Li et al. 2008).

Nanoparticles can also enter the nucleus either by penetrating the nuclear membrane, or being transported through the nuclear pore complexes, or becoming enclosed in the nucleus by chance during mitosis. Nanoparticles can cause genotoxic effect through ROS production, direct mechanical interference with the mitotic spindle and DNA or interaction with nuclear proteins and enzymes (Gonzalez et al. 2008, Singh et al. 2009).

Nanoparticles at different subcellular locations can interact with macromolecules and thus influence cellular functions.

g) Exposure routes, biodistribution, and fate

Nanoparticles can enter the human body through the skin, respiratory, or gastrointestinal tract, or by injection into the circulation (Oberdorster et al. 2005a). The actual exposure route depends on the exposure scenario (Fig. 4). Ambient nanoparticles from natural sources such as combustion processes enter the human body mainly via inhalation. Manufactured nanoparticles can also be inhaled if they get into the air during production. Nanoparticles in food or water can get into the body through the gastrointestinal tract. Nanoparticles in cosmetics and sun creams come into contact with the skin. Nanoparticles can be cleared from these organs, e.g. from the respiratory tract, by the mucociliar system, or they might be deposited. Importantly, nanoparticles can translocate from these organs into the blood vessels and reach any tissue of the body through the systemic circulation.

DOI:10.14753/SE.2016.1824

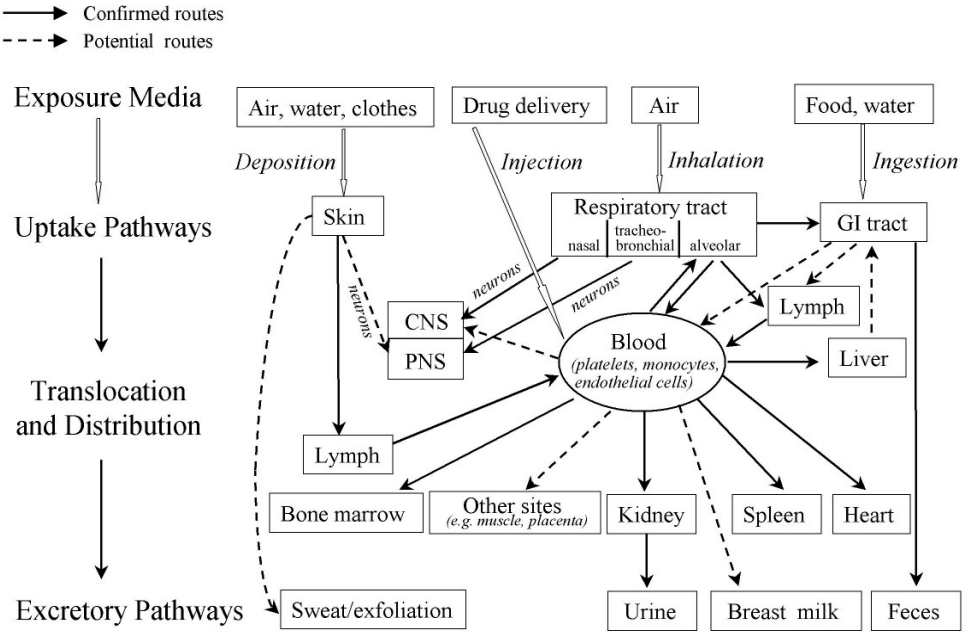

Fig. 4. *Confirmed (solid arrow) and potential (dashed arrow) exposure routes of nanoparticles in the human body. Nanoparticles can be taken up into the human body from the air through the respiratory tract, from food and water through the gastrointestinal tract, or they can be deposited from air, water, or clothes onto the skin. Nanoparticles might translocate from these organs into the blood, or in medical applications they can also be directly injected into the systemic circulation. Circulating nanoparticles can reach any organs of the body and be excreted by the kidney, liver, or skin. GI tract: gastrointestinal tract, CNS: central nervous system, PNS: peripheral nervous system. (Oberdorster et al. 2005a)*

Several experimental studies have shown that a small fraction of inhaled nanoparticles, depending on their size, can cross the air-blood barrier in the lungs and translocate into the systemic circulation. Kreyling and coworkers have shown that depending on particle size about 1-10 % of deposited ^{192}Ir particles translocated from the lungs into the blood and deposited in secondary organs, such as liver, spleen, heart, and brain (Kreyling et al. 2002). Nemmar and coworkers confirmed this observation in a human study. They found that inhaled ^{99m}Tc-labelled ultrafine carbon particles pass rapidly into the systemic circulation (Nemmar et al. 2002a). The mechanism of translocation is supposed to be via pores (Conhaim et al. 1988, Hermans and Bernard 1999) or by diffusion through the cells of the alveoli (Geiser et al. 2005). Translocation

from the lungs was shown for different types of nanoparticles: ^{192}Iridium particles (Kreyling et al. 2002), ultrafine particles (Nemmar et al. 2002a), Tc-labelled albumin molecules (Nemmar et al. 2001), carbon black (Shimada et al. 2006), gold nanoparticles (Lipka et al. 2010), nano-ceria (He et al. 2010), and fullerenes (Naota et al. 2009).

Another main exposure route is through the gastrointestinal tract. It is estimated that 10^{12}-10^{14} fine and ultrafine particles, including mainly silicates and titanium dioxide, are ingested per person per day in the Western world (Lomer et al. 2002). Experiments in rats and also human studies have shown that TiO_2 particles (150–500 nm) taken in via food can translocate into the blood and accumulate in the liver and spleen (Jani et al. 1990, Borm et al. 2006).

Regarding the contact of nanoparticles with the skin, numerous studies have demonstrated that TiO_2 or ZnO nanoparticles do not penetrate into or translocate through normal skin (Nohynek et al. 2007, Nohynek et al. 2008, Nohynek et al. 2010). However, small quantum dots can penetrate broken skin to lodge in other tissues and organs (Mortensen et al. 2008).

In diagnostic or therapeutic medical applications, nanoparticles are directly injected into the systemic circulation. Nanoparticles translocated from the respiratory or gastro-intestinal tract into the systemic circulation or nanoparticles directly injected into the bloodstream can reach all the organs of the body and finally pass the microcirculation of any tissue (Borm et al. 2006, Geiser and Kreyling 2010). It has been shown that circulating nanoparticles can also cross the blood brain barrier and accumulate in the brain (Kreuter 2001, Hu and Gao 2010). A special route to the central nervous system is the direct pathway of nanoparticles from the nasal airways into the brain through the olfactory nerves (Elder et al. 2006).

The biodistribution of nanoparticles depends on their properties. The main uptake organs are the lungs, liver, and spleen. Nanoparticles have different half-lives in the body depending on their type and surface modifications, and they are excreted through renal or hepatic pathways. The way of excretion depends on size, shape, charge, and composition of the nanoparticles. Nanoparticles which are smaller than 6 nm can be filtered in the glomerulus and excreted by the kidney in the same way as small biological molecules. Interestingly, high aspect ratio nanoparticles, such as carbon nanotubes, which have a mean diameter of few nm and lengths in the micrometer range,

have been reported to be cleared from the blood also through the renal pathway. The other main organ of nanoparticle excretion is the liver, which is able to excrete nanoparticles that do not undergo renal clearance. Hepatocytes can take up nanoparticles from the blood, and eliminate them via the biliary pathway. For example, polystyrene nanoparticles have been found to be eliminated by the hepatic pathway, which was mediated by ApoE receptors. Also hepatic Kupffer cells, together with other cells of the reticuloendothelial system, contribute to the elimination of nanoparticles, mainly by degradation processes. On the other hand, nanoparticles such as quantum dots, which can not be degraded, deposit in the phagocytes, leading to long-term retention of these nanoparticles in the body. (Choi et al. 2007, Hagens et al. 2007, Longmire et al. 2008, Landsiedel et al. 2012)

3. Thrombus formation

Haemostasis is an essential physiological function maintaining the integrity of vessels based on a well-tuned interplay between endothelial cells, platelets, and the coagulation system. Haemostatic processes are able to stop bleeding from injured vessels by platelet plug formation and blood coagulation. On the other hand, pathological thrombus formation may induce thromboembolic diseases.

Vascular injury

Intact endothelial cells provide a non-thrombogenic surface to which neither platelets nor fibrin mesh can adhere (Fig 5). Additionally, endothelial cells actively inhibit thrombus formation. They produce prostacyclin and nitric oxide, which both suppress platelet activation. Endothelial cells also express CD39, an ecto-ADPase that blocks adenosindiphosphate (ADP) dependent secondary platelet activation. Heparan sulphate and thrombomodulin-protein C complex on the surface of endothelial cells, as well as the endothelial production of tissue factor pathway inhibitor (TFPI), inhibit the coagulation system. Finally, the production of plasminogen activators (tissue plasminogen activator and urokinase-type plasminogen activator) leads to lysis of erroneously generated thrombi (Ruggeri 2002).

DOI:10.14753/SE.2016.1824

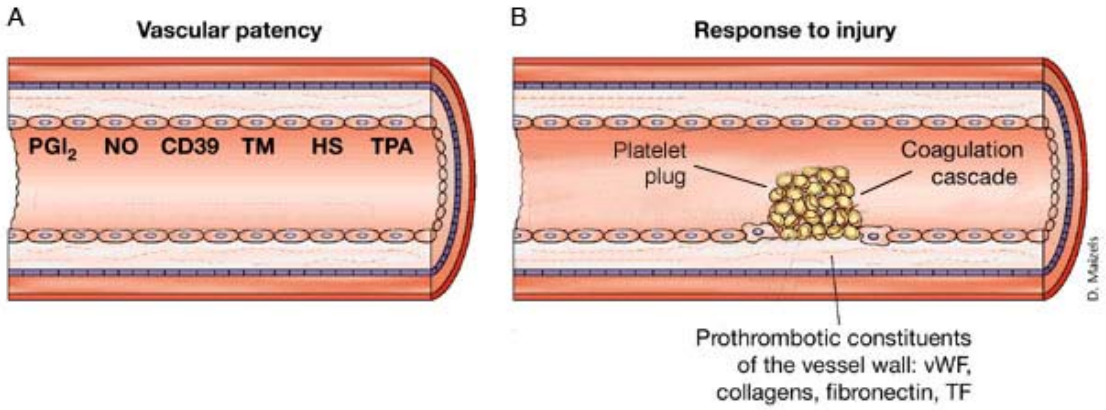

***Fig 5. A**. Vascular patency. Healthy endothelial cells inhibit thrombus formation. Prostacyclin (PGI_2), nitric monoxide (NO), and ecto-ADPase (CD39) suppress platelet activation. Thrombomodulin (TM), heparan sulphate (HS), and tissue plasminogen activator (TPA) counteract the coagulation process. **B**. Response to injury. Loss of antithrombogenic endothelial cells and interaction of platelets and plasma proteins with prothrombotic constituents of the subendothelial matrix induces thrombus formation: generation of a platelet plug and a fibrin mesh. Modified after Ruggeri at al. (Ruggeri 2002).*

At the site of vascular injury, the loss of antithrombogenic endothelial cells and the contact with the denuded subendothelial matrix evolve the formation of a platelet plug and initiate the coagulation cascade (Fig 5). The subendothelial matrix is, in contrast to endothelial cells, highly thrombogenic. Moreover, von Willebrand factor (vWF), the main ligand of platelet tethering, immediately deposits from plasma onto the denuded subendothelial layer. The interaction between subendothelial matrix proteins and platelets lead to the adhesion and activation of platelets. At the same time, tissue factor (TF) expressed on the surface of subendothelial cells initiates the coagulation process. During thrombus formation, platelets form a plug and the coagulation cascade forms a fibrin mesh, and these two processes aid one another (Ruggeri 2002).

DOI:10.14753/SE.2016.1824

Platelet adhesion and initial platelet activation

Platelets are small (2-5 µm) anuclear cell fragments with armature for adhesion and aggregation (Broos et al. 2012). Adhesion is a multistep process between elements of the subendothelial matrix of the vessel wall and the receptors of platelets (Fig 6). Platelets first tether through glycoprotein GPIb-V-IX to vWF immobilized on collagen fibres. This adhesive interaction is rapidly reversible and does not readily support stable platelet adhesion. However, the resulting rolling and deceleration of platelets allows the interaction of the two major collagen receptors GPVI and integrin $\alpha_2\beta_1$ with the subendothelial matrix resulting in firm adhesion and platelet activation. (Ruggeri 2002, Varga-Szabo et al. 2008, Nuyttens et al. 2011)

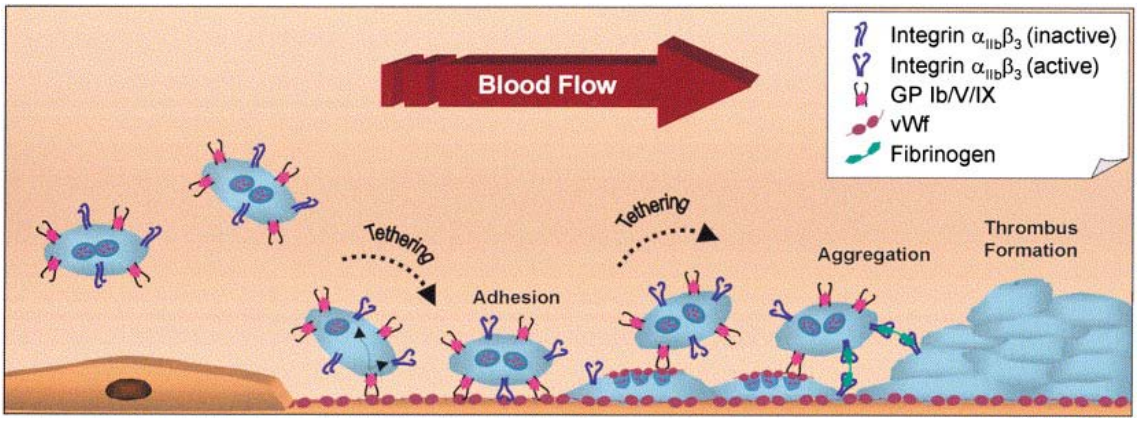

Fig. 6. *Formation of a platelet plug on the denuded subendothelial matrix. Platelets tether to vWF via GP-Ib-V-IX receptors. Interaction of platelet receptors with proteins of the subendothelial matrix induces platelet adhesion. Activation of* $\alpha_{IIb}\beta_3$ *receptors leads to aggregation of platelets bridged by fibrinogen molecules. (Jackson et al. 2000).*

Collagen-GPVI and vWF-GPIb-V-IX interactions are the key initiators of platelet activation (Fig. 7). Signal transduction through phospholipase C γ2 results in the release of secondary activation molecules, integrin activation, and procoagulant changes in platelets (Li et al. 2010).

DOI:10.14753/SE.2016.1824

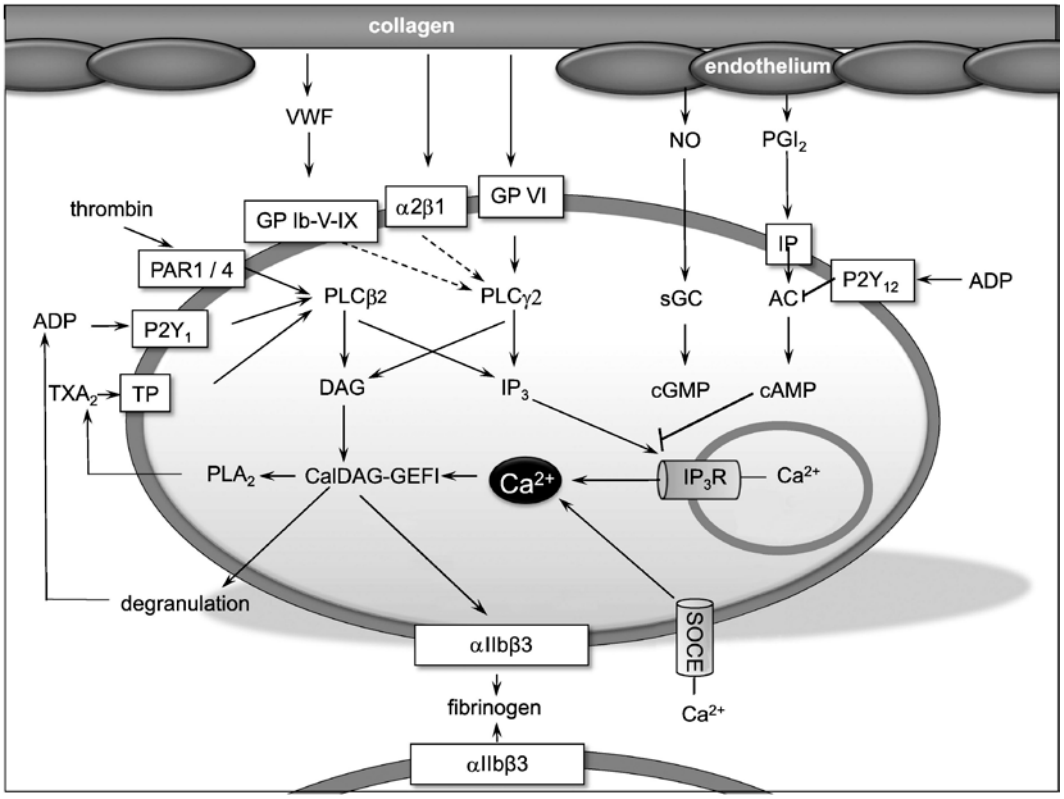

Fig. 7. *Platelet signalling. Exposure to the subendothelial matrix activates platelets: collagen-GPVI, collagen-$\alpha_2\beta_1$, and vWF-GPIb-V-IX interactions activate phospholipase Cγ2 (PLCγ2) inducing the formation of inositol triphosphate (IP_3) and diacylglycerol (DAG) second messengers. IP_3 mobilise Ca^{2+} from intracellular stores through inositol triphosphate receptor (IP_3R) which subsequently leads also to Ca^{2+} influx by store operated calcium entry (SOCE). Ca^{2+} and DAG activate calcium and DAG regulated guanine nucleotide exchange factor 1 (CalDEG-GEFI). This signal transduction results in degranulation, synthesis of thromboxane A2 (TXA_2) by phospholipase A2 (PLA_2), and inside-out activation of $\alpha_{IIb}\beta_3$ receptors. Platelet activation through second messengers and thrombin: ADP receptor $P2Y_1$, TXA_2 receptor TP, and thrombin receptors PAR1/4 activate PLCβ2, which further exaggerates the platelet activation. ADP can also bind to $P2Y_{12}$ receptor, which blocks the synthesis of inhibitory cAMP molecules. Endothelial cells inhibit platelets: Prostacyclin (PGI_2) binds to prostacyclin receptor (IP) and activates adenylate cyclase (AC) leading to increased cyclic adenosine monophosphate (cAMP) level. Nitric monoxide (NO) increases intracellular cyclic guanosine monophosphate (cGMP) through the soluble guanylate cyclase (sGC). Increased levels of cAMP and cGMP suppress platelet activation. Slightly modified after Broos et al. (Broos et al. 2012).*

Secondary platelet activation

After adhesion and activation of adhered platelets, secondary platelet activation molecules are released (Fig. 7). ADP and serotonin are released by degranulation of dense-granules upon activation of platelets. In contrast, thromboxane A2 is *de novo* synthesized from phospholipids. Thrombin, not a secondary platelet activator, is generated in the coagulation cascade and besides having a pivotal role in coagulation, contributes also to activation of platelets. All of these activator molecules act through G-protein coupled receptors. These autocrine and paracrine signals further excite already activated platelets and amplify the thrombus formation process by activating and recruiting other platelets to the growing thrombus. (Li et al. 2010, Broos et al. 2012)

Platelet aggregation

Aggregation means the binding of platelets to each other, leading to a growing thrombus and finally to a haemostatic platelet plug. Platelets adhere to each other by binding to both sides of a fibrinogen molecule through $\alpha_{IIb}\beta_3$ receptors (Fig. 6). In resting platelets, the receptor only has a low affinity to fibrinogen, but the affinity dramatically increases upon platelet activation. This change in fibrinogen activity requires an inside-out activation of the $\alpha_{IIb}\beta_3$ integrin receptor (Fig 7). The activated $\alpha_{IIb}\beta_3$ receptor is able to bind fibrinogen, leading to the aggregation of platelets. Ligand binding of the $\alpha_{IIb}\beta_3$ receptor also induces signalling events, i.e. outside-in signalling leads to platelet spreading, granule secretion, and clot retraction. (Ruggeri 2002, Jackson 2007, Li et al. 2010).

Procoagulant changes in platelets

Platelet activation also induces procoagulant changes in platelets. Activation of scramblase leads to the exposure of negatively charged phosphatidylserine molecules on the plasma membrane, providing a platform for the coagulation cascade. Vitamin K-dependent clotting factors in the presence of Ca^{2+} can bind to the platelet plasma membrane. In these compartments, coagulation factors can build complexes that accelerate the speed of enzymatic reactions by 10^5-10^7 times. In addition, activated platelets produce procoagulant microparticles that further increase the active surface for the coagulation process (Machovich 2006, Tanaka et al. 2009, Broos et al. 2012, Clemetson 2012).

DOI:10.14753/SE.2016.1824

Formation of platelet-leukocyte complexes

Activation of platelets does not only induce platelet-platelet adhesion but also the formation of heterotypic platelet-leukocyte aggregates (Fig. 8). Platelets can form complexes with granulocytes, monocytes, and with subsets of lymphocytes. These interactions play an important role in platelet-dependent leukocyte recruitment and also in the augmentation of thrombus formation.

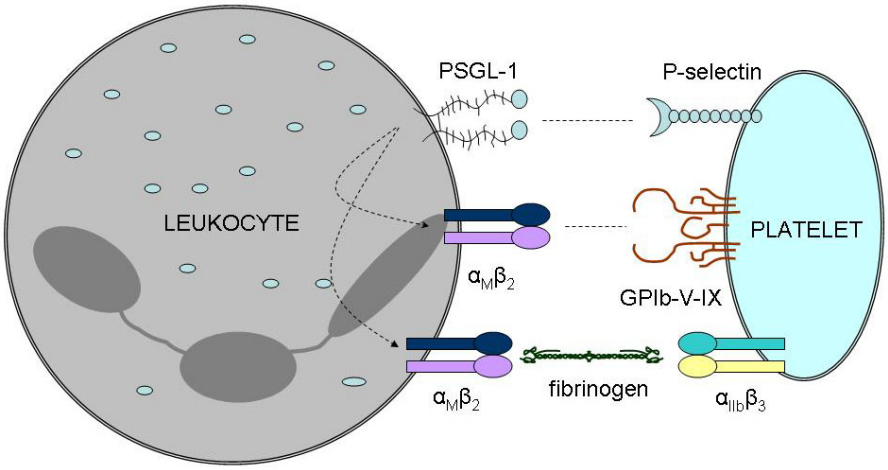

Fig. 8. *Platelet-leukocyte adhesion. Tethering of platelets to leukocytes through P-selectin and PSGL-1 induces activation of $\alpha_M\beta_2$ receptors. Binding of activated $\alpha_M\beta_2$ to $\alpha_{IIb}\beta_3$ through fibrinogen and to GPIb-V-IX directly leads to firm adhesion. Modified after Ley at al. (Ley 2011)*

The initial adhesion of platelets to leukocytes is mediated by P-selectin on platelets and P-selectin glycoprotein ligand-1 (PSGL-1) on leukocytes. Ligation of PSGL-1 leads to Src family kinase-dependent signalling that results in conformational change of leukocyte β2 integrins and also induces delayed responses in leukocytes by the activation of nuclear factor κB and the transcription of proinflammatory molecules (Totani and Evangelista 2010). On the other hand, the loose connection between P-selectin and PSGL-1 holds platelets and leukocytes close to each other, enabling the formation of firm connections, and also activates leukocyte integrins necessary for the strong adhesion. Firm platelet-leukocyte adhesion is mediated mainly due to the formation of a fibrinogen bridge between $\alpha_{IIb}\beta_3$ on platelets and macrophage 1-antigen ($\alpha_M\beta_2$ integrin) on leukocytes, and due to the direct interaction of leukocyte macrophage

1-antigen ($\alpha_M\beta_2$ integrin) and GPIb-V-IX receptor of platelets (May et al. 2007). These interactions recruit leukocytes to the site of the thrombus formation. In these heterotypic conjugates, the interaction of platelet P-selectin with leukocyte PSGL-1 and platelet CD40 ligand with leukocyte CD40 induces TF expression of leukocytes contributing to initiation of the coagulation cascade and consequently to fibrin production (Cerletti et al. 2012). Moreover, activated neutrophils recruited to the thrombus produce neutrophil extracellular traps. Neutrophil extracellular traps serve as a scaffold primarily composed of extracellular DNA fibres, which are able to trap pathogens circulating in blood. Neutrophil extracellular trap fibres also contribute significantly to thrombus formation by adhering and activating platelets as well as by stimulating fibrin formation (Fuchs et al. 2012).

Initiation of the coagulation cascade

At the same time as platelet plug formation, blood coagulation factors become activated at the sites of vascular lesions. The initial step of the coagulation cascade (Fig. 9) is triggered by the interaction of activated factor VII plasma protein with subendothelial TF at the site of vascular injury (extrinsic pathway). The activated factor VII-TF complex cleaves factor X. Activated factor X together with activated cofactor V cleaves prothrombin to thrombin. In the initial phase of coagulation, activated factor X generates just a trace amount of thrombin. There are two main inhibitors of the initiation of the coagulation cascade: TFPI blocking factor X, and antithrombin III blocking factor X and thrombin. For the initialization of the coagulation cascade, the TF concentration has to be high enough to overcome the barrier given by TFPI and antithrombin III in order to propagate the coagulation reaction. This mechanism prevents the false activation of the coagulation cascade (Tanaka et al. 2009).

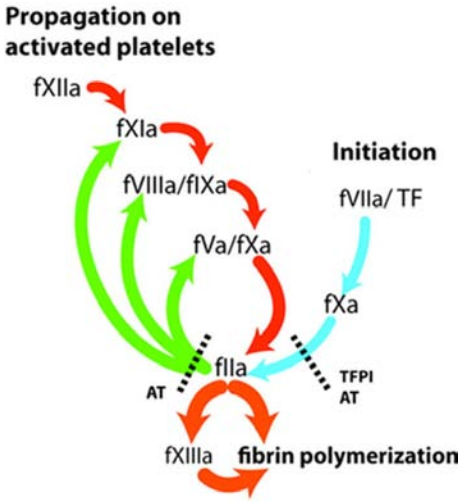

Fig. 9. *Initiation and propagation of the coagulation cascade. The coagulation cascade is triggered by the interaction of TF with factor VII. Activated factor VII-TF complex (fVIIa/TF) leads to the activation of factor X (fXa) and factor II (fIIa). The propagation of the coagulation cascade is due to a positive feedback loop involving the activation of factor XII (fXIIa), XI (fXIa), X (fXa), II (fIIa), and cofactor VIII (fVIIIa) and V (fVa) on activated platelets. Activated factor II cleaves fibrin, resulting in fibrin polymerisation. Activated factor XIII (fXIIIa) strengthens the fibrin mesh. Antithrombin III (AT) and TFPI are inhibitors of the coagulation cascade. Slightly modified after Tanaka et al. (Tanaka et al. 2009)*

Propagation of thrombin production

After initiation of the coagulation cascade, thrombin generation is further exaggerated due to positive feedback loops involving coagulation factors of the intrinsic pathway (Fig 9). Thrombin activates factor XI, VIII, and V. Activated factor XI mediates the activation of factor IX. Activated factor IX together with activated cofactor VIII mediates the cleavage of factor X leading to thrombin generation. Thus, thrombin exaggerates its own production by activating serine proteases of the intrinsic pathway. Thrombin has a central role in haemostasis: it mediates the generation and stabilisation of the fibrin mesh and it is also a very potent platelet activator.

Contact activation

Coagulation might also be initiated in an alternative way due to contact activation. The biological relevance of this kind of activation has not been fully elucidated, but this

mechanism is relevant to thrombus formation upon the interaction of foreign materials with blood. This phenomenon is also widely utilised in the measurement of the activated partial thromboplastin time when silica or kaolin particles are added to blood to initiate the intrinsic coagulation. The contact system consists of factor XII, plasma kallikrein, as well as the cofactor high-molecular-weight-kininogen that assembles on negatively charged surfaces. When particles with a negatively charged solid surface are incubated with blood, factor XII is able to become activated non-enzymatically. Alternatively, plasma kallikrein can cleave and activate the surface-bound factor XII. Activated factor XII also cleaves prekallikrein to kallikrein, resulting in a positive amplification loop. Activated factor XII activates factor XI and thus initiates the intrinsic pathway of the coagulation process (Maas and Renne 2012).

Fibrin mesh

Once thrombin is generated, it cleaves fibrinogen molecules, leading to the release of fibrin monomers. These monomers aggregate spontaneously in a regular array, forming a fibrin clot. In addition to fibrin formation, thrombin activates factor XIII, a highly specific transglutaminase that introduces cross-links composed of covalent bonds between the glutamines and lysines in the fibrin monomers.

Fibrinolysis

Erroneously or excessively produced fibrin mesh can be degraded by fibrinolysis. At first plasminogen, the proenzyme of plasmin, binds to the lysine side chains of the fibrin mesh. This interaction leads to a conformational change of plasminogen molecules, enabling cleavage of plasminogen by plasminogen activators (tissue plasminogen activator and urokinase-type plasminogen activator). The generated plasmin cleaves fibrin into soluble fibrin degradation products, making more and more lysine side chains available where new plasminogen molecules can adhere and become activated. The fibrinolysis is controlled by plasminogen activator inhibitor-1, plasmin inhibitor and trombin activatable fibrinolysis inhibitor. The latter inhibits fibrinolysis by removing lysine side chains from the fibrin mesh. (Machovich 2006, Schaller and Gerber 2011, Foley et al. 2013)

Thrombus formation in the microcirculation

Disturbances in haemostasis can also occur in the microcirculation, inducing alteration of blood flow in tissues. Augmented microcirculatory thrombus formation has been implicated in the pathophysiology of sepsis, disseminated intravascular coagulation, and multiple organ dysfunctions (Gando 2010, Semeraro et al. 2012). Microvascular thrombosis also plays an important role in thrombotic microangiopathies, which comprise a spectrum of diseases such as typical and atypical haemolytic uremic syndrome, thrombotic thrombocytopenic purpura, antiphospholipid syndrome, paroxismal nocturnal haemoglobinuria, malignant hypertension, drugs or systemic autoimmune diseases or antibody-mediated rejection (Benz and Amann 2010).

4. Nanoparticles and thrombus formation

a) Thrombus formation on foreign surfaces

There is a great deal of information about the interaction between blood and foreign material devices such as oxygenators, plasmapheresis equipment, hemodialysers, catheters, stents, vascular grafts, or heart valves. Thrombosis and embolization are well-known complications of these cardiovascular devices. The interaction of blood with foreign surfaces induces thrombus formation by a combination of several mechanisms, involving the coagulation system, platelets, the complement system, and leukocytes (Gorbet and Sefton 2004)

Upon interaction with blood, biomaterials are immediately covered by plasma proteins. Among these proteins are fibrinogen, vWF, factor XII, high molecular weight kininogen, C3 complement, and IgG (Ekdahl et al. 2011).

Factor XII becomes non-enzymatically activated upon adhesion onto negatively charged surfaces and initiates the coagulation cascade (Gorbet and Sefton 2004, Vogler and Siedlecki 2009).

Platelets can adhere to foreign materials mediated by $\alpha_{IIb}\beta_3$ or GPIb-V-IX receptors binding to fibrinogen or vWF adhering to the surface of biomaterials. Adhesion leads to platelet activation. However, the interaction with biomaterials often induces platelet activation without adhesion, which is characterised by a decreased platelet count due to

the removal of activated platelets from the circulation. In the presence of cardiovascular devices, platelets also adhere to leukocytes and induce the formation of platelet-leukocyte aggregates (Mickelson et al. 1996, Bonomini et al. 1999, Gorbet and Sefton 2004) (see also section II/3). The amount of platelet-leukocyte aggregates can also be considered as a parameter for biocompatibility (Gorbet and Sefton 2004).

The complement cascade, which is part of the innate immune system, also contributes to the thrombus formation on biomaterials. The complement cascade results in the formation of the terminal C5b-9 complement complex that can be incorporated into platelet membranes inducing platelet activation. Platelets are also activated by the interaction of C1q and C3a ligands with their platelet receptors. (Gorbet and Sefton 2004, Markiewski et al. 2007, Ekdahl et al. 2011)

Leukocytes can also adhere to the surface of foreign materials. Upon adhesion and due to complement activation, leukocytes express TF. Interaction of TF with factor VII initiates the extrinsic pathway of coagulation. Adhered leukocytes also contribute to the recruitment of platelets by binding platelets to biomaterials through platelet-leukocyte interactions (Gorbet and Sefton 2004, Vogler and Siedlecki 2009).

b) Epidemiology of particulate matter-associated diseases

Relevant information about the toxicity of nanoparticles comes from the investigation of the detrimental effect of air pollution on the human body. Although air pollution is composed not just of nanosized particles, but also larger particulate matter, gaseous and liquid components, this knowledge gives some clues about the possible effects of nanoparticles.

There is a well-known epidemiological association between air pollution and cardiovascular or pulmonary diseases (Brook et al. 2010). The detrimental health effects of air pollution were first realised in the 20th century after major incidents involving acute air pollution (Meuse Valley, Belgium 1930; Donora, USA 1948; and Greater London, UK 1952,) caused sudden deaths, increased illness, and hospital admissions (Simkhovich et al. 2008).

Further investigations revealed that the particulate matter fraction of air pollution is the major contributor to these toxic effects. A number of epidemiological studies have demonstrated the close relationship between particulate matter levels and

cardiopulmonary mortality both in short and long-term studies. Overall evidence from meta-analysis of about 100 research papers since the early 1990s and recent comprehensive analysis of large number multicity studies assume that a short-term (1 to 5 days) 10 μg/m^3 elevation of $PM_{2.5}$ results in an ~1% increase in mortality (Pope and Dockery 2006, Samoli et al. 2008, Brook et al. 2010, Emmerechts and Hoylaerts 2012). Long-term prospective cohort studies have provided more evidence about the health effects of particulate matter. The Harvard Six Cities Study investigated about 8000 persons over 14-16 years (Dockery et al. 1993), the American Cancer Society study analysed data from more than 500,000 adults over 16 years (Pope et al. 2002, Pope et al. 2004, Franchini and Mannucci 2012) and recent large cohort studies of 13.2 million US Medicare participants were analysed for the time period 2000 to 2005. The overall evidence from the cohort studies show on average 10% increase for all case mortality per 10 μg/m^3 elevation in long-term $PM_{2.5}$ exposure. The cardiovascular mortality risk ranges from 3% to 76% in the different cohort studies (Brook et al. 2010).

The role of the nano-sized fraction in particulate matter induced detrimental effects has been gathered from studies collecting data at the source of combustion-derived particles. Ultrafine particles generated by combustion-related processes have a very short life (minutes to hours) and rapidly grow to form a larger complex. Therefore, ultrafine particulate matter concentration is at its highest near the source of primary particles, such as in the vicinity of busy roads. Interestingly, Peters et al. found in a survey of 691 patients a correlation between exposure to traffic and the onset of a myocardial infarction within one hour afterwards (Peters et al. 2001, Peters et al. 2004). An association was also found between short-term exposure to ultrafine particles and hospital admissions for stroke (Andersen et al. 2010). A linear relationship was described between the distance from major traffic roads and the risk of deep vein thrombosis (Baccarelli et al. 2009), indicating the role of ultrafine particles in this process.

There are also epidemiological data that substantiate the influence of air pollution on haemostasis (Emmerechts and Hoylaerts 2012). A positive association was found between particulate matter exposure and plasma fibrinogen concentration, plasminogen activator inhibitor-1 level, and changes of coagulation tests towards hypercoagulability (Pekkanen et al. 2000, Su et al. 2006, Baccarelli et al. 2007, Chuang et al. 2007, Bigert

et al. 2008). Particulate matter exposure is also associated with platelet activation. Chronic inhalation of particulate matter emitted from biomass burning during household cooking in India was shown to induce platelet activation (increased CD62P expression) and to increase the amount of platelet-leukocyte aggregates (Ray et al. 2006). Positive associations were found between soluble P-selectin (shedding after platelet activation) and ambient ultrafine particles (Delfino et al. 2008). Also an immediate increase of a plasma soluble CD40 ligand and a decrease in platelet count was found to be associated with ultrafine particles (Ruckerl et al. 2007).

c) Particulate matter and thrombus formation

To find out how inhaled particulate matter induces detrimental cardiovascular effects several experimental studies have been carried out. Inhaled particles have been found to deposit in the lungs and to induce the production of inflammatory mediators. Based on these findings, the first (classical) hypothesis was that the release of inflammatory agents from the lungs into the blood circulation alters the cardiovascular system or haemostasis (Fig. 10) (Brook et al. 2004, Mills et al. 2009).

The role of inflammatory mediators in inducing prothrombotic effects is supported by experiments in which mice were intratracheally exposed to particulate matter. These studies observed shortened bleeding time and increased thrombus formation 24 hours after application (Mutlu et al. 2007). The prothrombotic effect was attributed to an IL-6-dependent increased activity of the coagulation cascade, and a tumour necrosis factor alpha-dependent decreased fibrinolysis due to increased plasminogen activator inhibitor-1 activity (Mutlu et al. 2007, Budinger et al. 2011). Also controlled human exposure to diesel exhaust particles (DEP) was shown to reduce the release of endothelial tissue plasminogen activator (Mills et al. 2005, Mills et al. 2007). Furthermore, increased TF expression was demonstrated upon incubation of different cells with particulate matter *in vitro* and in the aorta after long-term exposure to particulate matter *in vivo* (Gilmour et al. 2005, Sun et al. 2008).

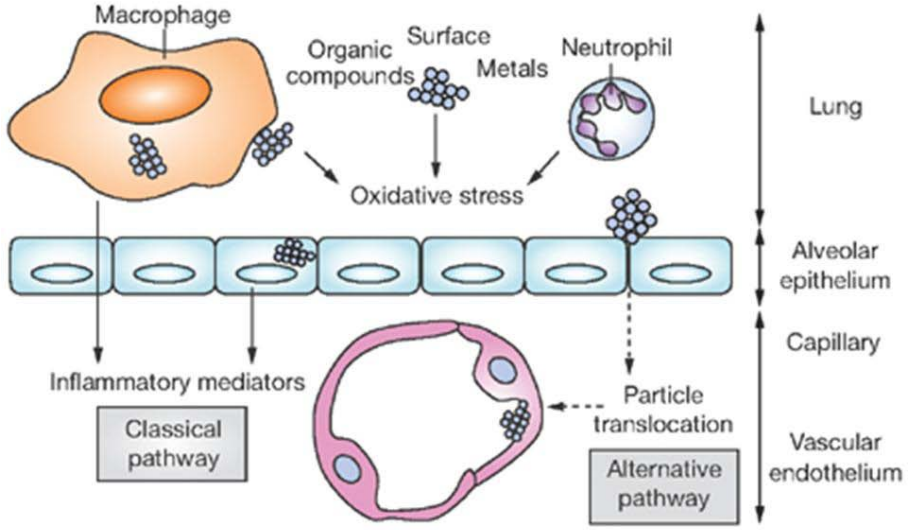

Fig. 10. *Classical and alternative pathways through which airborne nanoparticles induce cardiovascular effects. Classical pathway: Nanoparticles deposited in the lung induce oxidative stress through chemically active organic or metal compounds given on the surface of nanoparticles or through activation of neutrophils and macrophages. In this way they initiate the production of inflammatory mediators from macrophages and alveolar epithelial cells, which are released into the systemic circulation and induce cardiovascular effects. Alternative pathway: Nanoparticles translocate from the lungs through the alveolar epithelium into the blood circulation, where they alter cardiovascular functions. (Mills et al. 2009)*

In further epidemiological studies about the detrimental effects of particulate matter, the important role of its ultrafine fraction has been indicated. Knowing that nano-sized particles are able to translocate from the lungs into the blood (see section II/2/g), an alternative hypothesis was suggested emphasizing that translocated ultrafine particles can reach remote tissues via the circulation and influence organ functions directly (Fig. 10) (Brook et al. 2004, Mills et al. 2009).

The first experimental findings supporting the alternative hypothesis that intratracheally administered nanoparticles are able to augment thrombus formation were published by Nemmar et al. The authors demonstrated in an *in vivo* hamster model that intratracheally instilled or intravenously injected amine-modified polystyrene nanoparticles activate platelets and enhance thrombosis in femoral arteries and veins within 1 hour after application (Nemmar et al. 2002b). Interestingly, just nano-sized (60

nm) and not coarse (400 nm) polystyrene beads influenced thrombus formation, while both nano-sized and coarse polystyrene beads induced lung inflammation suggesting different mechanisms for these two processes (Nemmar et al. 2003b). Later, not just polystyrene beads but also DEP were shown to activate blood platelets and augment thrombus formation (Nemmar et al. 2003a). The prothrombotic effect of DEP was augmented even 6 and 24 hours after instillation and the instillation of DEP nanoparticles also induced an inflammatory reaction in the lung, i.e. increased granulocyte count and elevated histamine concentration in the bronchoalveolar lavage. Interestingly, H1 histamine receptor antagonist inhibited the increase in granulocyte counts in the bronchoalveolar lavage and the late (6- and 24-hour) prothrombotic effects, but did not affect the acute (1 hour) DEP-induced thrombosis or platelet activation (Nemmar et al. 2003c). These findings suggest that both mechanisms contribute to the prothrombotic effect of DEP nanoparticles: translocated nanoparticles induce early prothrombotic effects by direct activation, while lung inflammatory mediators generate late prothrombotic effects.

The above investigations evoked further studies to find out how the interaction of ultrafine particles with blood can influence haemostasis. Several experiments demonstrated the role of platelet activation in the prothrombotic effects of ultrafine particles. *In vitro* experiments found increased P-selectin expression, augmented platelet aggregation, and the formation of platelet-leukocyte aggregates upon the incubation of blood with ultrafine particles (Nemmar et al. 2002b, Nemmar et al. 2003a, Nemmar et al. 2003b, Nemmar et al. 2003c, Radomski et al. 2005, Khandoga et al. 2010, Nemmar et al. 2010, Forestier et al. 2012, Kim et al. 2012). Using *in vivo* microscopy, platelet accumulation was found in the hepatic microcirculation in mice upon injection of carbon black ultrafine particles. Platelet adhesion to endothelial cells was strongly associated with fibrin deposition, and the blockade of the fibrinogen receptor $\alpha_{IIb}\beta_3$ inhibited platelet accumulation in the liver (Khandoga et al. 2004). In the recent work of our research group (Khandoga et al. 2010), a similar experiment was carried out, but instead of systemic injection, inhalative exposure was used for the application of carbon black nanoparticles. The experiment showed the same result: platelets accumulated in the microcirculation of the liver. Fibrin deposition was found on the endothelial surfaces of the microcirculation in the liver and heart. In contrast, according to data obtained

from the bronchoalveolar lavage, a significant pulmonary inflammatory response did not occur and neither the plasma levels of proinflammatory cytokines nor blood cell counts were affected. These data suggest that inhaled carbon black nanoparticles generate prothrombotic effects, also without inducing an inflammatory response in the lungs.

These data were further confirmed by controlled human exposure experiments. Inhalation of elemental carbon ultrafine particles by patients with type 2 diabetes mellitus for 2 hours increased the CD40 ligand expression of platelets and the number of platelet-leukocyte aggregates (Stewart et al. 2010). In the experiment of Lucking et al. healthy volunteers were exposed to DEP, and thrombus formation was measured in a Badimon *ex vivo* perfusion chamber. The Badimon chamber consists of a pump to draw blood from the cubital vein through a perfusion chamber with a strip of porcine aorta. Diesel exhaust particles increased thrombus formation and the formation of platelet-leukocyte aggregates (Lucking et al. 2008).

Ambient nanoparticles were also found to activate the coagulation system (Nemmar et al. 2010, Kilinc et al. 2011). The authors concluded that early procoagulant effects are dependent on the TF-driven extrinsic pathway, whereas long-lasting thrombogenic actions are due to translocated ultrafine particles inducing contact-dependent activation of the coagulation cascade (Kilinc et al. 2011).

Summarising the experimental data about prothrombotic mechanisms of inhaled particulate matter suggests that larger ambient particles deposit in the lung and induce procoagulative changes through inflammatory mediators, whereas nano-sized ambient particles immediately translocate in the circulation, directly activate platelets, and later on activate the coagulation system via contact activation.

d) Manufactured nanoparticles and thrombus formation

The research performed on biomaterials and particulate matter indicates that manufactured nanoparticles might also influence thrombus formation. In spite of the fact that manufactured nanoparticles are produced in high amounts, their effects on the thrombotic process have been investigated to a lesser extent.

Most information concerning the prothrombotic effects of nanoparticles have been obtained from *in vitro* experiments. Increased platelet activation and aggregation were

found to be induced by amine-modified polystyrene beads (Nemmar et al. 2002b, Mayer et al. 2009, McGuinnes et al. 2011), quantum dots (Geys et al. 2008), titanium dioxide nanorods (Nemmar et al. 2008), and gold nanoparticles (Deb et al. 2011). However, in another study gold nanoparticles failed to affect platelet function or coagulation (Dobrovolskaia et al. 2009). Silver nanoparticles were found to prevent platelet activation, adhesion, and aggregation in a concentration-dependent manner, and to inhibit fibrin polymerisation (Shrivastava et al. 2009, Shrivastava et al. 2011). Coagulation was induced by synthetic amorphous silica and organically modified silica nanoparticles (Tavano et al. 2010), polylactic acid nanoparticles (Sahli et al. 1997), and titanium dioxide nanotubes, whereas titanium dioxide nanoparticles inhibited the coagulation system (Roy et al. 2007). Nano-sized copper (II) oxide caused up-regulation of plasminogen activator inhibitor-1 in endothelial cells (Yu et al. 2010).

There is much less data about the effect of nanoparticles on thrombus formation *in vivo.* It has been shown that amine-modified polystyrene nanoparticles augmented and carboxyl-modified polystyrene nanoparticles inhibited thrombus formation in femoral vessels (Nemmar et al. 2002b). Carbon nanotubes were found to augment ferric chloride-induced thrombosis *in vivo* (Radomski et al. 2005). TiO_2 rutile nanorods decreased the platelet count *in vivo* (Nemmar et al. 2008). Intravenous administration of quantum dots (Geys et al. 2008) or mesoporous silicate nanoparticles (Hudson et al. 2008) were shown to induce pulmonary thrombosis.

The above studies have investigated thrombus formation in large vessels. Although nanoparticles also reach the microcirculation, there are only a few recent publications that have analysed the effects of nanoparticles on thrombus formation in the microvasculature. Amine-modified polystyrene nanoparticles as benchmark particles were shown to induce a dose-dependent enhancement of thrombus formation in the microcirculation (Silva et al. 2005). Additionally, a previous study from our research group has demonstrated that systematically administered carbon black nanoparticles enhanced platelet accumulation on the endothelium of postsinusoidal venules and sinusoids in the hepatic microcirculation (Khandoga et al. 2004). However, the effects of manufactured nanoparticles on thrombus formation in the microcirculation have not been investigated yet.

DOI:10.14753/SE.2016.1824

III. Aims

The main objective of my research work was to investigate platelet activating and microcirculatory prothrombotic effects of manufactured nanoparticles. To achieve these aims, some methodological problems also had to be solved, i.e. the preparation of nanoparticle dispersions in physiological solutions and the optimisation of the platelet-granulocyte complex measurement.

1. Optimisation of the preparation method of nanoparticle dispersions

For investigations of *in vitro* and *in vivo* prothrombotic effects, nanoparticles have to be dispersed in physiological solutions. However, nanoparticles in solutions with physiological salt concentrations and pH values form coarse agglomerates. To avoid the formation of coarse agglomerates, a steric stabiliser has to be added to the nanoparticle dispersions. To optimise the dispersion method, we varied the following factors while preparing the nanoparticle dispersions:

i) ultrasound energy levels

ii) type of dispersion stabilizer: human, bovine, or mouse albumin, Tween 80, or mouse serum

iii) concentration of dispersion stabilizer

iv) concentration of nanoparticles

v) sequence of preparation steps

vi) stability of the dispersion over time

vii) We also tested our method on a broad range of various types of nanoparticles.

2. Optimisation of platelet-granulocyte complex measurement

For the evaluation of platelet activation, also the amount of platelet-granulocyte complexes was measured. The measurement of platelet-granulocyte complexes with a flow cytometer is based on the simultaneous detection of fluorescent signals from both cell types. However, these double-positive signals can also originate from the coincidence of non-interacting platelets and granulocytes in the detection volume. Our aim was to develop a method that measures the real amount of platelet-granulocyte complexes without overestimating it due to coincidence.

DOI:10.14753/SE.2016.1824

3. Prothrombotic effects of nanoparticles

Ambient nanoparticles have been shown to exert prothrombotic effects, but manufactured nanoparticles are less well investigated in this regard. Although circulating nanoparticles also reach the microcirculation, the effects of manufactured nanoparticles on microcirculatory thrombus formation have not been investigated yet. Thus the aim of this study was:

i) to characterize the effects of DEP, titanium dioxide rutile, and single-walled carbon nanotube nanoparticles on platelet activation and

ii) on the formation of platelet-granulocyte complexes *in vitro*

iii) to assess their impact on thrombus formation in small arteries and in the microcirculation *in vivo,* and

iv) to compare these effects with those induced by surface-modified polystyrene beads as benchmark particles.

DOI:10.14753/SE.2016.1824

IV. Materials and Methods

1. Materials

a) Nanoparticles

Table 3. *Nanoparticles used in our study, name of company, and size of nanoparticles as given by the manufacturer.*

Nanoparticle	Size	Company
Titanium(IV) oxide nanopowder 99.5% rutile	~10 nm × 40 nm	Sigma-Aldrich, Schnelldorf, Germany
Titanium(IV) oxide nanopowder 99.7% anatase	<25 nm	Sigma-Aldrich, Schnelldorf, Germany
Zinc oxide nanopowder	<100 nm	Sigma-Aldrich, Schnelldorf, Germany
Plain polystyrene beads	60 nm	Bangs Laboratories, Fishers, USA
Carboxyl-modified polystyrene beads	60 nm	Bangs Laboratories, Fishers, USA
Amine-modified polystyrene beads	65 nm	Bangs Laboratories, Fishers, USA
S-purified SWNT	outer diameter < 2 nm, length 1–5 μm	SES research, Houston, USA
S-purified MWNT	outer diameter 10–30 nm, lengths 1–2 μm	SES research, Houston, USA

Nanoparticle	Size	Company
DEP - SRM 2975	no data	National Institute of Standards and Technology, Gaithersburg, USA
Silicon oxide 99.5%	10 nm	Nanostructured and Amorphous Materials Inc, Los Alamos, USA
Silver synthesized 99.5%	30–50 nm	Nanostructured and Amorphous Materials Inc, Los Alamos, USA

b) Reagents

Mouse serum albumin (MSA), bovine serum albumin (BSA), 10 × concentrated phosphate buffered saline (PBS), and 10 × concentrated RPMI 1640 medium, fluorescein isothiocyanate (FITC) dextran 150 kD, epinephrine-bitartrate, ADP, ethylenediaminetetraacetic acid (EDTA), and lipopolysaccharide (LPS) from Escherichia Coli O111:B4 were purchased from Sigma-Aldrich, Schnelldorf, Germany. Human serum albumin (HSA) 50 g/l was from Baxter Deutschland Gmbh, Heidelberg, Germany. BSA-Tyr buffer contained: 0.35% BSA, 10 mM Hepes, 137 mM NaCl, 2.8 mM KCl, 1 mM $MgCl_2$, 12 mM $NaHCO_3$, 0.4 mM Na_2HPO_4, 5.5 mM glucose, pH 7.4.

c) Mouse serum

C57BL/6NCrl male mice (Charles River, Sulzfeld, Germany) were anaesthetised with isoflurane-N_2O (FiO_2 0.35, 0.015 l/l isoflurane; Forene; Abbott GmbH, Wiesbaden, Germany). Blood was taken by heart puncture and allowed to clot. The blood was centrifuged at 1400 g for 20 minutes and the supernatant was taken. Serum samples were pooled and aliquots were stored at -20°C until use.

d) Antibodies and fluorescent beads for flow cytometry

For the flow cytometric detection of platelets, PE-labelled anti-CD62P (Dako, Glostrup, Denmark), FITC-labelled anti-CD41 (Immunotech, Marseilles, France), and mouse IgG1-FITC isotype control (DAKO, Denmark, Glostrup) as well as for detection of

granulocytes PC5-labelled anti-CD15 (Immunotech, Marseilles, France) antibodies were used. For modelling coincidence, FL1 fluorescent FITC (Calibrite, Becton Dickinson, USA) and FL3 fluorescent Starfire Red™ labelled (QuantumPlex, Level IV, Bangs Laboratories, USA) beads were applied.

2. Characterisation of nanoparticles

The characterisation of nanoparticle dispersions involved the measurement of size distribution and zeta potential, visualisation with transmission electron microscopy, and determination of the endotoxin content.

a) Size distribution and zeta potential measurement

The size distribution and the zeta potential of nanoparticles were analysed in aqueous dispersion with a Zetasizer Nano ZS instrument (Malvern, Malvern Hills, United Kingdom).

Dynamic light scattering is used by the instrument to determine the size distribution of particles by measuring dynamic fluctuations of the scattered light intensity due to the Brownian motion of the particles.

This technique yields the Z-average hydrodynamic diameter of the particles calculated from the peak values of the hydrodynamic diameter distribution via the Stokes-Einstein equation. This type of measurement also provides the polydispersity index (PdI) that describes the width of the particle size distribution. The PdI scale ranges from 0 to 1, where a higher number means higher polydispersity. Each assigned size and PdI value was the mean of 10 runs. All measurements were carried out in triplicate with a temperature equilibration time of 1 minute at 25°C. The following parameters were used in the instrument settings to allow for a correct optical model: The refractive index values of the nanoparticles were taken from the literature. For the dispersant, a refractive index of 1.330 and a viscosity of 0.8872 cP were chosen. The data processing mode was set to high multi-modal resolution.

The measurement technique used by the Zetasizer Nano ZS to measure the zeta-potential of particles in a solution is known as phase analysis light scattering. This technique uses a laser which is passed through the sample to measure the velocity of the

particles in an applied electric field of known value. Among other factors, velocity depends on the zeta potential of the nanoparticles. The optical model for zeta potential measurements was interpreted using Smoluchowski's method, since the particles were dispersed in polar solvents.

For measuring the accuracy of size and zeta potential measurement, 60 nm plain carboxyl- and amine-modified particles were prepared at a concentration of 0.02 mg/ml in distilled water.

b) Transmission electron microscopy

Nanoparticles were visualised with a transmission electron microscope (Jeol JEM 2010) operated at 200 kV. Samples for transmission electron microscopy were prepared by letting a drop of nanoparticle dispersion dry onto a perforated carbon layer-covered copper mesh grid (Agar Scientific Ltd., Stansted, UK). The mean particle size in the TiO_2 (rutile) dispersions prepared with HSA was analysed by measuring the diameter of 100 particles using Image J software (National Institutes of Health, Bethesda, USA).

c) Endotoxin measurement

Nanoparticle dispersions prepared by the above method were tested with the LAL (Limulus amoebocyte lysate) kinetic chromogenic assay (Lonza, Verviers, Belgium). The endotoxin content in DEP, TiO_2 (rutile), and SWNT dispersions was below 0.5 EU/ml.

3. Optimisation of the nanoparticle dispersion method

For *in vitro* and *in vivo* studies, a new dispersion method was needed to avoid formation of nanoparticle agglomerates in physiological solutions. The preparation had to be optimised. The optimal conditions for each preparation step and the best preparation sequence were tested in terms of their effect on the agglomeration state of nanoparticle dispersions. The agglomeration state of aqueous dispersions was analysed with dynamic light scattering and transmission electron microscopy (see above). The following factors were tested and optimised:

a) Effect of different ultrasound energies

A TiO_2 (rutile) stock solution was prepared at a concentration of 0.02 mg/ml in distilled water. One ml of the nanoparticle dispersion was sonicated with a Hilscher UP50H 50 watt, 30 kHz sonicator (Hilscher Ultrasonics GmbH, Teltow, Germany) using different intensities (20%, 50% or 100%) and different time intervals (10 sec, 1 min or 5 min). The power consumption of the sonicator was measured with a power-measuring device during sonication of the particles (working operation) and during sonication of air (no-load operation). The specific energy was calculated as: $E_{spec}= (P_{work}-P_{no\text{-}load}) \times t/V$, where P_{work} and $P_{no\text{-}load}$ are the power consumptions of working and no-load operations, t is the duration of the sonication, and V is the volume of the dispersion (Hilscher 2005).

b) Various sequences of preparation steps

To evaluate the effect of various sequences of preparation steps, a TiO_2 (rutile) stock solution was prepared at a concentration of 0.02 mg/ml in distilled water with or without sonication with 4.2×10^5 kJ/m^3 specific energy. Thirty µl of HSA (end concentration 1.5 mg/ml) or Tween 80 (end concentration 0.1%) was given to 870 µl of dispersion before or after the addition of 100 µl of a 10 × concentrated PBS solution.

c) Mediums and dispersion stabilisers

The TiO_2 (rutile) dispersion was also prepared in a similar way using RPMI 1640 cell culture medium and with the addition of other dispersion stabilisers, i.e. 1.5 mg/ml MSA, 1.5 mg/ml BSA, 0.1% Tween 80, or 30 µl mouse serum.

The effect of different TiO_2 rutile (0.002, 0.02, 0.2, 2 mg/ml) and HSA (0.0015, 0.015, 0.15, 1.5, and 15 mg/ml) concentrations was tested.

d) Different types of nanoparticles

Dispersions were also prepared from TiO_2 (anatase), ZnO, SWNT, MWNT, silver, SiOx, and SRM 2975 DEP by preparing 0.02 mg/ml stock solutions, sonicating with 4.2×10^5 kJ/m^3 specific ultrasound energy, adding 1.5 mg/ml HSA, 0.1% Tween, or 30 µl serum prior to the addition of concentrated PBS.

DOI:10.14753/SE.2016.1824

e) Evaluation of the stability of nanoparticle dispersions

The stability of 0.02 mg/ml TiO_2 (rutile) dispersions prepared by sonication with 4.2×10^5 kJ/m^3 energy and by the addition of 1.5 mg/ml HSA followed by PBS was measured for 1 week.

4. Dispersion of nanoparticles

Based on the previous optimisation, the following dispersion method was used for *in vitro* and *in vivo* experiments. DEP, TiO_2 (rutile), or SWNT stock solutions were prepared at a concentration of 0.23 mg/ml in distilled water using sonication with 4.2×10^5 kJ/m^3 specific energy. For *in vitro* experiments with human blood, 30 µl of 50 mg/ml human serum albumin (end concentration 1.5 mg/ml) and for *in vivo* mouse experiments 30 µl of mouse serum was given to 870 µl of dispersion before the addition of 100 µl of a ×10 concentrated PBS solution. To prepare dispersions at lower concentrations, dilutions of the stock solution were used. The end concentrations of nanoparticles in the dispersion were 0.002, 0.02 and 0.2 mg/ml. The vehicle was prepared in the same way, but instead of nanoparticle dispersion, 870 µl of distilled water was added to human serum albumin or mouse serum and to concentrated PBS. Dispersions with amine- and carboxyl-modified polystyrene nanoparticles were prepared in PBS at 0.2 mg/ml without sonication or addition of human serum albumin or mouse serum.

5. Blood collection for *in vitro* studies

For flow cytometric and aggregometry measurements, blood was collected from the cubital vein of healthy volunteers into citrate anticoagulant-containing Vacuette (Greiner, Austria, Kremsmünster) test tubes. In some cases, when platelet–granulocyte coincidence was modelled, EDTA was used as anticoagulant. All samples were obtained with the approval of the local Ethical Committee after the donor had given informed consent.

DOI:10.14753/SE.2016.1824

6. Optimisation of the platelet-granulocyte complex measurement

a) Experimental analysis of coincidence

Measurement of fluorescent beads

To model platelet–granulocyte coincidence experimentally, FL1 fluorescent and FL3 fluorescent beads were mixed at 225,000/µl and 5000/µl final concentrations respectively, corresponding to the platelet and granulocyte concentrations in the blood. Bead mixtures were measured in the flow cytometer after 10–320-fold dilutions with PBS (n=4).

Measurement in EDTA anticoagulated blood

To measure coincidence of platelets and granulocytes in the flow cytometer, EDTA anticoagulated blood samples (n=7) were stained by fluorescent-labelled antibodies: 20 µl anti-CD15-PC5 as a granulocyte marker and 10 µl anti-CD41-FITC as a platelet marker were added to 100 µl of blood. The non-specific binding of antibodies was measured using appropriate isotype controls. The samples were incubated for 30 min in the dark at room temperature. After incubation, samples were diluted with 2 mM Na2-EDTA containing PBS. The final blood dilutions were 6.625-, 20-, 40-, 80-, 160- and 320-fold. To minimize platelet activation, no washing or vortexing procedures were used (Hagberg and Lyberg 2000).

Measurement in citrate anticoagulated blood

To measure platelet–granulocyte complexes, citrated blood samples (n=9) were kept at room temperature for 30 ± 10 min to ensure *in vitro* complex formation (Li et al. 1999, Peters et al. 1999, Hagberg and Lyberg 2000) and stained in the same way as the EDTA anticoagulated blood samples. Then, 130 µl of stained sample was made up to 1 ml with PBS containing 1% paraformaldehyde and 0.38% Na3-citrate (final dilution of blood: 10-fold) and kept at room temperature for 1 h to stabilize the *in vitro* formed complexes. These samples were further diluted with PBS containing 1% paraformaldehyde and 0.38% Na3-citrate, as in the case of the EDTA samples. The final blood dilutions were

6.625-, 20-, 40-, 80-, 160- and 320-fold. No washing or vortexing procedures were used.

Detection of platelet-granulocyte complexes using fluorescent beads

To determine the extent of coincidence in the presence of real complexes, citrated blood samples were stained only for CD 41, fixed and diluted as above. Right before flow cytometric measurement 10 µl (~10^7/ ml) of FL3 fluorescent beads were mixed into 500 µl of fixed diluted citrated blood samples to ensure a bead concentration comparable to that of granulocytes.

Flow Cytometry

Samples were run on a Becton Dickinson FACScan flow cytometer at high (1 µl/s) flow rate and at 488 nm excitation wavelength. Data acquisition was triggered by the FL3 signals detected at 650 nm. To ensure that granulocytes or fluorescent beads triggered the data collection, the appropriate threshold was determined in separate measurements based on the FL3 histogram and on the light scattering profile. 5000 events were collected in every measurement. The FL1 positive events (CD41+ platelets or FITC labelled beads, detected at 530 nm) were evaluated as a percentage of FL3 positive ones (Fig. 11).

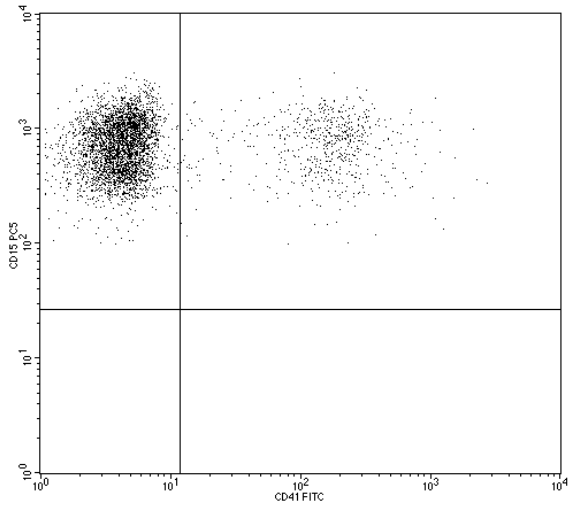

Fig. 11. *Representative dot plot of an EDTA anticoagulated blood sample at 40-fold dilution. Only CD15 positive data were acquired. The ratio of double (CD15+ and CD41+) positive events is 14.8%. (Bihari et al. 2008a)*

DOI:10.14753/SE.2016.1824

Cell Counts

Granulocyte and platelet counts were determined in undiluted blood samples by standard procedures on an Abbott Celldyn 3500 haematological analyser.

b) Mathematical description of coincidence

The phenomenon of coincidence occurring during the sorting of cells at high-speed by a flow cytometer has been discussed by Keij et al. (Keij et al. 1991). Instead of the time bins used by them, it seemed more practical to introduce the detection volume as a way to describe coincidence of platelets and granulocytes (Fent et al. 2008). The detection volume is that fraction of the sample volume in which fluorescent signal collection occurs during the detection of one event (Fig 12.).

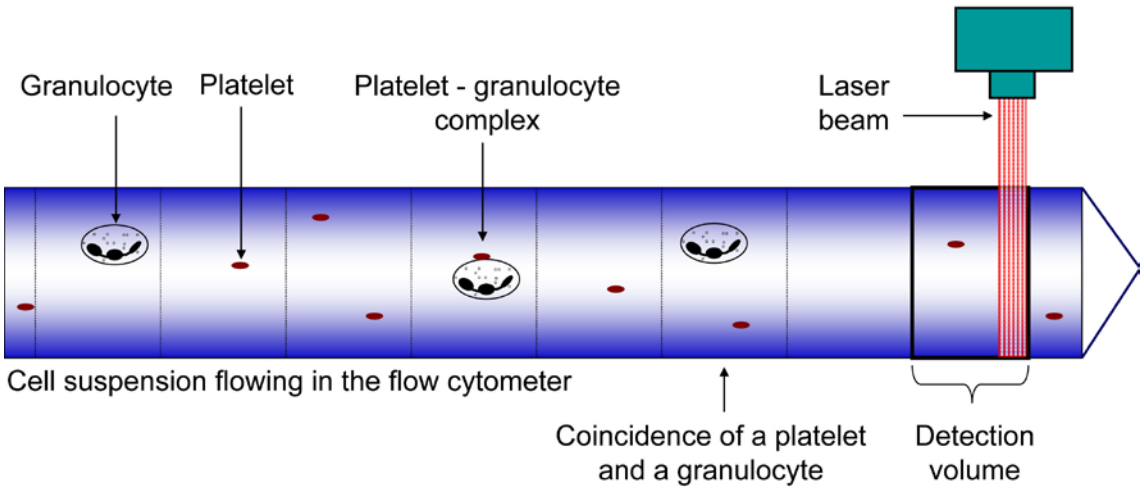

Fig. 12. *Principle of flow cytometric measurement of platelet-granulocyte complexes. Real platelet-granulocyte complexes are undistinguishable from separated platelets and granulocytes that coincide in the detection volume. The detection volume is given by multiplication of the volume flow rate of the cell suspension and the time duration of the detection. Slightly modified after Fent et al. (Fent et al. 2008).*

The easiest way to describe coincidence mathematically, in a complex system where a different number of platelets can adhere to or can coincide with a granulocyte in the detection volume, is to determine the probability of the complementary event, i.e. the

probability that triggering originates from a platelet marker negative granulocyte (p_n). The probability p_n can be given as the product of two probabilities:

(1) $$p_n = p_0 p_c$$

p_0 denotes the probability that no free platelets are in the detection volume and p_c is the probability that the triggering event originates from a single granulocyte and not from a platelet–granulocyte complex.

(2) $$p_c = 1 - \frac{[\mathrm{C}]}{[\mathrm{G}]}$$

where [G] and [C] represent the concentration of granulocytes and complexes in the blood sample respectively. The probability that a given number of platelets occurs in the detection volume (V_d) can be calculated from the Poisson distribution. Poisson distribution describes the probability (p_k) of a given number of events (k) occurring within a time or space (e.g. volume) interval, when a single event occurs with a steady probability (p). For calculation purposes, platelets and granulocytes are considered point-like particles without dimension, where n is the number of platelets given in the examined blood.

(3) $$p_k = \frac{(np)^k}{k!} e^{-np}$$

When no free platelets are in the detection volume, k=0 and the probability (p_0) can be calculated as follows:

(4) $$p_0 = \frac{(np)^0}{0!} e^{-np} = e^{-np}$$

where n, the number of platelets in the volume of blood examined (V_{all}) can be calculated from the platelet concentration ([T]):

(5) $$n = V_{all}[\mathrm{T}]$$

and p is the probability of platelet–granulocyte coincidence if only one platelet was to be found in V_{all}

(6) $$p = \frac{V_d}{V_{all}}$$

From Eqs. (4), (5) and (6) one gets:

(7) $$p_0 = e^{-np} = e^{-[\mathrm{T}]V_d}$$

Combining Eqs. (1), (2) and (7):

(8) $$\ln p_n = -V_d[\mathrm{T}] + \ln\left(1 - \frac{[C]}{[G]}\right)$$

If "D" means the percentage of platelet marker positive events in the granulocyte gate, p_n can be estimated from the flow cytometric measurements in the following way:

(9) $$p_n = 1 - D/100$$

and thus plotting

(10) $$Y = \ln(1 - D/100)$$

as a function of platelet concentrations results in a straight line if [C]/[G] and V_d are independent of [T] (Eq. (8)). [C]/[G] independence of [T] means that the sample contains only dilution-resistant complexes. V_d independence of [T] means that the velocity of cell suspension or the duration of event detection does not change depending on the event count. The intercept of that straight line contains information on the amount of dilution resistant stable complexes. The negative slope of the straight line equals the detection volume.

7. Measurement of platelet activation *in vitro*

a) Incubation of whole blood with nanoparticles

Platelet activation and formation of platelet-granulocyte complexes in the presence of nanoparticles in human whole blood was determined by flow cytometry. 100 µl of citrated blood was incubated with 100 µl of vehicle or 100 µl of nanoparticle dispersion for 10 minutes at room temperature. Dispersions of amine-, carboxyl-modified polystyrene bead, DEP, and TiO_2 (rutile) nanoparticles had a concentration of 0.2

mg/ml and SWNT dispersions had concentrations of 0.002, 0.02 or 0.2 mg/ml. After incubation, samples were diluted 5-fold with BSA-Tyr buffer. As a positive control, blood samples diluted 10 times with BSA-Tyr buffer were incubated with 1 μM ADP (final concentration) for 10 minutes.

b) Flow cytometry

Measurement of platelet P-selectin

Samples were stained with PE-labelled anti-CD62P antibodies and FITC-labelled anti-CD41 antibodies according to the manufacturer's instructions. To check non-specific binding of the antibodies, appropriate isotype control antibodies were used. After staining, samples were diluted 50-fold with BSA-Tyr buffer (500-fold final dilution of blood). To minimize the spontaneous activation of platelets, no washing steps were used. Samples were run on a Becton Dickinson FACScan flow cytometer. 5000 events were collected in every measurement. The CD41 platelet marker was used as a trigger signal for data collection. Platelets were gated on the FS-SS dot plot, and the mean CD62P fluorescence intensity was analysed for CD41 positive events.

Measurement of platelet-granulocyte complexes

For the measurement of platelet-granulocyte complexes, the previously optimised flow cytometric method with high sample dilution was used (see results and discussion of the optimisation below in section V/2 and VI/2). Samples were stained according to the manufacturer's instructions with FITC-labelled anti-CD41 and PC5-labelled anti-CD15 antibodies. To check the non-specific binding of the antibodies, appropriate isotype control antibodies were used. After staining, samples were diluted 50-fold with BSA-Tyr buffer (500-fold final dilution of blood). To minimize the spontaneous activation of platelets, no washing steps were used. Samples were run on a Becton Dickinson FACScan flow cytometer. 5000 events were collected in every measurement. Platelet-granulocyte complexes were detected as double-positive events in the granulocyte gate. Here, the CD15-PC5 granulocyte marker was used as a trigger signal. The amount of platelet-granulocyte complexes was determined as a percentage of CD41 positivity in the CD15-positive gate.

c) Aggregometry

In vitro aggregation of human platelets in the presence of nanoparticles was detected with a Chronolog Whole Blood Lumi-Aggregometer type 560 C (Chrono-Log, Havertown, USA) by measuring the optical density in plastic cuvettes at 37 ^{o}C with continuous stirring (1000 RPM). The reaction mixture contained 400 µl of platelet-rich plasma (PRP) and 100 µl of 0.5 mg/ml nanoparticles. Platelet-poor plasma (PPP) containing the same amount of nanoparticles served as reference. After running samples for at least 10 minutes, 1 µM of ADP was added to check the aggregation ability of platelets. Data were collected with both a two-channel recorder and a computer. Aggregation in the presence of nanoparticles is given as a percentage of that induced by ADP.

8. Detection of *in vivo* thrombus formation

a) Animals

C57BL/6NCrl mice were purchased from Charles River (Sulzfeld, Germany). All experiments were performed with male mice with a body weight of 15 to 22 g (18.6 ± 1.6 g) for mesenteric thrombosis and 20 to 27 g (24.0 ± 1.5 g) for cremasteric thrombosis experiments. Animals were raised in a specific pathogen-free environment and later housed under conventional conditions with free access to food and water. All experiments were performed according to the German legislation for the protection of animals.

b) Ferric chloride-induced thrombosis in small mesenteric arteries

Surgical procedure

Mice were anaesthetised using a ketamine (100 mg/kg) / xylazine (10 mg/kg) mixture administered by intraperitoneal injection. The carotid artery was cannulated in a retrograde manner for the administration of FITC-dextran, nanoparticles, or vehicle. For intravital microscopy, the mesentery was exteriorized gently through a midline abdominal incision. At the end of the experiment blood was collected from the heart and

blood cell counts were measured with a Coulter Ac T 8 haematology analyser (Beckman Coulter, Fullerton, USA).

Intravital microscopy

The set-up for intravital microscopy was centred around a Zeiss Axiotech upright microscope, equipped for fluorescence epi-illumination microscopy. Light from a 100-W HBO source was directed onto the specimen via a FITC filter cube (Ex 450-490, FT 510, LP 520). Microscopic images were obtained with Epiplan lenses (10x / NA 0.2) and recorded with a black and white CCD video camera (FK 6990A-IQ, Pieper, Schwerte, Germany) and a digital video recorder (Sony DSR-45P DVCAM).

Experimental protocol

The experiments were performed as described earlier (Andre et al. 2003) with minor modifications. After surgical preparation, either DEP, TiO_2 (rutile), SWNT nanoparticles at a concentration of 1 mg/kg (in a volume of 5 µL/g body weight), polystyrene nanoparticles at a concentration of 0.5 mg/kg body weight (in a volume of 2.5 µL/g body weight), vehicle, or physiological saline were injected through the catheter into the mice 10 minutes prior to induction of thrombosis in order to yield a uniform distribution of the particles in the microcirculation. One small mesenteric artery (diameters 140-230 µm) per animal was recorded. Vessel wall injury was generated at 10 minutes after nanoparticle application by placing a 1 x 2 mm filter paper saturated with a 5% $FeCl_3$ solution over the artery for 7 minutes (Fig. 13). Cessation time was defined as time between induction of vessel wall injury and complete occlusion of the artery. In vessels without complete occlusion until the end of the recording, the cessation time was considered to be 40 min. As a positive control, mice were given epinephrine intra-arterially at a blood concentration of 12.5 µM (blood volume was estimated to be 2 ml) immediately prior to the induction of thrombosis.

DOI:10.14753/SE.2016.1824

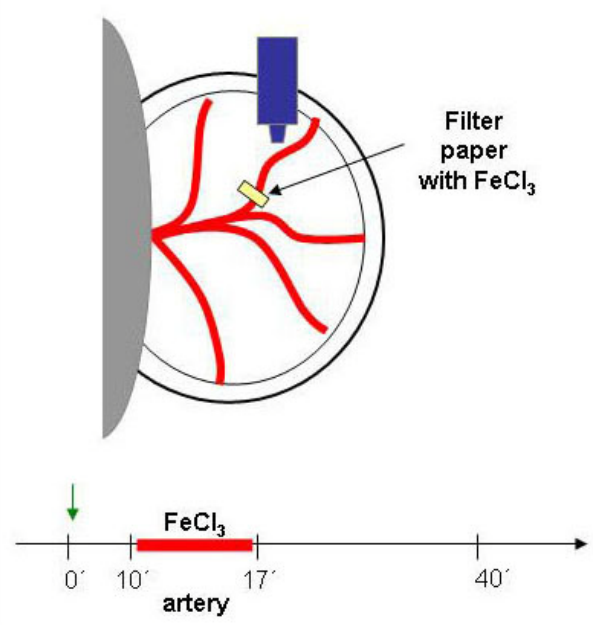

Fig. 13. *Ferric chloride-induced thrombosis in mesenteric arteries. The mesentery is exteriorized through a midline abdominal incision and thrombus formation is induced by placing a 1 x 2 mm filter paper saturated with a 5% $FeCl_3$ solution over the artery (140-230 µm) for 7 minutes.*

c) Light/dye-induced thrombosis in the cremasteric microcirculation

Surgical procedure

Light/ dye-induced thrombosis in the cremaster microcirculation was carried out in a separate set of experiments. The surgical preparation of the cremaster muscle was performed as originally described by Baez (Baez 1973) with minor modifications. Mice were anaesthetised using a ketamine (100 mg/kg) / xylazine (10 mg/kg) mixture administered by intraperitoneal injection. The left femoral artery was cannulated in a retrograde manner for the administration of FITC-dextran and nanoparticles or vehicle. The right cremaster muscle was exposed through a ventral incision of the scrotum. The muscle was opened ventrally in a relatively avascular zone, using careful electrocautery to stop any bleeding, and spread over the pedestal of a custom-made microscopic stage. Epididymis and testicle were detached from the cremaster muscle and placed into the abdominal cavity. Throughout the surgical procedure, the muscle was superfused with warm Ringer solution. At the end of each experiment, blood was collected from the heart for measurement of blood cell counts.

Intravital microscopy

The set-up for intravital microscopy was centred around an Olympus BX 50 upright microscope (Olympus Microscopy, Hamburg, Germany). Light from a 75-W xenon source was narrowed to a near monochromatic beam of a wavelength of 488 nm by a galvanometric scanner (Polychrome II, TILL Photonics, Gräfelfing, Germany) and directed onto the specimen via a FITC filter cube equipped with dichroic and emission filters (DCLP 500, LP515, Olympus Microscopy). Microscopic images were obtained with Olympus water immersion lenses [20x /NA 0.5 and 60x/NA 0.9], recorded with a CCD camera (IMAGO S/N 382KLO345; TILL Photonics GmbH, Gräfelfing, Germany) and subjected to digital image analysis (TILLvisION 4.0; TILL Photonics GmbH, Gräfelfing, Germany).

Experimental protocol

Light/dye-induced thrombosis was performed as described earlier (Rumbaut et al. 2006) with slight modifications (Fig. 14). The light intensity was measured by a photodiode at 488 nm at the exit of the light source daily and maintained to be between 2.65 and 2.75 mA. After surgical preparation either polystyrene nanoparticles at a concentration of 0.5 mg/kg body weight (in a volume of 2.5 µL/g body weight), or DEP or TiO_2 (rutile) at a concentration of 1 mg/kg body weight (in a volume of 5 µL/g body weight), or SWNT at a concentration of 0.01, 0.1 and 1 mg/kg body weight (in a volume of 5 µL/g body weight) or vehicle or physiological saline (control) were injected through the catheter. The nanoparticles were administered 10 minutes prior to induction of thrombosis in order to yield a uniform distribution of the particles in the microcirculation. Thereafter, 4 ml/kg body weight FITC-dextran (2.5%) was given. To verify comparable intravascular FITC concentrations among experimental groups, digital images were taken from one venule and the mean grey fluorescence intensity was measured.

Ten minutes after the application of nanoparticles, photoactivation was induced by exposing a vessel segment of 300 µm length to continuous epi-illumination with a wavelength of 488 nm. An Olympus water immersion lens [60x / NA 0.9] was used to focus the light onto the cremaster and to obtain fluorescent images. Thrombus formation was quantified in one arteriole (25-35 µm) and one venule (30-50 µm) by analysing the

time when platelets became adherent to the vessel wall (onset) and the time required for complete occlusion of the vessel (cessation). The cessation time in vessels without complete occlusion until the end of the recording was considered 20 min for venules and 40 min for arterioles. As a positive control, mice were given 4 mg/kg body weight LPS intraperitoneally 4 hours prior to the induction of thrombosis.

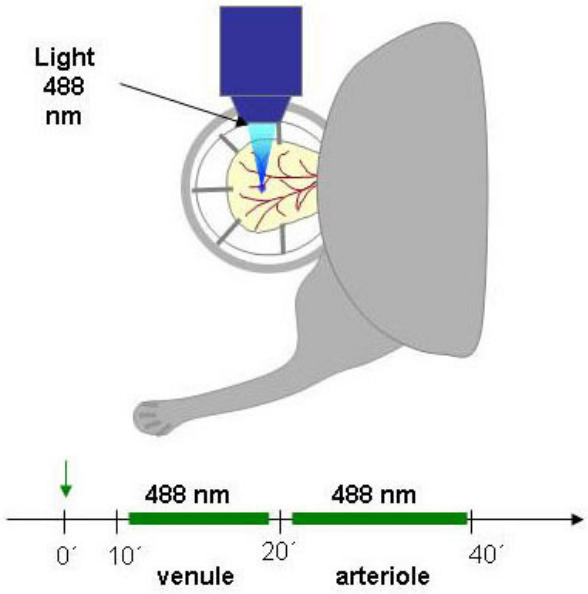

Fig. 14. *Light/dye-induced thrombosis in cremasteric microvessels. The right cremaster muscle was exposed through a ventral incision of the scrotum and spread over the pedestal of a custom-made microscopic stage. Thrombus formation was induced in cremasteric microvessels (25-35 µm) by photoactivation of intravascular FITC-dextran molecules with 488 nm light.*

9. Statistics

Data analysis was performed with a statistical software package (SigmaStat v3.0 for Windows, Jandel Scientific, Erkrath, Germany).

For analysis of the data of the dispersion study, one way ANOVA followed by either the Dunnett (comparison versus control) or the Student-Newman-Keuls (all pairwise comparison) tests were used for the estimation of stochastic probability. The t-test was used to compare two groups.

Transformed flow cytometric data as a function of platelet concentration were fitted by the least squares method. Regression analysis was used to estimate the significance level of correlation coefficients and to judge the zero character of intercepts.

ANOVA followed by Dunnett test (comparison versus control) for *in vivo* data and repeated measures ANOVA followed by Holm-Sidak test for human *in vitro* data was used for the estimation of stochastic probability. For the analysis of the aggregometry data, one-sample t-test was used.

Data are given as mean values and standard error except the methodological studies, where mean values and standard deviation were used. P values < 0.05 were considered significant.

DOI:10.14753/SE.2016.1824

V. Results

1. Physical characterisation of nanoparticles and optimisation of the dispersion method

Nanoparticles tend to form agglomerates in physiological solutions. Thus, for *in vitro* and *in vivo* studies where nanoparticles are in contact with physiological solutions, a new dispersion method for preparation of nanoparticles was necessary. To optimise the dispersion method, the effect of different factors on the agglomeration state of TiO_2 (rutile) nanoparticles was tested. Thereafter, using the optimal technique, other nanoparticles were prepared and physically characterised.

a) Measurement of polystyrene beads

First, the accuracy of size distribution and zeta potential measurements was verified by measuring 60–65-nm polystyrene beads with different surface charges in distilled water and also in PBS. The size measurements demonstrated almost identical results to those reported by the manufacturer. Amine-modified particles had positive while carboxyl and unmodified particles negative zeta potential (Tab. 4).

Table 4. *Size and zeta potential data of polystyrene beads. Polystyrene bead dispersions were prepared in distilled water (DI H_2O) or in PBS at a concentration of 0.02 mg/ml without sonication. The measurements were made in triplicate. The average value (bold text) and the standard deviation (normal text) of the measurements are shown. (Bihari et al. 2008b)*

Particle	Average Diameter (nm)	PdI	Zeta-Potential (mV)	Electrophoretic Mobility (µmcm/Vs)	Conductivity (mS/cm)
Plain polystyrene beads (60 nm)					
DI H_2O	**67**	**0.030**	**-57.0**	**-4.466**	**0.009**
	0.4	0.004	5.3	0.412	0.010
PBS	**73**	**0.135**	**-24.8**	**-1.947**	**18.267**
	7	0.068	5.7	0.446	0.289

DOI:10.14753/SE.2016.1824

Particle	Average Diameter (nm)	PdI	Zeta-Potential (mV)	Electrophoretic Mobility (µmcm/Vs)	Conductivity (mS/cm)
Carboxyl-modified polystyrene beads (60 nm)					
DI H_2O	**60**	**0.046**	**-56.7**	**-4.443**	**0.003**
	0.3	0.021	0.3	0.021	0.000
PBS	**58**	**0.057**	**-32.5**	**-2.550**	**17.833**
	0.9	0.018	2.5	0.193	0.208
Amine-modified polystyrene beads (65 nm)					
DI H_2O	**68**	**0.062**	**59.7**	**4.676**	**0.006**
	0.5	0.035	4.9	0.379	0.002
PBS	**86**	**0.204**	**19.0**	**1.493**	**18.100**
	8	0.029	3.4	0.268	0.100

b) Ultrasound energy

The effects of different ultrasound energies were tested on TiO_2 (rutile) suspensions in distilled water. A specific ultrasound energy of 4.2×10^5 kJ/m^3 (power consumption: 7 W, 1 ml dispersion, 60 sec sonication) was sufficient to disaggregate TiO_2 (rutile) nanoparticles as indicated by the reduction of the particle diameter from 527.6 ± 34.2 to 159.7 ± 2.3 nm (Fig. 1) and of the PdI from 0.434 ± 0.086 to 0.166 ± 0.015 (data not shown). However, higher energy input did not further improve size reduction (Fig. 15).

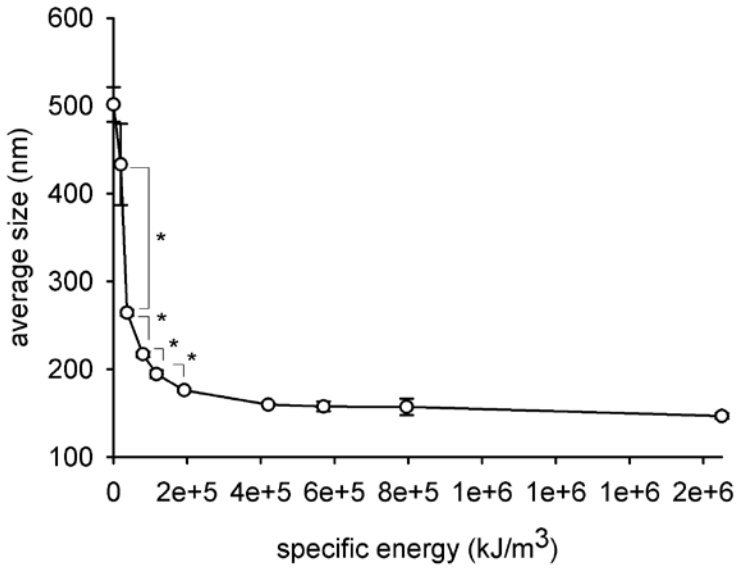

Fig. 15. *Effect of intensity of sonication on TiO_2 (rutile) particle size.* *TiO_2 (rutile) dispersed in distilled water at a concentration of 0.02 mg/ml was sonicated with different specific energies, and the average of the hydrodynamic diameter of the particles was measured. The experiments were carried out in triplicate (*, $p < 0.05$). (Bihari et al. 2008b)*

c) Sequence of preparation steps

Various sequences of preparation steps of particle dispersions were assessed on TiO_2 (rutile) (Fig. 16). The average diameter and PdI of TiO_2 (rutile) in PBS without sonication was 912 ± 48 nm and 0.509 ± 0.017, respectively. Addition of HSA or Tween 80 to the TiO_2 (rutile) dispersion without previous sonication did not reduce the particle diameter in PBS. However, the TiO_2 (rutile) particle diameter was reduced in PBS when HSA or Tween 80 was added to the dispersion after sonication. In the case of HSA, the diameter of TiO_2 (rutile) particles was further reduced when the stabilizer was added prior to the addition of PBS. Best results were obtained with HSA as dispersion stabilizer when we first sonicated the TiO_2 (rutile) nanoparticles in distilled water, then added the dispersion stabilizer, and at the end added buffered salt solution to the dispersion (average diameter = 186.4 ± 9.9 nm, PdI = 0.212 ± 0.03). In this case, the addition of HSA prior to the addition of PBS prevented the TiO_2 (rutile) particles from reagglomeration (Fig. 17). Interestingly, the diameter of TiO_2 (rutile) particles was slightly but significantly elevated after HSA addition (from 159.7 ± 2.3 to 174.2 ± 2.2,

Fig. 3). This dispersion protocol also worked well when RPMI 1640 cell culture medium was used as a dispersion medium. Similar results were obtained using BSA, MSA, or mouse serum as dispersion stabilizers (Fig. 18).

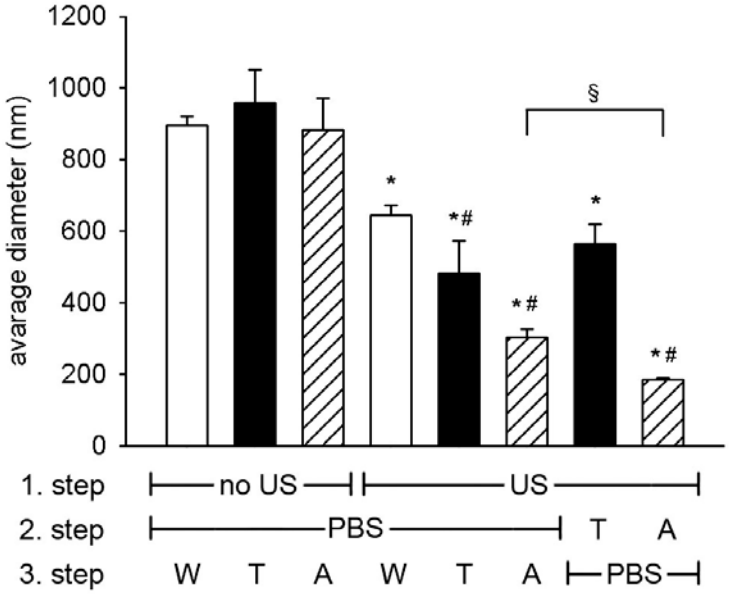

Fig. 16. *Role of the sequence of preparation steps.* *TiO_2 (rutile) dispersed in distilled water at a concentration of 0.02 mg/ml was sonicated with 4.2 × 10^5 kJ/m^3 specific energy (US) or not sonicated (no US). Tween 80 0.1% (T), HSA 1.5 mg/ml (A) or distilled water (W) was given to the dispersion before or after the addition of concentrated PBS. The average hydrodynamic diameter of the particles was measured (n = 4; *, p < 0.05 vs. dispersion in distilled water (W) without sonication (no US), #, p < 0.05 vs. dispersion in distilled water (W) with sonication (US), § p < 0.05). Slightly modified after Bihari et al. (Bihari et al. 2008b)*

DOI:10.14753/SE.2016.1824

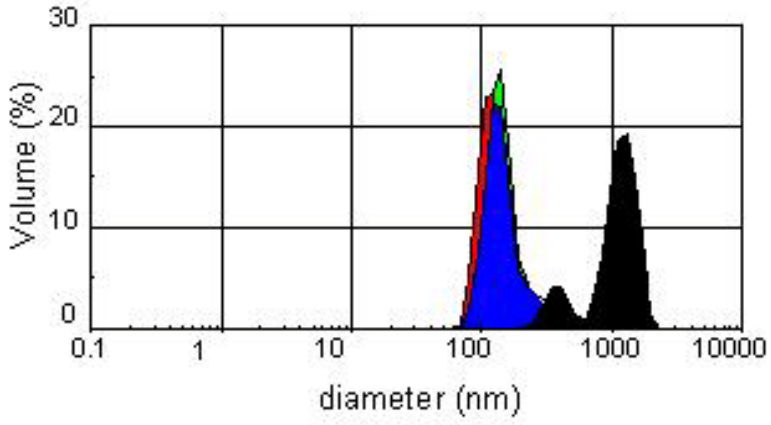

Fig. 17. *Size distribution by volume of a TiO_2 (rutile) dispersion measured after each preparation step.* ***TiO_2*** *(rutile) was dispersed in distilled water and sonicated (red), then HSA (blue) and finally concentrated PBS (green) was given to the dispersion. TiO_2 (rutile) was also prepared in the same way but without HSA (black). (Bihari et al. 2008b)*

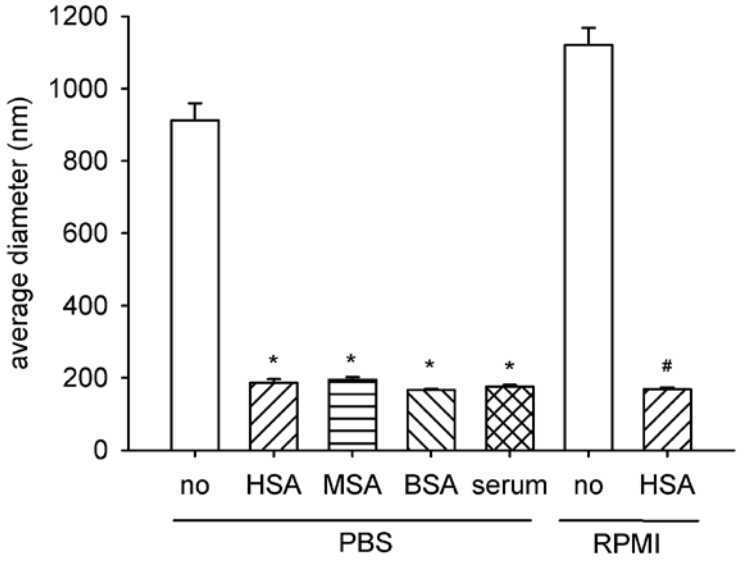

Fig. 18. *Albumin from different species and serum as dispersion stabilizer.* ***TiO_2*** *(rutile) dispersed in distilled water at a concentration of 0.02 mg/ml was sonicated, and HSA, MSA, BSA or mouse serum was given to the dispersion before the addition of concentrated PBS. The average hydrodynamic diameter of the particles was measured. The experiments were carried out in triplicate (*, $p < 0.05$ vs. dispersion without albumin in PBS; #, $p < 0.05$ vs. dispersion without albumin or serum in RPMI). (Bihari et al. 2008b)*

DOI:10.14753/SE.2016.1824

d) Albumin and nanoparticle concentration

To optimize the HSA concentration for stabilization of dispersions, we prepared dispersions with different HSA or TiO_2 (rutile) concentrations. When changing HSA concentration at a constant (0.02 mg/ml) TiO_2 (rutile) concentration, we found that an HSA concentration between 0.015 mg/ml and 15 mg/ml prevented the formation of coarse TiO_2 (rutile) agglomerates. However, at 0.0015 mg/ml HSA concentration, the average diameter and the PdI value of TiO_2 (rutile) were increased (Fig. 19, 20). At an HSA concentration of 15 mg/ml, the average diameter of TiO_2 (rutile) particles was slightly decreased. This decrease is not the result of a real change in the TiO_2 (rutile) particle size, but the consequence of the presence of particles with a diameter of 7.1 ± 0.1 nm (data not shown) in the dispersion. The presence of these particles, corresponding to free HSA molecules, causes a shift in the average diameter. The presence of the two types of particles with different diameters (TiO_2 (rutile) and free HSA molecules) in the dispersion is also reflected in the strong increase of the PdI.

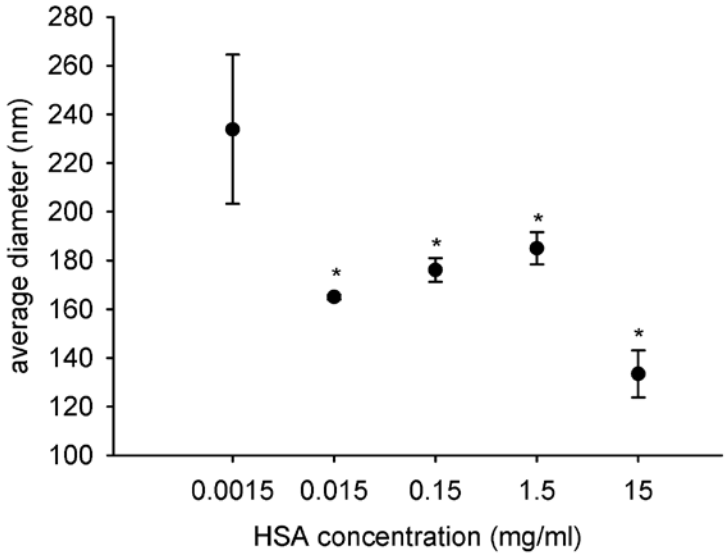

Fig. 19. *TiO_2 (rutile) particle size in dispersions with different HSA concentrations.* *TiO_2 (rutile) dispersed in distilled water at a concentration of 0.02 mg/ml was sonicated and HSA at concentrations ranging from 0.0015 to 15 mg/ml was given to the dispersion prior to addition of concentrated PBS. The average hydrodynamic diameter of the particles was measured. The experiments were carried out in triplicate (*, $p < 0.05$ vs. dispersion with 0.0015 mg/ml HSA). (Bihari et al. 2008b)*

DOI:10.14753/SE.2016.1824

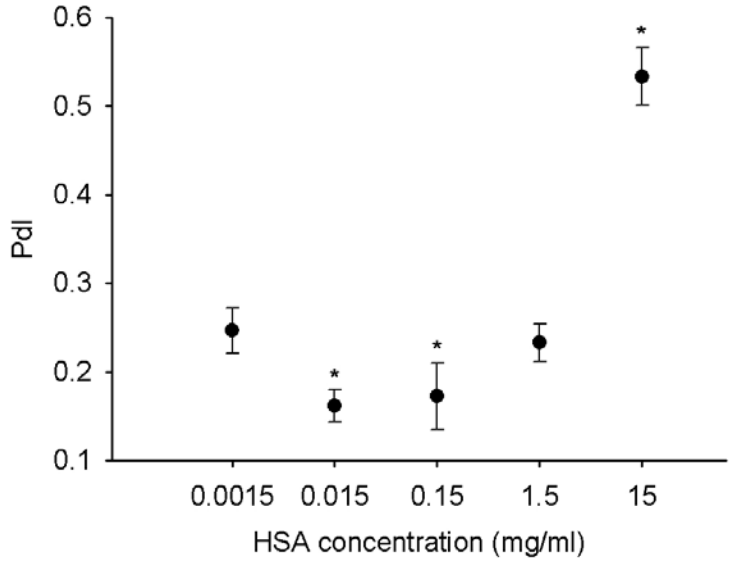

Fig. 20. *Polydispersity index of TiO_2 (rutile) in dispersions with different HSA concentrations.* ***.*** *TiO_2 (rutile) dispersed in distilled water at a concentration of 0.02 mg/ml was sonicated and HSA at concentrations ranging from 0.0015 to 15 mg/ml were given to the dispersion prior to addition of concentrated PBS. Polydispersity index (PdI) of the particles was measured. The experiments were carried out in triplicate (*, $p < 0.05$ vs. dispersion with 0.0015 mg/ml HSA). (Bihari et al. 2008b)*

Next, we prepared dispersions with different TiO_2 (rutile) concentrations, but the same HSA (1.5 mg/ml) concentration. We found that HSA prevented the formation of coarse agglomerates at TiO_2 (rutile) concentrations ranging from 0.002 to 0.2 mg/ml. As in the case of the highest HSA concentration, at the lowest TiO_2 (rutile) concentration the presence of particles of about 7 nm caused a shift in the average diameter. At a TiO_2 (rutile) concentration of 2 mg/ml, the average diameter and the PdI value were increased. However, this increase in particle size could be avoided by increasing the amount of HSA by 10 times in the dispersion (Fig. 21, 22).

DOI:10.14753/SE.2016.1824

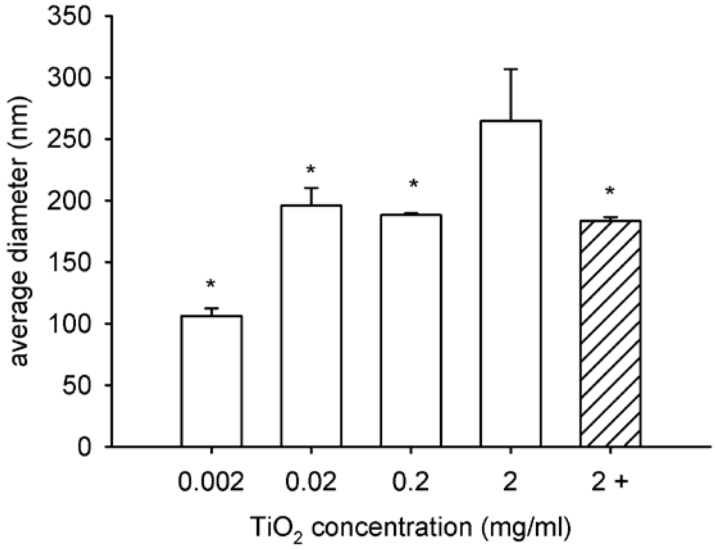

Fig. 21. *TiO_2 (rutile) particle size in dispersions at different TiO_2 concentrations.* ***TiO_2*** *(rutile) dispersed in distilled water at concentrations ranging from 0.002 to 2 mg/ml was sonicated and before concentrated PBS 1.5 mg/ml HSA was added to the dispersion. TiO_2 (rutile) dispersions at a concentration of 2 mg/ml were also prepared in the same way but with the addition of 10 times more (15 mg/ml) HSA (hatched bar). The average hydrodynamic diameter of the particles was measured. The experiments were carried out in triplicate (*, $p < 0.05$ vs. dispersion with 2 mg/ml TiO_2 (rutile)). (Bihari et al. 2008b)*

DOI:10.14753/SE.2016.1824

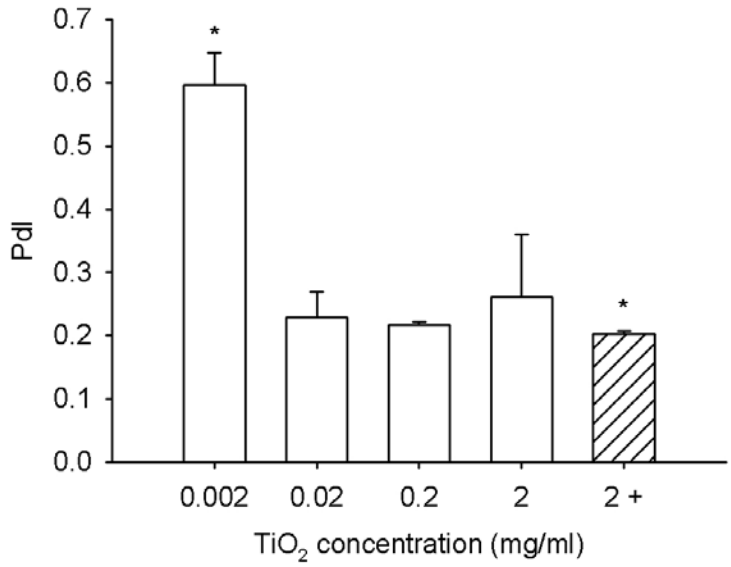

Fig. 22. *Polydispersity index of TiO_2 (rutile) dispersions with different TiO_2 concentrations.* ***TiO_2*** *(rutile) dispersed in distilled water at concentrations ranging from 0.002 to 2 mg/ml was sonicated and before concentrated PBS 1.5 mg/ml HSA was added to the dispersion. TiO_2 (rutile) dispersions at a concentration of 2 mg/ml were also prepared in the same way but with addition of 10 times more (15 mg/ml) HSA (hatched bar). The polydispersity index (PdI) of the particles was measured. The experiments were carried out in triplicate (*, $p < 0.05$ vs. dispersion with 2 mg/ml TiO_2 (rutile)). (Bihari et al. 2008b)*

e) Stability

The stability of the TiO_2 (rutile) dispersions prepared with 1.5 mg/ml HSA was determined over a time period of one week (Fig. 23). During this period, the TiO_2 (rutile) PBS dispersions prepared with HSA remained stable without coarse agglomerates, whereas in dispersions without HSA the average diameter and the PdI values continuously increased, approaching a plateau at 24 hours.

DOI:10.14753/SE.2016.1824

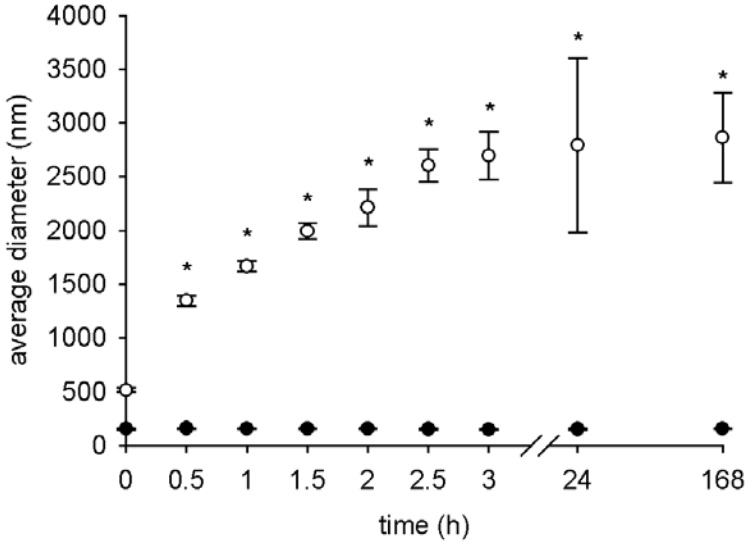

Fig. 23. *Stability of TiO_2 (rutile) dispersions. TiO_2 (rutile) dispersions were prepared in distilled water at a concentration of 0.02 mg/ml with (closed circles) or without (open circles) addition of HSA, before giving concentrated PBS to the dispersion. The average hydrodynamic diameter of the particles was measured at different time points for up to one week. The experiments were carried out in triplicate (*, $p < 0.05$, dispersions with vs. without HSA at the same time point). (Bihari et al. 2008b)*

f) Different types of nanoparticles

To test the applicability of our optimised method for other nanoparticles and to physically characterise these nanoparticle dispersions, we prepared and measured TiO_2 (anatase), ZnO, SWNT, MWNT, Silver, SiO_x, and nanosized DEP using HSA, Tween 80, or mouse serum as dispersion stabilizers (Tab. 5). In all dispersions, the average diameter of the particles was greater then the size of the primary particles given by the manufacturer, indicating the presence of some agglomerates. For all nanoparticles tested, the addition of HSA, Tween 80, or mouse serum resulted in a decreased average diameter. With HSA as dispersion stabilizer, the average diameter of TiO_2 (rutile), ZnO, SWNT, MWNT, Silver, SiO_x, and DEP was below 290 nm. For TiO_2 (anatase) particles, our method was less effective as indicated by a higher average diameter of the particles. In dispersions of SWNT, MWNT, and SiO_x nanoparticles, the PdI value was rather high.

Table 5. *Size and zeta potential data of different types of nanoparticles. Nanoparticles were prepared in distilled water at a concentration of 0.02 mg/ml with (DI H_2O) or without (DI H_2O no US) sonication. For other measurements, nanoparticles were prepared in distilled water at a concentration of 0.02 mg/ml by sonication and addition of human serum albumin (PBS, HSA), Tween 80 (PBS, Tween), mouse serum (PBS, mserum) or distilled water (PBS) previous to addition of PBS. The measurements were made in triplicate. The average value (bold text) and the standard deviation (normal text) of the measurements are shown. (Bihari et al. 2008b)*

Particle	Average Diameter (nm)	PdI	Zeta-Potential (mV)	Electrophoretic Mobility (µmcm/Vs)	Conductivity (mS/cm)
TiO_2 (rutile) (~10 nm × 40 nm)					
DI H_2O no US	**502**	**0.434**	**-44.2**	**-3.465**	**0.003**
	34	0.086	0.3	0.018	0.000
DI H_2O	**160**	**0.166**	**-40.9**	**-3.210**	**0.005**
	2	0.015	3.0	0.238	0.002
PBS	**641**	**0.263**	**-19.5**	**-1.531**	**18.200**
	69	0.022	6.3	0.493	0.265
PBS, HSA	**186**	**0.212**	**-8.8**	**-0.687**	**17.500**
	10	0.030	0.9	0.067	0.436
PBS, Tween	**578**	**0.248**	**-13.3**	**-1.041**	**17.900**
	132	0.017	4.4	0.347	0.173
PBS, mserum	**175**	**0.270**	**-10.7**	**-0.836**	**18.100**
	5	0.046	1.5	0.115	0.656
DEP - SRM 2975 (mean diameter by volume distribution: 31.9 ± 0.6 µm)					
DI H_2O no US	**347**	**0.397**	**-45.2**	**-3.543**	**0.004**
	21	0.047	2.7	0.215	0.001
DI H_2O	**144**	**0.132**	**-48.4**	**-3.791**	**0.011**
	1	0.009	1.7	0.129	0.010
PBS	**684**	**0.249**	**-32.0**	**-2.511**	**18.233**
	284	0.064	2.8	0.224	0.351
PBS, HSA	**163**	**0.152**	**-9.6**	**-0.750**	**17.967**
	3	0.008	0.6	0.043	0.321
PBS, Tween	**151**	**0.143**	**-7.0**	**-0.551**	**17.333**
	1	0.012	0.2	0.015	0.289
PBS, mserum	**168**	**0.209**	**-9.2**	**-0.722**	**18.233**
	13	0.033	1.4	0.111	0.289
Silver (30-50 nm)					
DI H_2O no US	**403**	**0.455**	**-20.1**	**-1.580**	**0.012**
	125	0.039	3.9	0.308	0.009
DI H_2O	**161**	**0.338**	**-29.8**	**-2.337**	**0.003**

DOI:10.14753/SE.2016.1824

Particle	Average Diameter (nm)	PdI	Zeta-Potential (mV)	Electrophoretic Mobility (µmcm/Vs)	Conductivity (mS/cm)
	12	0.055	0.3	0.026	0.002
PBS	**223**	**0.343**	**-24.5**	**-1.919**	**17.933**
	8	0.026	3.1	0.243	0.961
PBS, HSA	**172**	**0.343**	**-11.3**	**-0.889**	**18.167**
	22	0.018	0.3	0.020	0.153
PBS, Tween	**194**	**0.368**	**-9.8**	**-0.765**	**17.267**
	23	0.014	1.9	0.145	0.252
PBS, mserum	**158**	**0.305**	**-11.0**	**-0.863**	**18.333**
	5	0.063	0.6	0.045	0.289
TiO_2 (anatase) (<25 nm)					
DI H_2O no US	**1169**	**0.462**	**13.8**	**1.084**	**0.011**
	48	0.020	2.1	0.162	0.011
DI H_2O	**517**	**0.431**	**-18.7**	**-1.467**	**0.012**
	60	0.055	0.4	0.035	0.012
PBS	**890**	**0.369**	**-23.0**	**-1.805**	**17.700**
	230	0.077	1.7	0.132	0.458
PBS, HSA	**521**	**0.475**	**-9.6**	**-0.749**	**18.733**
	25	0.023	1.1	0.088	0.709
PBS, Tween	**818**	**0.358**	**-14.0**	**-1.096**	**17.633**
	11	0.029	2.5	0.200	0.513
PBS, mserum	**574**	**0.474**	**-10.7**	**-0.841**	**18.300**
	92	0.111	1.1	0.090	0.964
ZnO (<100 nm)					
DI H_2O no US	**1298**	**0.721**	**10.6**	**0.832**	**0.008**
	252	0.072	2.0	0.157	0.001
DI H_2O	**278**	**0.414**	**-29.4**	**-2.301**	**0.015**
	72	0.086	6.0	0.475	0.004
PBS	**517**	**0.445**	**-29.3**	**-2.294**	**17.967**
	174	0.053	2.8	0.219	0.462
PBS, HSA	**267**	**0.288**	**-11.6**	**-0.907**	**18.300**
	6	0.059	0.6	0.045	0.500
PBS, Tween	**457**	**0.360**	**-14.6**	**-1.148**	**18.000**
	135	0.041	7.3	0.570	0.265
PBS, mserum	**190**	**0.544**	**-7.7**	**-0.603**	**18.033**
	8	0.103	1.1	0.090	0.231
SiO_x (15nm)					
DI H_2O no US	**1121**	**0.593**	**-33.4**	**-2.616**	**0.021**
	304	0.014	1.8	0.136	0.010
DI H_2O	**370**	**0.488**	**-21.1**	**-1.655**	**0.004**
	49	0.047	19.8	1.551	0.005
PBS	**852**	**0.617**	**-14.5**	**-1.135**	**17.867**
	267	0.025	0.2	0.015	0.058

DOI:10.14753/SE.2016.1824

Particle	Average Diameter (nm)	PdI	Zeta-Potential (mV)	Electrophoretic Mobility (µmcm/Vs)	Conductivity (mS/cm)
PBS, HSA	**251**	**0.880**	**-10.4**	**-0.815**	**18.533**
	27	0.107	0.7	0.052	0.153
PBS, Tween	**398**	**0.532**	**-3.7**	**-0.288**	**17.900**
	51	0.040	0.4	0.029	0.200
PBS, mserum	**132**	**0.497**	**-11.1**	**-0.868**	**19.100**
	49	0.192	0.6	0.044	0.265
SWNT (outer diameter: <2nm, length: 1-5µm)					
DI H_2O no US	**689**	**0.569**	**-7.0**	**-0.550**	**0.010**
	111	0.100	7.6	0.595	0.009
DI H_2O	**372**	**0.560**	**-23.1**	**-1.814**	**0.004**
	59	0.076	10.4	0.813	0.001
PBS	**977**	**0.526**	**-2.6**	**-0.203**	**11.533**
	46	0.131	2.3	0.178	9.989
PBS, HSA	**285**	**0.605**	**-10.1**	**-0.790**	**17.600**
	79	0.143	0.7	0.054	0.400
PBS, Tween	**291**	**0.531**	**-8.5**	**-0.667**	**16.933**
	89	0.103	3.3	0.259	1.124
PBS, mserum	**115**	**0.666**	**-7.7**	**-0.602**	**18.433**
	51	0.132	1.6	0.126	1.168
MWNT (outer diameter: 10-30 nm, lengths: 1-2µm)					
DI H_2O no US	**309**	**0.304**	**-2.7**	**-0.215**	**0.007**
	48	0.027	2.2	0.175	0.005
DI H_2O	**262**	**0.397**	**-22.5**	**-1.765**	**0.004**
	101	0.048	19.2	1.502	0.003
PBS	**486**	**0.424**	**-19.6**	**-1.535**	**18.000**
	173	0.079	5.8	0.458	0.608
PBS, HSA	**269**	**0.406**	**-9.7**	**-0.760**	**19.733**
	56	0.027	1.1	0.087	2.136
PBS, Tween	**206**	**0.292**	**-4.8**	**-0.375**	**17.733**
	13	0.037	0.5	0.039	0.208
PBS, mserum	**166**	**0.415**	**-7.8**	**-0.610**	**18.233**
	10	0.006	0.4	0.029	0.666
TiO_2 (rutile, NA) (30-40 nm)					
DI H_2O no US	**1702**	**0.351**	**-34.5**	**-2.708**	**0.016**
	372	0.290	3.8	0.300	0.013
DI H_2O	**418**	**0.306**	**-29.5**	**-2.312**	**0.016**
	2	0.008	3.0	0.235	0.008
PBS	**617**	**0.305**	**-20.6**	**-1.615**	**16.800**
	99	0.037	1.0	0.076	0.200
PBS, HSA	**414**	**0.319**	**-11.5**	**-0.899**	**17.667**
	17	0.038	1.5	0.117	0.473
PBS, Tween	**663**	**0.291**	**-12.1**	**-0.946**	**17.933**

Particle	Average Diameter (nm)	PdI	Zeta-Potential (mV)	Electrophoretic Mobility (µmcm/Vs)	Conductivity (mS/cm)
	123	0.016	4.4	0.343	0.351
PBS, mserum	**548**	**0.358**	**-10.7**	**-0.842**	**18.433**
	78	0.092	1.3	0.099	0.231

g) Zeta potential

All particles had a negative zeta potential in distilled water after sonication (Table 5). Interestingly, ZnO, and TiO_2 (anatase) had a positive zeta potential upon dispersion in distilled water and became negative after sonication. The particles were less negative when prepared with HSA, Tween 80, or serum in PBS. TiO_2 (rutile) prepared with HSA in RPMI cell culture medium had a positive zeta potential (data not shown).

h) Transmission electron microscopy

To visualize nanoparticles in dispersions, we used transmission electron microscopy. Similarly to the dynamic light scattering measurements, transmission electron microscope images showed smaller nanoparticle agglomerates in dispersions prepared with HSA or mouse serum as stabilizers (Fig. 24, 25, 26). In the case of TiO_2 (rutile) dispersions prepared with HSA, we determined the particle size with an image analysing software. The mean particle size was 134 ± 71 nm.

DOI:10.14753/SE.2016.1824

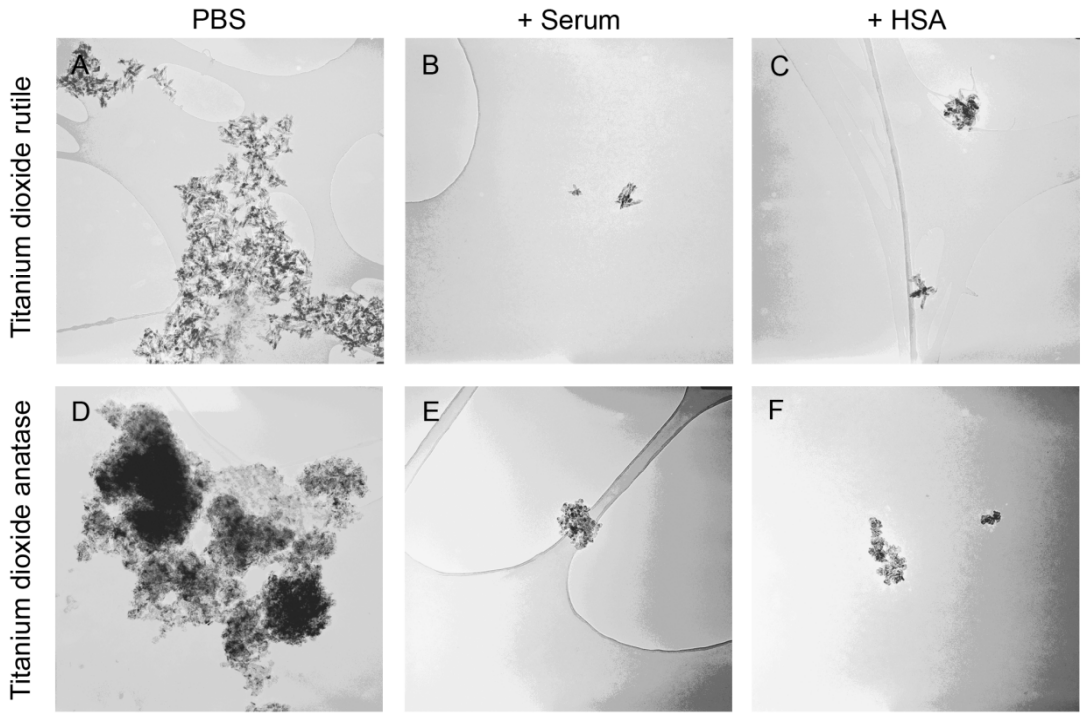

Fig. 24. *Electron microscopy of titanium dioxide (rutile and anatase) nanoparticles. Magnification: 100,000 (950 × 950 nm) Nanoparticle dispersions were prepared in distilled water at a concentration of 0.02 mg/ml without stabilizer (PBS) or with the addition of human serum albumin (+HSA) or mouse serum (+Serum) before giving concentrated PBS to the dispersion. (Bihari et al. 2008b)*

DOI:10.14753/SE.2016.1824

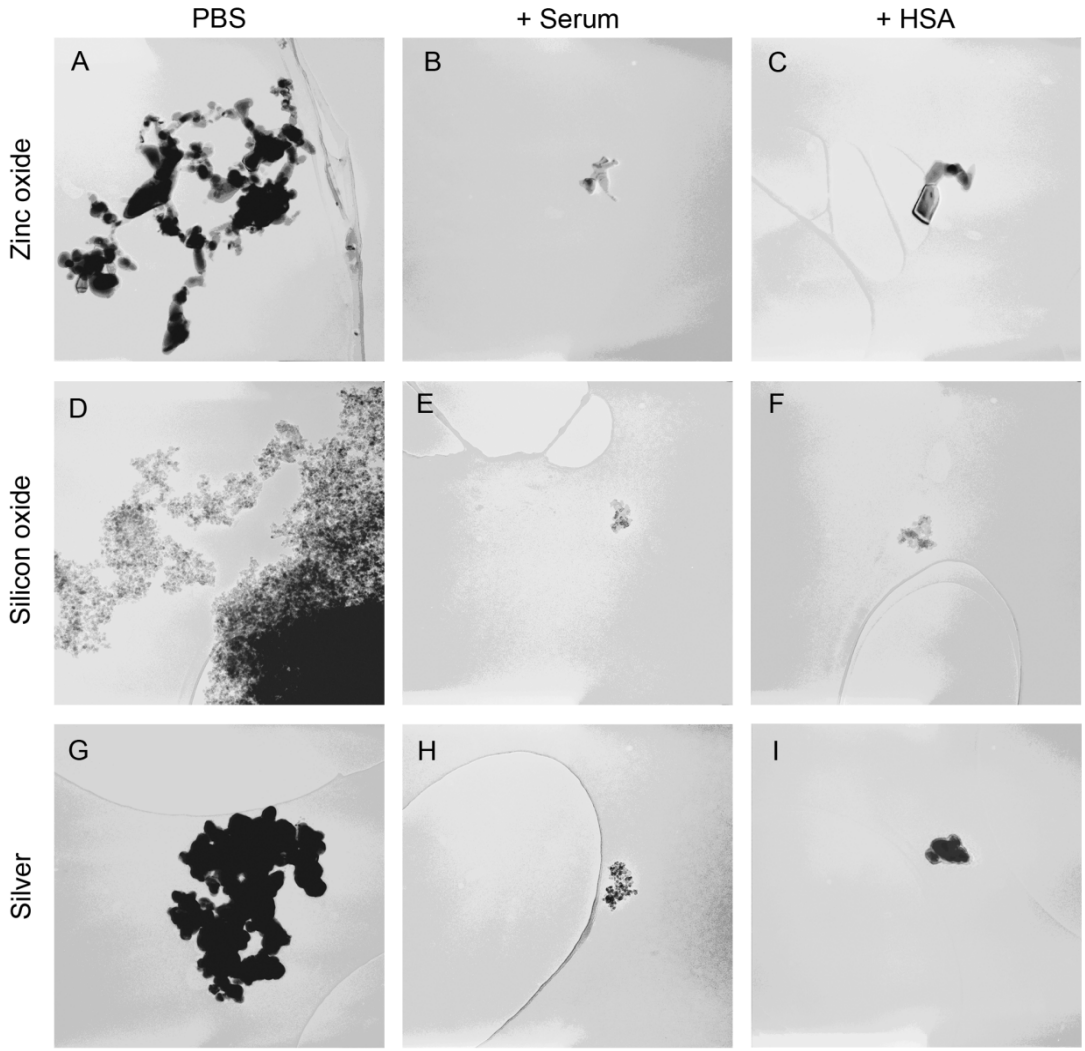

Fig. 25. *Electron microscopy of zinc oxide, silicon oxide, and silver nanoparticles. Magnification: 100,000 (950 × 950 nm) ZnO, SiO_x and silver nanoparticle dispersions were prepared in distilled water at a concentration of 0.02 mg/ml without stabilizer (PBS) or with the addition of human serum albumin (+HSA) or mouse serum (+Serum) before giving concentrated PBS to the dispersion. (Bihari et al. 2008b)*

DOI:10.14753/SE.2016.1824

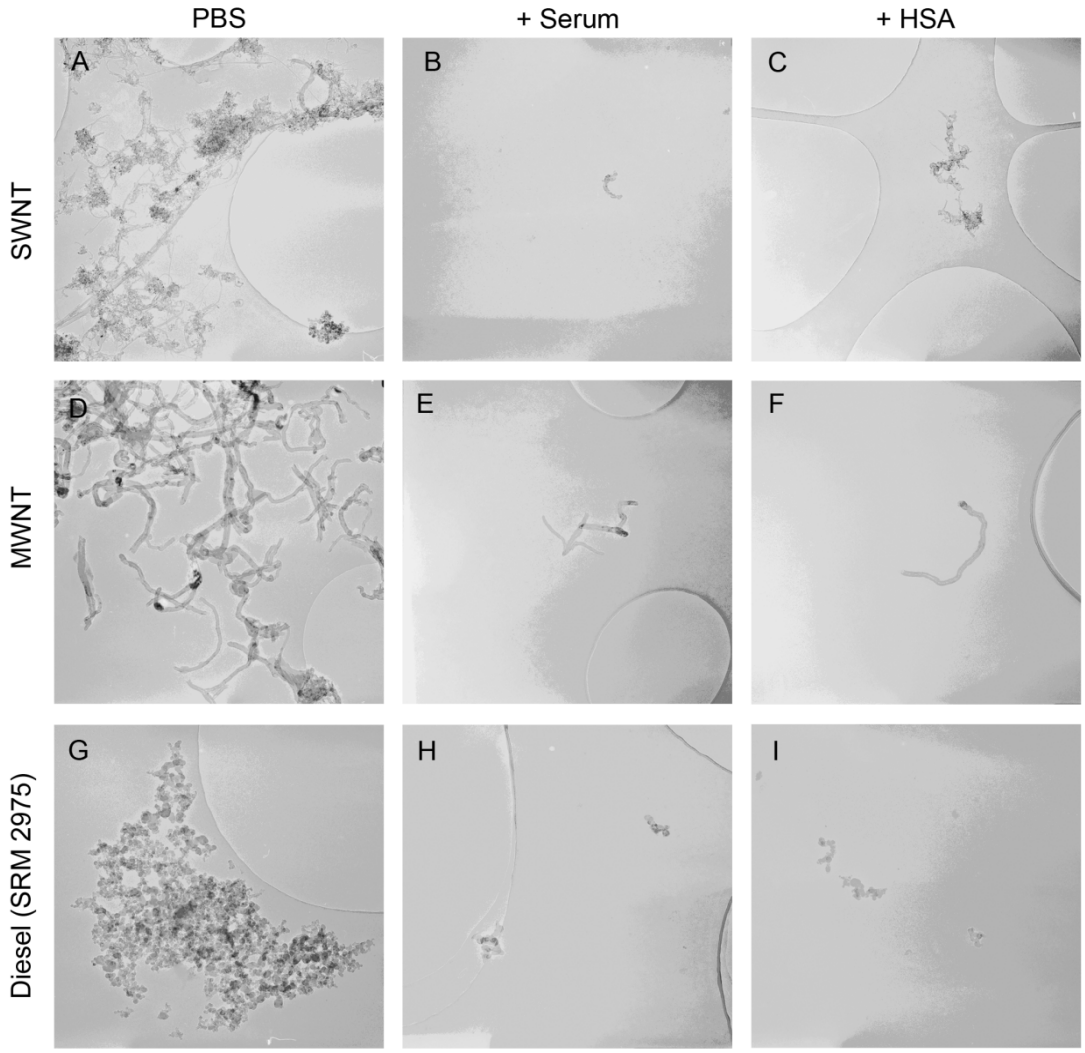

Fig. 26. *Electron microscopy of nanotubes and diesel exhaust particles**.** Magnification: 100,000 (950 × 950 nm) SWNT, MWNT and diesel exhaust particle (SRM 2975) dispersions were prepared in distilled water at a concentration of 0.02 mg/ml without stabilizer (PBS) or with the addition of mouse serum (+serum) or human serum albumin (+HSA) before giving concentrated PBS to the dispersion. (Bihari et al. 2008b)*

DOI:10.14753/SE.2016.1824

2. Optimisation of platelet-granulocyte complex measurement

a) Flow cytometric analysis of platelet-granulocyte coincidence

To model platelet-granulocyte coincidence experimentally, the mixture of two non-interacting fluorescent beads was measured at various dilutions. FITC-labelled beads with fluorescent signals for the FL1 detector of the flow cytometer were given at a higher concentration representing platelets and Starfire Red™-labelled beads with fluorescent signals for the FL3 detector were given at a lower concentration representing leukocytes. Fig. 27 shows the average percentage of FL1 and FL3 double positivity among the FL3 positive events as a function of dilution. The value of double positivity (mean ± SD) changes between 37.3 ± 1.3% and 2.1 ± 0.2% with the sample dilution in the range of 10–320 fold. This means that coincidence occurs often at low dilutions and that the rate of coincidence decreases exponentially with increasing dilution.

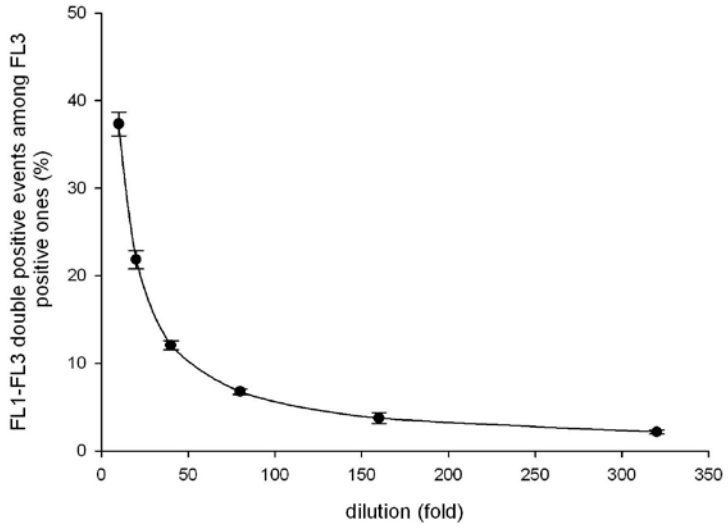

Fig. 27. *Percentage of average double positivity ± standard deviation (n = 4) measured in the mixture of FITC (FL1) and Starfire Red (FL3) labelled non-interacting fluorescent beads as a function of sample dilution. Data collection was triggered by FL3 signal. (Bihari et al. 2008a)*

DOI:10.14753/SE.2016.1824

To further analyse coincidence, data were transformed according to Eq. (10) (see section IV/6/b)

(10) $$Y = \ln\left(1 - D/100\right),$$

where D means the percentage of platelet marker-positive events in the granulocyte gate. As described in the Methods section, this transformation should result in a straight line. The intercept contains information on the amount of dilution-resistant stable complexes and the negative slope of the straight line equals the detection volume. Fig. 28 shows the transformed data as a function of FITC (FL1) labelled bead concentration. Data of each dilution series transformed according to Eq. (10) result in straight lines as well ($r^2 > 0.999$, $p < 0.001$). None of the intercepts of these straight lines differ from zero at 95% confidence level as judged by regression analysis. The average detection volume (mean ± SD) calculated from the slopes of the individual straight lines is 20.4 ± 1.0 pl.

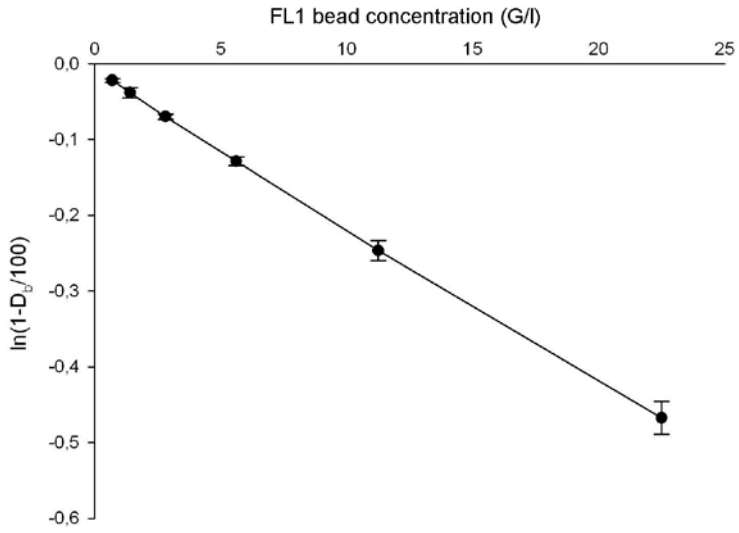

Fig. 28. *Data of Fig. 27 transformed according to Eq. (10) (n = 4) as a function of FITC (FL1) labelled bead concentration. (Bihari et al. 2008a)*

After modelling coincidence by fluorescent beads, the coincidence of platelets and leukocytes was studied in EDTA-anticoagulated blood. EDTA is known to inhibit formation of platelet-granulocyte complexes (Hamburger and McEver 1990), thus

double positivity should originate only from coinciding platelets (labelled with CD41-FITC) and granulocyte (labelled with CD15-PC5).

When EDTA-anticoagulated blood of our healthy donors (platelet concentration: 254 ± 36 G/l) was diluted 6.7–320 fold, the percentage of CD15/CD41 double-positive events among the CD15+ events exhibited a similar concentration dependence as that of the bead mixture (Fig. 29).

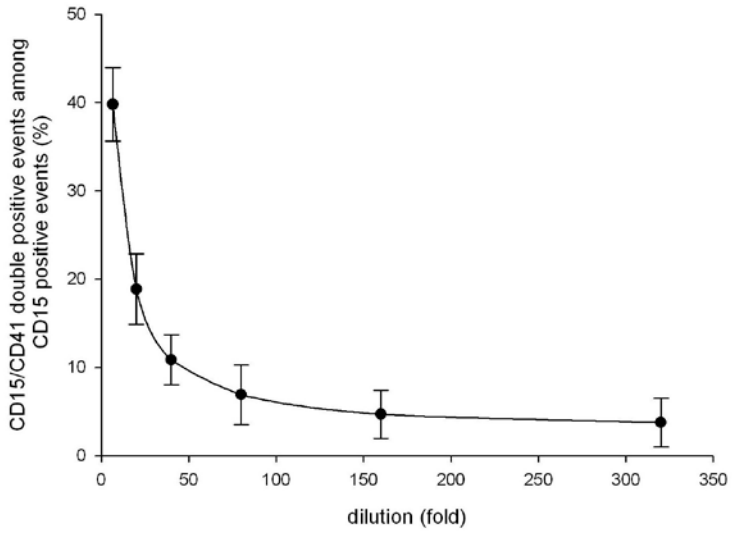

Fig. 29. *Average percentage with standard deviation of CD41/CD15 double positivity among CD15 positive events as a function of dilution (n = 7) for EDTA anticoagulated blood samples. Data collection was triggered by FL3 (CD15) signal. (Bihari et al. 2008a)*

In Fig. 30 the natural logarithm of ratios of CD41 negative events in the granulocyte gate is plotted as a function of platelet concentration for the EDTA anticoagulated blood samples of our donors (cf. Eq. (10)). All seven data sets can be fitted with straight lines ($p < 0.001$; the minimum of r^2 is 0.996). From the slopes of these lines the average detection volume for the EDTA anticoagulated blood in the dilution range tested is 13.5 ± 1.6 pl. The intercepts of these straight lines do not deviate significantly from zero at $p < 0.01$ significance level for four of our donors as judged by regression analysis. However, it is noteworthy that three of our donors exhibited a non-zero intercept, which indicates the presence of 5.7 ± 0.7 % of stable complexes (cf. Eq. (8)).

DOI:10.14753/SE.2016.1824

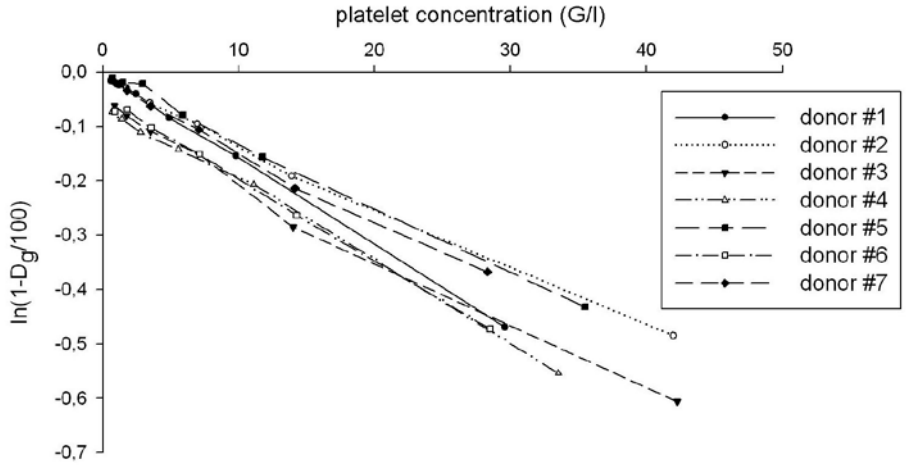

Fig. 30. *Individual data of CD41/CD15 double positivity measured in EDTA anticoagulated blood samples of our seven donors transformed according to Eq. (10) as a function of platelet concentration. (Bihari et al. 2008a)*

In the next set of experiments, paraformaldehyde-treated citrated blood samples were studied, in which also real platelet-granulocyte complexes exist. To be able to distinguish between double positivity originating from real platelet-granulocyte complexes and from coincidence, two different stainings were applied for each blood sample. To measure all double-positive events, platelets (CD41 FITC) and leukocytes (CD15 PC5) were stained. To measure coincidence, platelets (CD41 FITC) were stained and instead of staining leukocytes, FL3 fluorescent beads were given to blood. Fig. 31 shows a representative data set of donor #2 at various dilutions. CD 41 positivity measured as a function of dilution exhibits similar concentration dependencies whether data collection is triggered by fluorescent beads (open circles) or fluorescent-labelled granulocytes (solid squares). CD 41 positivity is always higher when data collection is triggered by granulocytes than in the case of beads. Data of Fig. 31 after transformation according to Eq. (10) result in two straight lines (Fig. 32): one having a practically zero intercept (beads in the sample, which do not interact with platelets), the other having a non-zero intercept indicating the presence of dilution independent stable complexes.

DOI:10.14753/SE.2016.1824

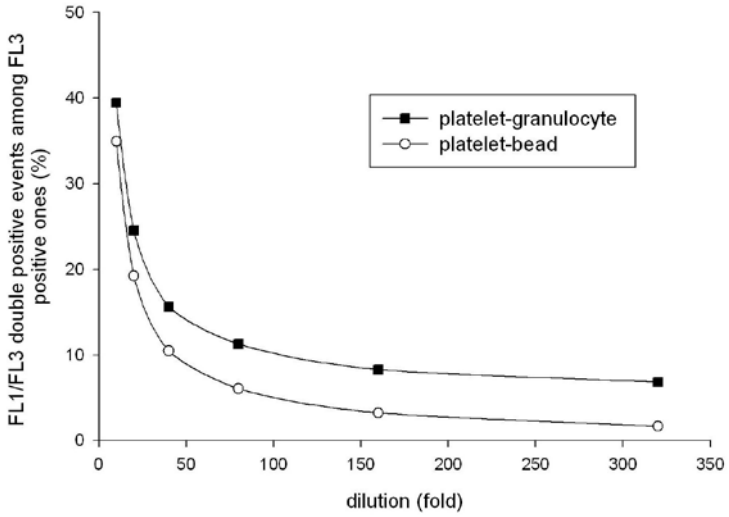

Fig. 31. *Percentage of platelet–granulocyte (solid squares) and platelet-bead (open circles) double positive data as a function of sample dilution measured in paraformaldehyde-treated citrated blood samples of donor #2. Data collection was triggered by FL3 signal. (Bihari et al. 2008a)*

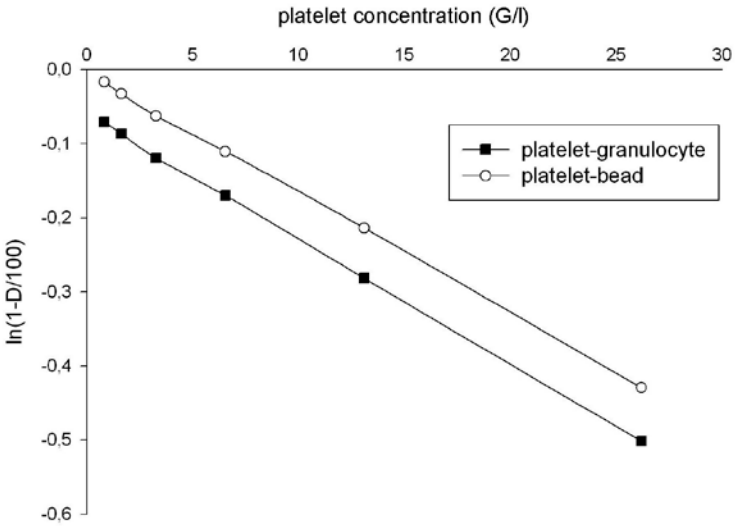

Fig. 32. *Platelet–granulocyte (solid squares) and platelet-bead (open circles) data of Fig. 31 transformed according to Eq. (10) as a function of platelet concentration. (Bihari et al. 2008a)*

The same qualitative results were obtained for each of our donors. Straight lines obtained from the data of our seven donors measured either with or without beads have a correlation coefficient of at least 0.992. Straight lines representing bead-containing

DOI:10.14753/SE.2016.1824

samples have practically zero intercepts (mean ± SD = − 0.006 ± 0.006) which means that no more than 0.61 ± 0.64 % of beads are positive for platelet markers. Slopes of the corresponding straight line pairs for each donor are identical within the limit of error, which means that the detection volume does not change when one replaces the granulocyte trigger with the bead one. The average detection volume when granulocytes or beads are used as triggers is: V_d = 15.2 ± 1.7 pl and 15.0 ± 1.9 pL, respectively.

b) Mathematical description of platelet-granulocyte complexes

The experiments outlined above provide the means to estimate the percentage of complexes at any platelet concentration. Let C denote the concentration of complexes, and D_b and D_g the percentage of CD41 positive events at the same dilution, in the case when FL3 bead or granulocyte fluorescence were used as triggers, respectively. According to Eqs. (8) and (9) (see section IV/6/b) one gets:

$$\ln\left(1-\frac{D_g}{100}\right)=-V_d[\mathrm{T}]+\ln\left(1-\frac{[C]}{[G]}\right) \quad (11a)$$

$$\ln\left(1-\frac{D_b}{100}\right)=-V_d[\mathrm{T}] \quad (11b)$$

Combining the two above equations, the percentage of platelet–granulocyte complexes (D_r) among granulocytes can be calculated:

$$D_r=\frac{[\mathrm{C}]}{[\mathrm{G}]}\cdot 100=\frac{100\cdot(D_g-D_b)}{100-D_b} \quad (12)$$

This simple formula is applicable to any blood dilution using CD41 positive data pairs (D_g and D_b) in the case when event collection is triggered alternately by granulocytes and beads.

According to our experience for a given donor, D_r is constant within the limit of error at each dilution of the paraformaldehyde treated blood samples (see Table 6).

DOI:10.14753/SE.2016.1824

Table 6. *The amount of stable complexes in the paraformaldehyde-treated citrated blood of the individual donors expressed as a percentage of granulocytes (D_r). The averages and standard deviations for each individual donor were calculated from values obtained at six different dilutions. (Bihari et al. 2008a)*

Donor	**#1**	**#2**	**#3**	**#4**	**#5**	**#6**	**#7**	**#8**	**#9**
D_r	17.6	5.9	18.6	30.8	0.5	18.1	15.0	10.1	16.2
SD	1.6	0.7	1.2	0.5	0.4	1.1	1.1	0.8	0.7

3. Effect of nanoparticles on platelet activation *in vitro*

a) Platelet P-selectin expression

Human platelet P-selectin expression was measured to analyse the direct effects of nanoparticles on platelet activation. Carboxyl-modified polystyrene, DEP, and TiO_2 (rutile) nanoparticles did not change CD62P (P-selectin) expression on platelets as compared to controls. In contrast, the addition of ADP, amine-modified polystyrene, or SWNT nanoparticles to human whole blood increased P-selectin expression on platelets (Fig 33).

DOI:10.14753/SE.2016.1824

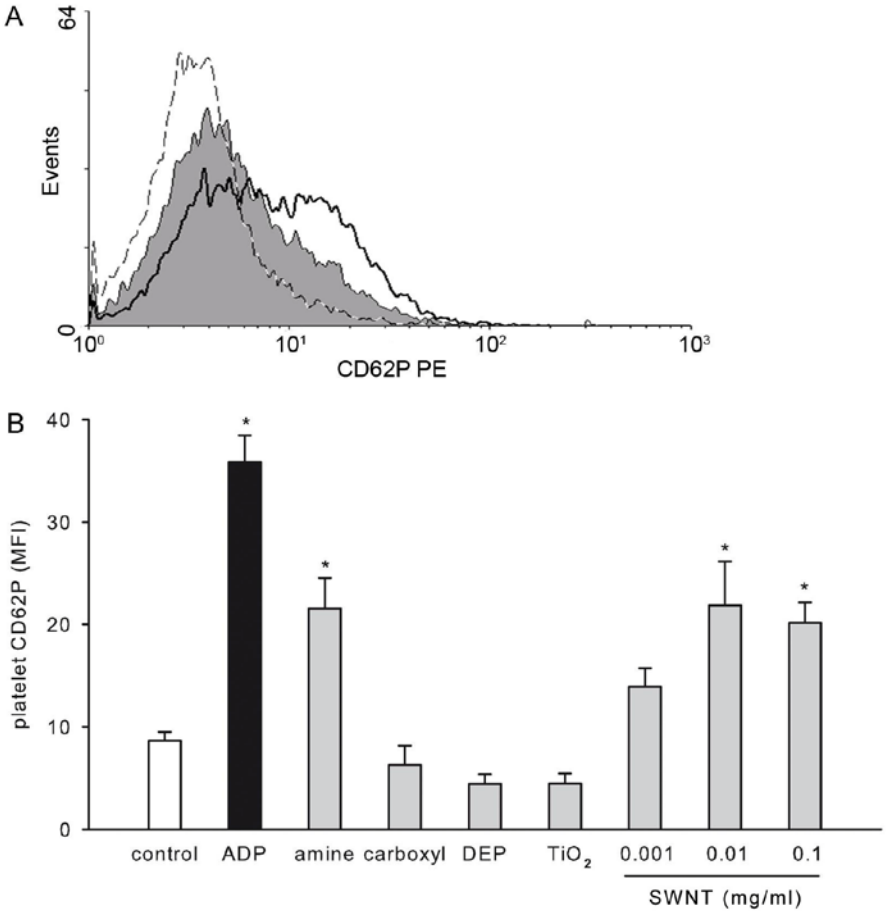

Fig. 33. A. *Representative flow cytometry histograms of platelet P-selectin measurements after 10 minutes incubation of human whole blood, either with PBS (dashed line), or with 1 µM ADP (thick solid line) or with 100 µg/ml SWNT (thin solid line).* ***B.*** *Platelet P-selectin expression. Human whole blood was incubated with PBS (n=44), ADP (n=44) or nanoparticle dispersion for 10 minutes. The concentrations of amine- (n=23), carboxyl-modified polystyrene (n=18), DEP (n=16), or TiO_2 rutile (n=15) nanoparticles were 100 µg/ml each. SWNT concentrations were 1 µg/ml (n=11), 10 µg/ml (n=14) and 100 µg/ml (n=25). ADP was added at a final concentration of 1 µM. Mean CD62P fluorescence intensities (MFI) of CD41-positive events were analysed (*, $p<0.05$ vs. control). (Bihari et al. 2010)*

b) Platelet-granulocyte complexes

As an additional marker of platelet activation, the formation of platelet-granulocyte complexes was analysed. Similar to the results of the P-selectin expression

measurements, ADP, amine-modified polystyrene, and SWNT nanoparticles significantly increased the percentage of CD41 positivity in the granulocyte gate as compared to control experiments. In contrast, carboxyl-modified polystyrene, DEP, and TiO_2 (rutile) nanoparticles had no effect on the number of platelet-granulocyte complexes (Fig 34).

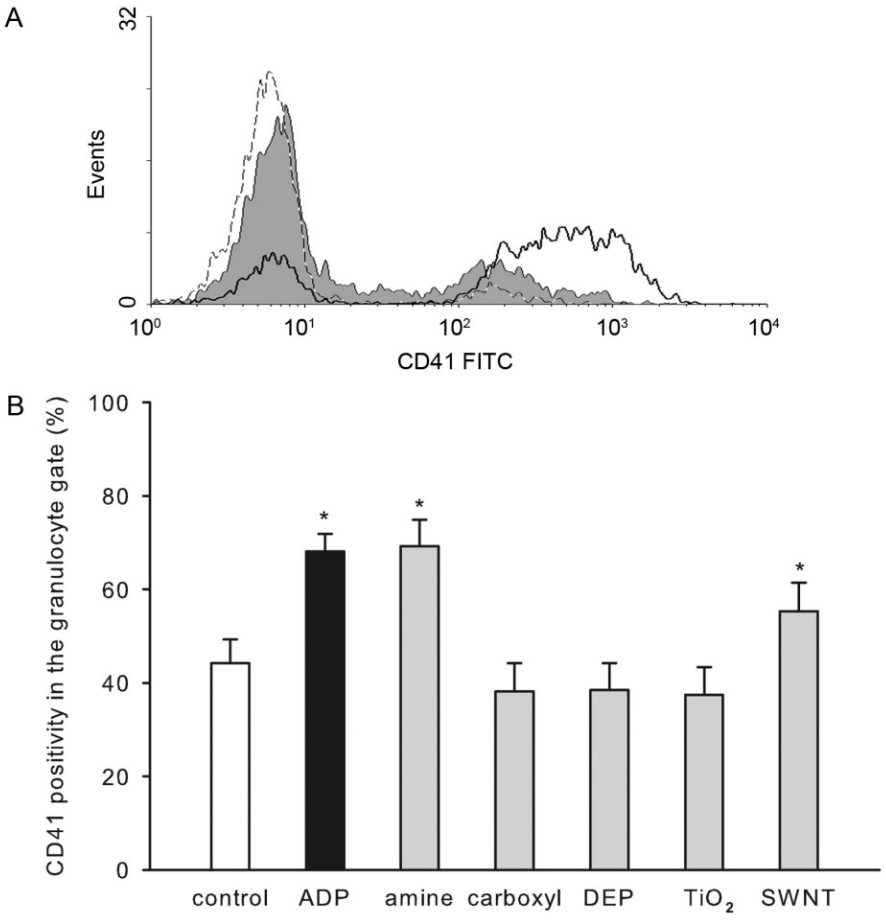

Fig. 34. A. *Representative flow cytometry histograms of platelet-granulocyte complexes measured in human whole blood after incubation with PBS (dashed line), 1µM ADP (thick solid line), or 100 µg/ml SWNT (thin solid line) for 10 minutes.* ***B.*** *Platelet-granulocyte complexes. Human whole blood was incubated with PBS (n=16), ADP (n=16), or nanoparticles for 10 minutes. The concentration of amine- (n=9), carboxyl- (n=9) modified polystyrene, DEP (n=9), TiO_2 rutile (n=9) or SWNT (n=10) nanoparticles was 100 µg/ml. ADP was given at a final concentration of 1 µM. (*, p<0.05 vs. control). (Bihari et al. 2010)*

DOI:10.14753/SE.2016.1824

c) Platelet aggregometry

To further characterize platelet activation induced by amine-modified polystyrene and SWNT nanoparticles, the effect of these nanoparticles on human platelet aggregation was analysed. The addition of SWNT nanoparticles to PRP reduced the optical density as compared to PPP incubated with SWNT. Changes in the optical density after the addition of amine-modified polystyrene beads were below the threshold of background noise (Fig 35). It is noteworthy that in case of SWNT we could not detect the usual initial increase in optical density due to platelet shape change and that the optical density change was not as rapid as by ADP-induced platelet aggregation (Fig 36).

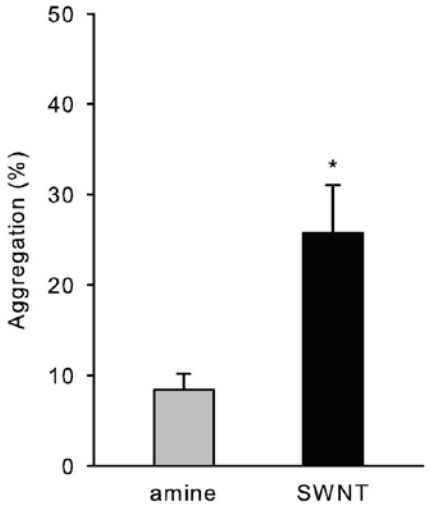

Fig. 35. *Platelet aggregation. Optical density changes of PRP versus PPP were measured after addition of amine-modified polystyrene (n=18) or SWNT (n=13) nanoparticles to both solutions. The final concentrations of nanoparticles were 100 µg/ml. After running samples for at least 10 minutes, ADP was added at a final concentration of 1 µM to PRP. Aggregation in the presence of nanoparticles is given as a percentage of that induced by ADP (*, p<0.05 vs. zero). (Bihari et al. 2010)*

DOI:10.14753/SE.2016.1824

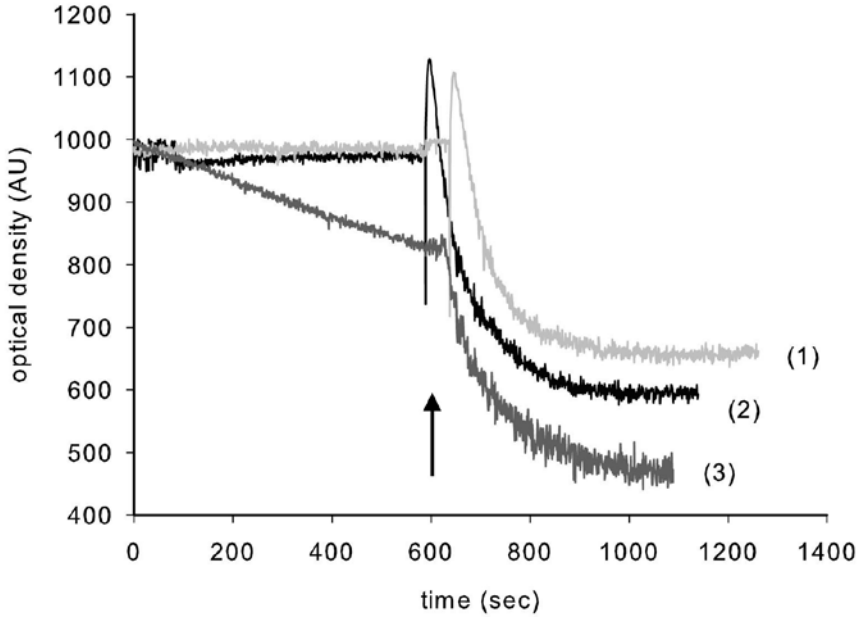

Fig. 36. *Platelet aggregation curves from three representative experiments. Optical density changes of PRP versus PPP were measured after the addition of PBS (1), amine-modified polystyrene (2), or SWNT (3) nanoparticles to both solutions. The final concentrations of nanoparticles were 100 µg/ml. After running samples for at least 10 minutes, ADP was added at a final concentration of 1 µM to PRP (arrow). Slightly modified after Bihari et al. (Bihari et al. 2010)*

4. Effect of nanoparticles on thrombus formation *in vivo*

a) Mouse blood counts

There were no differences in platelet, leukocyte, and erythrocyte counts, haematocrit, haemoglobin concentration, mean corpuscular volume, mean corpuscular haemoglobin, and mean corpuscular haemoglobin concentration of erythrocytes among groups treated with vehicle or nanoparticles (data not shown).

b) Mesenteric thrombosis

The effect of nanoparticles on thrombus formation were analysed in small mesenteric arteries. As a positive control, systemic administration of epinephrine significantly

decreased the cessation time compared to that which occurred when physiological saline was injected. Amine-modified polystyrene nanoparticles significantly decreased and carboxyl-modified polystyrene nanoparticles significantly increased the cessation time compared to that of the controls (Fig 37).

There were no significant differences in arterial cessation time in case of DEP-, TiO_2 (rutile)- or vehicle-treated animals. In contrast, cessation time was significantly decreased in SWNT- compared to vehicle-treated animals (Fig 38).

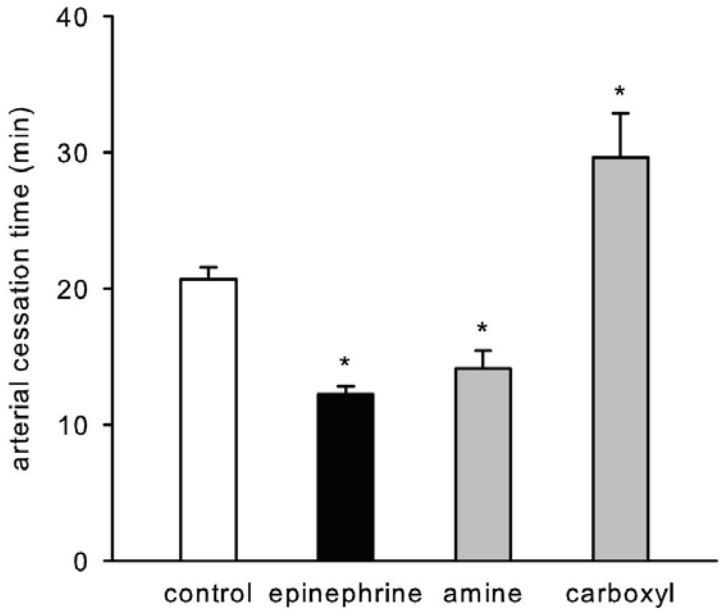

Fig. 37. *Cessation time in small mesenteric arteries after induction of ferric chloride-induced thrombosis. Epinephrine was given at a blood concentration of 12.5 µM intra-arterially immediately before thrombosis induction. Amine- or carboxyl-modified polystyrene nanoparticles at a concentration of 0.5 mg/kg body weight or physiological saline (control) were administered intra-arterially 10 minutes prior to the induction of thrombosis. (n=8; *, p<0.05 vs. control). (Bihari et al. 2010)*

DOI:10.14753/SE.2016.1824

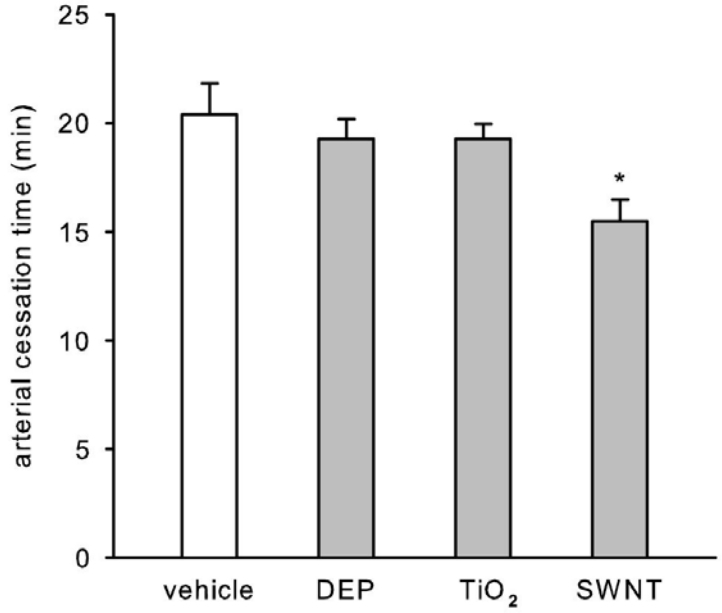

Fig. 38. *Cessation time in small mesenteric arteries after induction of ferric chloride-induced thrombosis. DEP, TiO_2 (rutile) or SWNT nanoparticles at a concentration of 1 mg/kg body weight or vehicle were administered intra-arterially 10 minutes before thrombosis induction. (n=8; *, p<0.05 vs. vehicle). (Bihari et al. 2010)*

c) Cremasteric thrombosis

Microvascular thrombotic effects of nanoparticles were analysed in the cremasteric microcirculation of mice. To ensure comparable intravascular FITC dextran concentrations in all experiments, the fluorescence intensity was measured in one venule in each experiment. There were no significant differences in the fluorescent intensities among experimental groups (data not shown). As a positive control, LPS significantly decreased the onset time and the cessation time in arterioles. In contrast to the small mesenteric arteries, onset and cessation times in arterioles of mice treated with amine- or carboxyl-modified polystyrene nanoparticles were the same as in the control groups (Fig 39). Furthermore, no significant differences were found in the onset time of thrombus formation in arterioles.

While the cessation times were not changed upon the application of DEP or TiO_2 (rutile), SWNT injection decreased the cessation time in arterioles dose-dependently as compared to the vehicle control. (Fig 40). Interestingly, no significant differences were found in venous thrombosis parameters (data not shown).

DOI:10.14753/SE.2016.1824

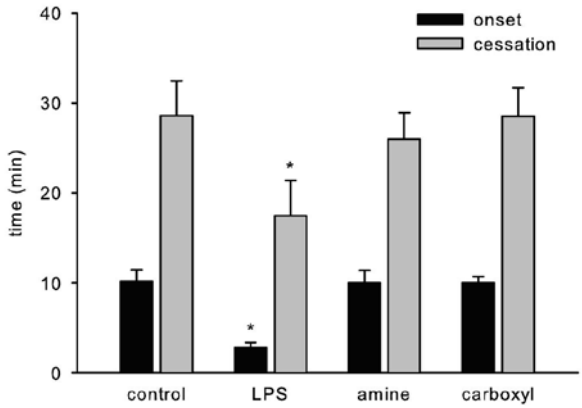

Fig. 39. *Light/dye-induced thrombosis in cremasteric arterioles. LPS (4 mg/kg body weight) was given i.p. 4 hours prior to the induction of thrombosis. Amine- or carboxyl-modified polystyrene nanoparticles at a concentration of 0.5 mg/kg body weight or physiological saline (control) were administered intra-arterially 10 minutes prior to the induction of thrombosis. Onset (black) and cessation times (grey) are shown. (n=8; *, p<0.05 vs. control). (Bihari et al. 2010)*

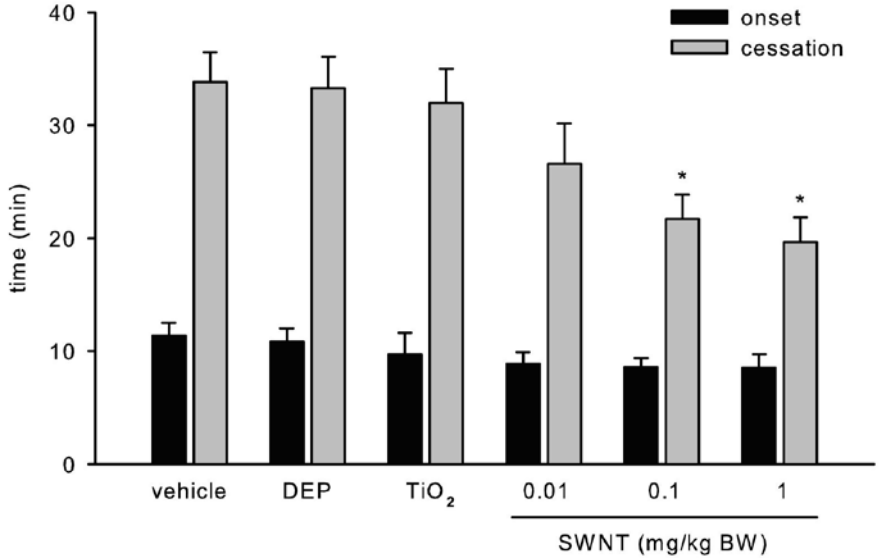

Fig. 40. *Light/dye-induced thrombosis in cremasteric arterioles. DEP, TiO_2 (rutile), nanoparticles at a concentration of 1 mg/kg body weight, SWNT at concentrations of 0.01, 0.1, 1 mg/kg body weight or vehicle were administered intra-arterially 10 minutes prior to the induction of thrombosis. Onset (black) and cessation times (grey) are shown. (n=8; *, p<0.05 vs. vehicle). (Bihari et al. 2010)*

DOI:10.14753/SE.2016.1824

VI. Discussion

The main goal of this dissertation was to analyse the influence of nanoparticles on platelet activation *in vitro* and on thrombus formation *in vivo*. In order to be able to carry out these measurements, we had to solve two problems: optimisation of the dispersion method of nanoparticles and optimisation of the platelet-granulocyte complex measurement. The discussion section begins with the consideration of these two methodological studies.

1. Optimisation of the nanoparticle dispersion method

To determine the toxicity of nanoparticles in biological *in vitro* or *in vivo* settings, the particles first have to be dispersed in a physiological fluid medium that is compatible with the biological material. Nanoparticles, however, tend to build coarse agglomerates in physiological solutions This phenomenon is described by the DLVO (named after Derjaguin, Landau, Verwey, Overbeek) theory: the stability of a particle dispersion depends on the balance between attractive (van der Waals) and repulsive (electrostatic) forces between particles (Müller 1996). Based on this theory, colloid science describes two fundamental ways for stabilising a dispersion: electrostatic and steric stabilisation (Fig 41). For the electrostatic stabilisation, the zeta potential of the electrostatic double layer around the particles provides repulsive forces. In practice, if the zeta potential of the particles is lower than -30 mV or higher than +30 mV, the repulsive forces are high enough to stabilise the dispersion. However, the zeta potential of the particles strongly depends on the pH and ionic strength of the dispersion medium (Müller 1996). At physiological pH and physiologic ionic strength, electrostatic repulsive forces are usually not high enough to stabilise the dispersion, and the nanoparticles form coarse agglomerates (Buford et al. 2007, Deguchi et al. 2007, Murdock et al. 2008). The other way of dispersion stabilisation is steric stabilisation, by which polymeric molecules are adsorbed onto the surface of nanoparticles preventing them from getting close to each other. As this kind of stabilisation is not dependent on the zeta potential of particles, i.e. the stability of the dispersion is independent of pH and ionic strength, it can also work in physiological solutions (Powers et al. 2006). This strategy has been found to be beneficial in different studies. Pulmonary surfactant, bronchoalveolar lavage fluid,

Tween, albumin, or serum were used as dispersion stabilising polymeric molecules to decrease the formation of coarse agglomerates (Buford et al. 2007, Sager et al. 2007, Murdock et al. 2008).

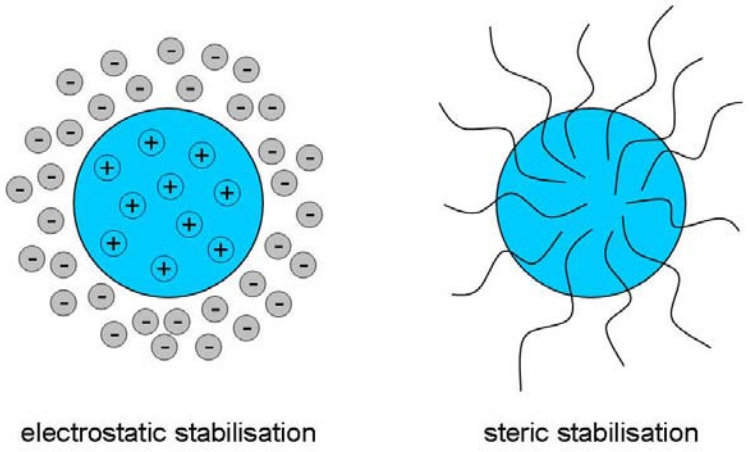

Fig. 41. *Electrostatic versus steric stabilisation of nanoparticle dispersions. Repulsive forces are given in electrostatic stabilisation by the zeta potential, whereas in steric stabilisation by the adsorbed molecules on the nanoparticle surface.*

Our aim was to optimise the factors that might influence the effectiveness of dispersing nanoparticles in physiological solutions using steric stabilisation, such as the ultrasound energy levels, various dispersion stabilizers (HSA, BSA, MSA, Tween 80, or mouse serum) at various concentrations and at different nanoparticle concentrations, and different sequences of preparation steps. We also tested our method on a broad range of different types of nanoparticles and measured the stability of the dispersion over time.

To analyse the effectiveness of steric stabilisation, we measured the size of nanoparticles in the dispersion with dynamic light scattering. This method was found to be reliable for measuring particle size and size distribution of dispersed spherical nanomaterials (Powers et al. 2006). Additionally, we measured the zeta potential of the particles with phase analysis light scattering and visualised dispersed nanoparticles using transmission electron microscopy.

First, we measured the effect of different sonication energies. Ultrasound heats up the fluid locally and generates steam bubbles (cavities). The rapid collapse of such gas

bubbles (implosion) gives rise to extremely high pressure waves. The energy of the pressure waves can break up nanoparticle agglomerates. It is known that the result of sonication, e.g. particle size reduction, depends on the applied energy per volume of the dispersion (specific energy) (Pohl et al. 2004, Hilscher 2005). The difficulty is that the sonication energy should be high enough to deagglomerate the particles, but at the same time it must not destroy them. We found that after rapid initial size reduction, a further increase in the specific energy did not lead to further reduction of the particle size. Thus, a specific energy of 4.2×10^5 kJ/m^3 was optimal for deagglomerating the nanoparticles. Our findings confirm previous observations of Mandzy et al. (Mandzy et al. 2005).

In the next set of experiments, we analysed the optimal sequence of particle preparation. The best sequence of dispersion preparation was when we first sonicated the nanoparticles, then added HSA as stabilizer, and finally added PBS to the dispersion. The addition of HSA molecules after sonication prevents the particles from the reagglomeration. Similar results were published for the preparation of dispersions of C60 nanoparticles (Deguchi et al. 2007). We found that the stabilising effect of albumin was species-independent as the agglomeration of nanoparticles could be avoided by the addition of either HSA, or MSA, or BSA; and it was also medium-independent since HSA worked in PBS as well as in RPMI cell culture medium.

When HSA molecules are added to the nanoparticles, they adhere to the surface of the particles, as indicated by a significant increase in the average diameter of the particles. This finding is in agreement with the prevailing opinion on the formation of a protein corona (Lynch and Dawson 2008) (see section II/2/e). Interestingly, in our measurements, the difference in average particle size between dispersions with and without HSA was 14.5 nm, consistent with approximately twice the diameter of one HSA molecule (7.1 ± 0.1 nm, our measurement with dynamic light scattering). These data suggest that the HSA molecules may completely cover the nanoparticles. Furthermore, the zeta potentials of different nanoparticles, ranging from -48.4 mV to -18.7 mV in distilled water, change uniformly to a value of about -10 mV after the addition of HSA (see Table 5). This change is presumably due to HSA molecules covering nanoparticles and masking their own zeta potential. Thus, the particles have a zeta potential near to the zeta potential of HSA (the zeta potential of the HSA molecules

in PBS is about -6 mV). This finding is corroborated by data from Lindman et al. (Lindman et al. 2007) who found, using the isothermal titration calorimetry technique, that particles with a diameter larger than 120 nm are covered with a dense monolayer of proteins.

To further analyse nanoparticle-albumin interactions, dispersions with different particle and albumin concentrations were prepared. HSA in a concentration higher than 0.015 mg/ml prevented the formation of coarse agglomerates, when the TiO_2 (rutile) concentration was 0.02 mg/ml. Elevating the HSA concentration in the dispersion resulted in a dose-dependent increase of particle size, obviously because the albumin layer on the nanoparticles was becoming complete. Further increase of the HSA concentration to 15 mg/ml results in saturation of the protein corona on the nanoparticle surface and the amount of free albumin molecules is high enough to be detectable as a separate peak in the size distribution measurements. From these experiments we could determine that the lowest HSA/TiO_2 (rutile) concentration ratio, at which particles are covered with HSA and dispersion is stable, was 0.75. We calculated that there are ~33000 HSA molecules per each TiO_2 (rutile) particle in the dispersion. This is ~7 times more than the amount calculated as necessary for a 100% HSA coverage of 200 nm spherical particles (4650 HSA molecules/particle) (Lindman et al. 2007). When we increase the TiO_2 (rutile) concentration 10-fold but use the same HSA concentration, the amount of HSA molecules is not high enough to cover TiO_2 (rutile) particles, resulting in insufficient protection against the agglomeration of particles. Consistent with this theory, we detected coarse agglomerates in that dispersion. However, when we increased the TiO_2 (rutile) and HSA concentrations equally (10-fold), generating the same HSA/TiO_2 (rutile) surface area ratio, the dispersion lacked the coarse agglomerates. These data suggest that the total surface area of particles in the dispersion determine the required amount of stabilizer. Thus, based on our measurements, for a nanoparticle concentration range relevant for toxicological studies (0.002 mg/ml – 0.2 mg/ml), we found 1.5 mg/ml HSA to be the optimal concentration to prevent formation of coarse agglomerates in the dispersion.

Adding mouse serum (30 μl mouse serum to 1 ml dispersion) to the dispersion containing similar amount of albumin when HSA was used also prevented the formation of coarse agglomerates. Thus, this amount of serum contains abundant proteins to cover

the particle surfaces. This is also supported by the publication of Cedervall et al., describing that ~100 µl plasma saturates 1 mg of 200 nm particles (Cedervall et al. 2007a), which is a similar concentration to the ones that we used.

Next we analysed whether particles prepared with HSA gave a stable dispersion. TiO_2 (rutile) prepared with HSA was found to be stable for at least one week, whereas without stabilizer the particles started to form agglomerates in PBS. Similar results were published for other particles (Deguchi et al. 2007).

We found that our optimised method was suitable for preparing dispersions without coarse agglomerates (average diameter < 290 nm) from nanosized TiO_2 (rutile), ZnO, Ag, SWNT, MWNT, and DEP (SRM2975). We measured high PdI values for SWNT, MWNT, and SiO_x. In the case of nanotubes, the size parameter should be interpreted differently from that of other particles since nanotubes have higher aspect ratios. In this case, the size parameter indicates the hydrodynamic diameter of a spherical particle that would move in the dispersion media at the same velocity as nanotubes. Thus the high PdI of SWNT and MWNT nanotubes is due to the shape of these particles. Although the size data obtained from the measurement of nanotubes are influenced by the shape of these nanoparticles, dynamic light scattering gives important information about the agglomeration state of these dispersions. If nanotubes agglomerate, they move more slowly in the dispersion medium and will be detected as if they had a higher average diameter. In contrast, well-dispersed nanotube dispersions show a lower average diameter. Such a difference could be detected when we compared the dispersions prepared in PBS with those prepared with our optimised method (see Table 5). For SiO_x and TiO_2 (anatase) particles, our method was less effective as indicated by a relatively high average diameter and PdI of particles.

The quantitative analysis of dispersions with transmission electron microscopy confirmed the data obtained from dynamic light scattering (see Fig. 24-26). Our optimised method generated an improved dispersion with any of the nanoparticles measured.

Besides the described methodological considerations, there are also some other options that have not been tested yet, but could theoretically further improve nanoparticle dispersions. As nanoparticles do not need to be in a physiological solution at the first stage of the preparation, also non-physiological chemical techniques might

be used to improve the quality of the dispersion at this stage. The point is to find techniques or chemical reagents that help deagglomerate nanoparticles, but at the same time do not hamper or even augment the binding of steric stabilizer. These techniques or chemicals should be chosen so that they could be neutralised or removed during the last stage of the preparation. For example, it could be helpful to change pH to the electrostatic optimum of the given nanoparticles at the beginning of the preparation, which would strengthen the repulsive forces, and to adjust pH to the physiological level after the addition of steric stabiliser.

Another option concerns sonication. After sonication, nanoparticles immediately start to agglomerate, and this process is stopped after the addition of a steric stabilizer. It is therefore important to keep this time period as short as possible. The best option for this is to use a second sonication step after the addition of the steric stabilizer (data not published). During the second sonication, the steric stabilizer is already in the dispersion, and this means it can immediately adhere to nanoparticle surfaces accessible due to deagglomeration. To avoid damage of the steric stabilizer by the second sonication step, less ultrasound energy, repeated short sonication periods, or cooling, might be necessary.

In biological studies, when nanoparticles get into the blood circulation they come into contact with albumin and other serum proteins, and these proteins cover the nanoparticles forming a protein corona. Our optimised method also uses albumin or serum, thus nanoparticles dispersed with our method are covered with the same proteins that nanoparticles encounter in the blood. Presumably later, after injection into the systemic circulation, proteins with higher affinity also integrate into the protein corona of these nanoparticles (Lynch and Dawson 2008).

We found that the following aspects are important in considering the preparation of nanoparticle dispersions in physiological solutions (Fig. 42):

i) the optimal sequence is first to sonicate the nanoparticles in distilled water, then to add the stabilizer, and finally to add buffered salt solution to the dispersion

ii) the usage of a sonication energy high enough to deagglomerate the particles ($>4.2 \times 10^5$ kJ/m^3)

iii) the addition of albumin or serum as stabilizers at a concentration sufficient to cover the nanoparticles (1.5 mg/ml HSA for dispersions with less than 0.2 mg/ml nanoparticle concentration or serum with a similar albumin concentration)

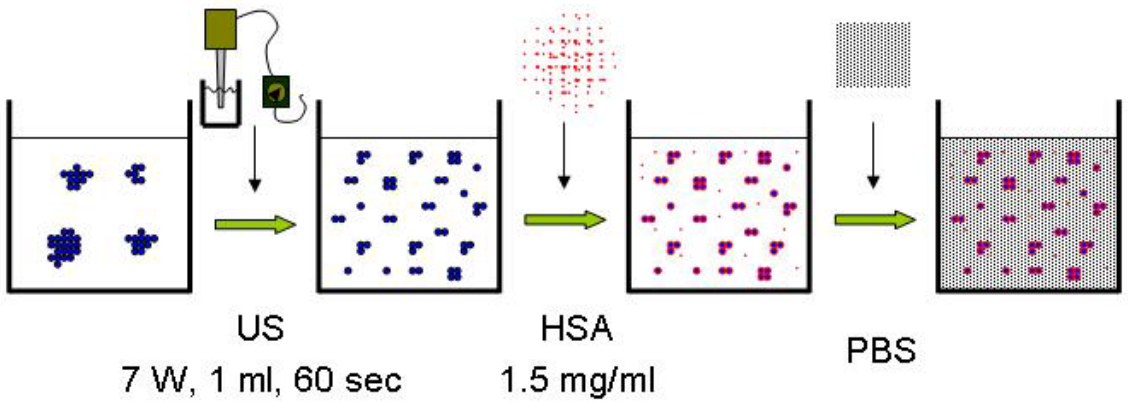

Fig. 42. *Preparation steps of nanoparticle dispersion. 1. Sonicate the nanoparticles in distilled water (power consumption: 7 W, 1 ml dispersion, 60 sec sonication, = 4.2 × 10^5 kJ/m^3). 2. Add stabilizer (1.5 mg/ml HSA or an amount of serum resulting in a similar albumin concentration for dispersions with less than 0.2 mg/ml nanoparticle concentration). 3. Add concentrated PBS to achieve physiological pH and salt concentration. (Bihari et al. 2008b)*

In conclusion, the optimised dispersion method appears to be effective and practical for preparing dispersions of nanoparticles in physiological solutions, without creating coarse agglomerates.

2. Optimisation of platelet-granulocyte complex measurement

Flow cytometry is the easiest and most often used way to measure platelet-granulocyte complexes. Platelets and granulocytes are labelled with various antibody-bound fluorescent probes and analysed with a flow cytometer (Li et al. 1999, Snow 2004, Fent et al. 2008). Platelet-granulocyte complexes can be identified as simultaneous fluorescent signals from both cell types. However, based on this kind of measurement,

DOI:10.14753/SE.2016.1824

one is unable to distinguish the real platelet-granulocyte complexes from the separated platelets and granulocytes that coincide in the detection volume (Fig. 12). To solve this problem we analysed the factors determining the rate of coincidence.

First, we measured coincidence in two different experimental models. In the first model, we mixed two different fluorescent beads in concentrations corresponding to that of platelets and granulocytes respectively. Since in this model non-interacting beads (Maehara et al. 1990) were used, simultaneous fluorescent signals from both types of beads could be detected just as in the case of coincidence. In the second model EDTA anticoagulated human blood was analysed, where according to literature data, in the absence of extracellular Ca^{2+}, no platelet-granulocyte complexes exist (Hamburger and McEver 1990). In these two models, the measured double positive events could only be derived from coincidence. In both systems, at 10-fold dilution, which ensures the manufacturer's recommended flow cytometric event rate ($10^2 - 4 \times 10^3$ particles/s), up to 40% double positivity was experienced (Fig. 27 and 29). When we increased the dilution the percentage of double positive events decreased. The dilution dependence of double positivity is understandable because the probability of the presence of platelets in the detection volume is lower in a diluted solution than in a concentrated one. In contrast, coincidence does not depend on granulocyte concentration, which can be explained by the data acquisition set-up of the flow cytometer. In our measurement the granulocyte signal was chosen as trigger for starting data acquisition. This means that data collection of a signal event starts only if a granulocyte is detected by the flow cytometer and lasts for a fixed time duration, i.e. a detection volume unit is defined.

According to our mathematical considerations (Eqs. (8)-(10), see section IV/6/b) in such systems where only coincidence exists, proper transformation of double positive events results in straight lines with zero intercept. This is the case for the bead mixture (Fig. 28) which reassures us that, in our bead model, double positive events derive solely from coincidence. Transformation of platelet-granulocyte double positive data obtained for EDTA anticoagulated blood samples also gives straight lines (Fig. 30). Four of our seven donors exhibit zero intercepts in accordance with the literature describing no platelet-granulocyte complexes in the absence of Ca^{2+} (Hamburger and McEver 1990). However, it is noteworthy that three of our donors seem to have complexes (the intercept of their straight lines in Fig. 30 is significantly different from

zero), also in EDTA anticoagulated blood, indicating the existence of some Ca^{2+}-independent platelet-granulocyte complexes. Further investigation is needed to clarify this phenomenon.

In citrated blood samples, platelet–granulocyte complexes are formed upon incubation at room temperature since citrate decreases but does not completely eliminates the Ca^{2+} concentration (Peters et al. 1997, Li et al. 1999, Peters et al. 1999, Hagberg and Lyberg 2000). Paraformaldehyde treatment of such citrated blood samples results in stable, dilution-independent platelet-granulocyte complexes. Transforming double positive data obtained for the paraformaldehyde-treated citrated blood (Fig. 32) can also be fitted with a straight line with a non-zero intercept, representing the amount of stable complexes (cf. Eq. (8), section IV/6/b). When platelet-bead double positivity was measured after mixing fluorescent beads into the same blood sample, transformation of the data resulted in a parallel straight line having a zero intercept (Fig. 32). This indicates that coincidence has the same probability whether granulocyte or bead is the triggering signal, and the difference in the intercepts corresponds to the amount of real complexes. Thus the amount of platelet-granulocyte complexes can be calculated according to Eq. (12) (section V/2/b).

The mathematical description of coincidence draws attention to the fact that the detection volume has a crucial impact on the extent of coincidence in a flow cytometer (cf. Eq. (8), section IV/6/b). The detection volume can be calculated from the technical data of the flow cytometer provided by the manufacturer. For the FACScan flow cytometer the estimated collection time period for fluorescence is 20 μsec. Considering the 1 μl/sec sample flow rate, the detection volume comes up as 20 pl. The same value (20.4±1.0 pl) was obtained within the limits of error when a mixture of the two non-interacting fluorescent beads was analysed. In EDTA anticoagulated blood a 13.5±1.6 pl detection volume was found. This smaller value can be attributed to a lower sample flow rate, which is a consequence of about a four-fold higher viscosity of undiluted blood than that of the PBS.

In the literature, various values were published (Peters et al. 1997, Jensen et al. 2001, Bunescu et al. 2002, Pitchford et al. 2003) for the amount of platelet-granulocyte complexes measured in citrated blood samples of healthy donors ranging from 1.8% to 25% in 416-fold (Jensen et al. 2001) and 15.2-fold dilutions (Peters et al. 1997),

respectively. Our findings may provide a possible explanation for the variation of data obtained in different laboratories. If the platelet concentration in the sample is not low enough, the contribution of coincidence to the measured amount of double positive events is no longer negligible, resulting in an overestimation of the platelet-granulocyte complexes.

Based on our findings, we suggest three methods to avoid overestimation of platelet-granulocyte complexes caused by coincidence if measured in a flow cytometer. The first possibility is that the contribution of platelet-granulocyte coincidence can be calculated when the detection volume and the platelet concentration are known (cf. Eqs. (8)-(10), section IV/6/b). Another possibility is to divide the blood sample into two parts: one part is stained for platelets and granulocytes, the other part is stained only for platelets and fluorescent beads are mixed into it. Then, by measuring platelet–granulocyte and platelet-bead double positivity at the same dilution (platelet concentrations need to be the same), the exact amount of platelet–granulocyte complexes can be calculated (cf Eq. (12), section V/2/b). The third and probably most practical method is to measure platelet-granulocyte complexes at dilutions high enough to make coincidence negligible. For measurement of the amount of platelet-granulocyte complexes upon incubation with nanoparticles, the dilution method was used.

3. Prothrombotic effects of nanoparticles

To use nanotechnology safely, one has to be aware of the possible hazards of nanomaterials. Previous research on biomaterials has shown that foreign materials in contact with blood induce thrombus formation. Moreover, investigation of air pollution has found that ambient nanoparticles, which can translocate from the lungs into the circulation, also exert prothrombotic effects. These scientific data suppose that manufactured nanoparticles may also influence haemostasis. Moreover, although nano-sized particles are deposited mainly in the microcirculation, the effect of nanoparticles on microcirculatory thrombus formation has not been investigated yet. Hence our aim was to examine whether manufactured nanoparticles exert prothrombotic potential in small arteries and in the microcirculation.

As in all toxicological studies, the choice of correct dosage is fundamental. We have chosen a concentration range that considers both of the following scenarios: (i)

manufactured nanoparticles are inhaled and translocate from the lungs into the circulation, and (ii) nanoparticles for medical use are directly injected into the blood. The background concentration of ambient ultrafine particles was found to be on average between 0.8 - 1.6 µg/m^3 (1-5 x 10^4 particle / cm^3) with peak concentrations reaching about 50 µg/m^3 (3 x 10^5 particle / cm^3) (Oberdorster 2001, Zhu et al. 2002). Similar concentrations were measured during the production of different manufactured nanoparticles: from 10^4 to 10^5 particle/cm^3, however with much higher peaks exceeding 1.2 x 10^6 particle/cm^3 (Maynard et al. 2004, Brouwer 2010). Thus assuming 500 µg/m^3 peak ambient nanoparticle concentration in the air would result in 6000 µg nanoparticle exposure daily at a normal ~12 m^3 air inhalation. Translocation of 10% of these inhaled nanoparticles (see section II/2/g) into the systemic circulation by a 70 kg person would result in about 0.01 mg/kg body weight concentration. A similar calculation was also used by Nemmar et al. to determine nanoparticle concentrations for their *in vivo* experiments (Nemmar et al. 2003a). Obviously nanoparticles injected directly into the blood circulation for medical applications might reach much higher concentration levels. Thus to cover a dosage range relevant for both exposure routes we applied a concentration range of 0.01-1 mg/kg body weight.

First, prothrombotic effects of polystyrene bead nanoparticles were tested. These nanoparticles are used in many nanotoxicological studies as benchmark particles because they can be produced in different sizes with various surface modifications, and can be dispersed easily. In our experiments amine-modified polystyrene nanoparticles injected into the systemic circulation reduced and carboxyl-modified polystyrene nanoparticles increased the time until vessel occlusion was complete in small mesenteric arteries. Furthermore, amine-modified polystyrene nanoparticles activated platelets as indicated by the increased expression of platelet P-selectin and an elevated number of platelet-granulocyte complexes in whole blood. These results are in agreement with previously published observations (Nemmar et al. 2002b). Interestingly, the incubation of amine-modified polystyrene nanoparticles with platelets did not induce platelet aggregation in our experiments. These observations suggest that positively charged polystyrene nanoparticles provoke only modest platelet activation. Indeed, in a recent publication, amine-modified polystyrene beads were found to induce a non-classical way of platelet activation characterized by perturbation of the platelet

membrane (McGuinnes et al. 2011). This observation is supported by the findings that positively and negatively charged polystyrene nanoparticles change the fluidity of phospholipid membranes by altering the tilt angle of the phosphocholine head groups (Wang et al. 2008). Although polystyrene nanoparticles affected the cessation times in small mesenteric arteries, they had no effect on thrombus formation in cremasteric microvessels. The inconsistent results of the two thrombosis models might be explained by the methodical differences in the induction of thrombosis. In the cremaster model, light/dye-induced thrombosis was used which, in contrast to ferric chloride application, activates endothelial cells without endothelial denudation (Rumbaut et al. 2006). Moreover, another difference is that the microcirculation has, due to the higher ratio of endothelial cells to blood, a larger endothelial cell dependent antithrombotic capacity than the vessels of the macrocirculation (Esmon and Esmon 2011).

Surprisingly, DEP failed to activate platelets or augment thrombosis in both small mesenteric arteries and in the microcirculation. These data are in contrast to previous findings demonstrating accelerated thrombus formation in large vessels after instillation (Nemmar et al. 2003a, Nemmar et al. 2003c, Nemmar et al. 2004) or systemic administration (Nemmar et al. 2007) of DEP. A possible explanation for these inconsistencies might be the different composition of DEP used in our study, or some changes in the physicochemical properties of nanoparticles during the dispersion procedure (sonication, interaction of nanoparticles with albumin). Missing prothrombotic effects upon DEP injection is also in contrast to our previous findings and to our recent investigations showing that carbon black, the main component of DEP, activates platelets, exerts prothrombotic effects and induces thrombus formation in the microcirculation.

In addition, two different manufactured nanoparticles (TiO_2 rutile and SWNT) were also tested in terms of the effect they exerted on platelet activation and thrombus formation. TiO_2 (rutile) nanoparticles had no effect on platelet activation or thrombus formation in small mesenteric arteries or in the microcirculation. In contrast, TiO_2 rutile nanorods increased ADP-induced platelet agglomeration *in vitro* and decreased the platelet count 24 hours after instillation (Nemmar et al. 2008). The distinct shape of the TiO_2 nanoparticles might explain their different prothrombotic effects.

SWNT, the other nanomaterial tested, decreased thrombosis time in small mesenteric arteries. This result is in agreement with the findings of Radomski at al. (Radomski et al. 2005) who found similar effects of SWNT on thrombus formation in the carotid artery of rats. Interestingly, SWNT had a more pronounced effect in the microcirculation. The cessation time decreased dose-dependently upon the application of SWNT. Even as low as 0.01 mg/kg body weight concentrations of SWNT augmented thrombus formation. Although the cessation times were decreased, there was only a slight, non-significant decline in the onset times. These results indicate that platelet-platelet binding or stabilisation of the thrombus rather than the initial platelet-endothelial interactions have changed.

To further analyse changes in platelet function upon exposure to SWNT nanoparticles, *in vitro* experiments were performed. SWNT increased P-selectin expression on platelets and induced a significant elevation in the number of platelet-granulocyte complexes. The simultaneous change of these two parameters is consistent with earlier findings that P-selectin plays an essential role in the formation of platelet-granulocyte complexes (Hamburger and McEver 1990). Aggregometry clearly detected a significant change in the optical density of PRP versus PPP upon the addition of SWNT to both samples. However, the shape of the platelet activation curve is unusual: the initial optical density increase, which represents platelet shape change at the beginning of the activation process, is missing, and the decrease in the optical density is also much slower than that induced by other platelet activators. Interestingly, the SWNT-platelet aggregometry curves published by Radomski and colleagues (Radomski et al. 2005) show the same unusual characteristics. This raises the question whether the change in optical density is a result of a typical platelet aggregation or whether platelets become connected to each other through SWNT strands. The aggregation of SWNT alone cannot explain the optical density decrease, as this was not detected in the control sample containing only SWNT in platelet-poor plasma. Similarly, Radomski at al. described platelet activation upon incubation with SWNT or MWNT. They also report the release of matrix metalloproteinases by SWNT-activated platelets which may further augment thrombus formation (Radomski et al. 2005). Semberova et al. found that Ca^{2+} influx by store operated calcium entry (SOCE, see also Fig. 7) plays an important role in MWNT-induced platelet activation and the subsequent release of platelet

microparticles (Semberova et al. 2009). Thus in our view SWNT might augment platelet aggregation by the direct activation of platelets, and by a mechanism where SWNT mediates adhesion between platelets.

The most interesting observation of our study therefore is that SWNT exerts prothrombotic effects not only in small mesenteric arteries but also in the micro-circulation. This finding is of particular importance because the microcirculation plays an essential role in various organ functions. Thrombotic events in the microcirculation reduce tissue perfusion and might result in functional disturbances.

Summarising our results we can conclude that SWNT and amine-modified polystyrene beads activate platelets and induce prothrombotic effects *in vivo*. In contrast, DEP and TiO_2 (rutile) nanoparticles as well as carboxyl-modified polystyrene beads do not activate platelets or induce thrombus formation. Moreover, carboxyl-modified polystyrene beads prolong thrombus formation in small mesenteric arterioles. This means that no general judgement can be concluded on the prothrombotic effects of nanoparticles. Further data from the scientific literature corroborate this opinion. Prothrombotic effects of amine-modified polystyrene beads (Nemmar et al. 2002b, Silva et al. 2005, Mayer et al. 2009, McGuinnes et al. 2011), quantum dots (Geys et al. 2008), gold (Deb et al. 2011), silica (Hudson et al. 2008, Tavano et al. 2010) and TiO_2 anatase (Haberl et al. 2015) nanoparticles, TiO_2 rutile nanorods (Nemmar et al. 2008), TiO_2 anatase nanotubes (Roy et al. 2007), CuO (Yu et al. 2010), carbon black (Khandoga et al. 2004, Radomski et al. 2005), DEP (Nemmar et al. 2003a), SWNT, and MWNT (Radomski et al. 2005, Semberova et al. 2009) have been published. According to the literature, no change in haemostasis was found in the presence of plain polystyrene beads (Nemmar et al. 2002b), gold (Dobrovolskaia et al. 2009), Ag, ZnO, TiO_2 rutile, SiO_2 nanoparticles (Haberl et al. 2015) or fullerenes (Radomski et al. 2005). Haemostasis was inhibited by nanoparticles isolated from calcified human and bovine tissues (Miller et al. 2009), silver nanoparticles (Shrivastava et al. 2009, Shrivastava et al. 2011), polylactic acid nanoparticles (Sahli et al. 1997), and carboxyl-modified polystyrene beads (Nemmar et al. 2002b).

The striking differences in the haemostatic effects of nanoparticles indicate that all kinds of nanoparticles need to be tested to exclude any prothrombotic effects. To keep up with the rapidly developing nanotechnology and the production of new types of

nanoparticles, screening methods are necessary. We suggest that flow cytometry could be a method for screening platelet-activating effects of nanoparticles. The flow cytometric data were in correlation with *in vivo* prothrombotic effects, reliably detecting nanoparticles that augment thrombus formation. The flow cytometric measurement of platelet activation, completed with tests of coagulation and endothelial cell activation, could be the first line of screening methods to detect the prothrombotic potential of nanoparticles.

Although the influence of nanoparticles on haemostasis has been discussed mainly from toxicological point of view, it can have therapeutic relevance too. Nanoparticles have been suggested for drug delivery applications. For effective drug delivery, however, drug-containing nanoparticles have to reach the target cells through the circulation. In this context, the microthrombotic effects of nanoparticles are relevant, because the trapping of nanoparticles by microthrombi may potentially reduce the availability of drugs and therefore result in therapy failure. Pro- and antithrombotic effects of nanoparticles have also been proposed in medical applications. Arg-Gly-Asp functionalized nanoparticles as synthetic platelets were recommended for early intervention in trauma to halt bleeding (Bertram et al. 2009). TiO_2 anatase nanotubes were suggested to control haemorrhage due to their enhanced coagulatory effect (Roy et al. 2007). Structured alignment of nanoparticles can be used to provide superhydrophobicity and thus antithrombotic properties for biomaterials (Sun et al. 2005). MWNT (Meng et al. 2005, Sun et al. 2005) were suggested as antithrombotic coatings for vascular grafts and stents.

Thus in summary, we think that the studies conducted by us and others indicate that some ambient and manufactured nanoparticles have a thrombogenic potential which ultimately may exert detrimental health effects. In contrast, some other nanoparticles do not influence thrombosis or even have antithrombotic properties that might be useful in the development of non- or anti-thrombotic biomaterials. Screening the platelet-dependent prothrombotic potential of manufactured nanoparticles might be carried out with flow cytometry.

DOI:10.14753/SE.2016.1824

VII. Conclusions

1. Optimisation of the nanoparticle dispersion method

To avoid creating coarse agglomerates when preparing dispersion of nanoparticles in physiological solutions, the following aspects were found to be important:

i) Usage of a sonication energy high enough to deagglomerate the particles (>4.2×10^5 kJ/m^3)

ii) Addition of albumin or serum as stabilizers at a concentration sufficient to cover the nanoparticles (1.5 mg/ml HSA or an amount of serum resulting in a similar albumin concentration for dispersions with less than 0.2 mg/ml nanoparticle concentration)

iii) The optimal sequence is first to sonicate the nanoparticles in distilled water, then to add the stabilizer, and finally to add buffered salt solution to the dispersion

2. Optimisation of platelet-granulocyte complex measurement

Based on our findings, we suggest three methods to avoid overestimation of platelet-granulocyte complexes caused by coincidence in the flow cytometer:

i) Calculate coincidence from the detection volume and platelet concentration, and correct the measured platelet-granulocyte double positivity with these data

ii) Measure coincidence by adding fluorescent beads to the blood sample and correct the measured platelet-granulocyte double positivity with these data

iii) Measure platelet-granulocyte complexes at dilutions high enough to render coincidence negligible

3. Prothrombotic effects of nanoparticles

Based on the investigation of ambient and manufactured nanoparticles on platelet activation *in vitro* and on thrombus formation in small arteries and in the microcirculation *in vivo*, we conclude that:

i) Amine-, but not carboxyl-modified polystyrene beads induce activation and aggregation of platelets. Amine-modified polystyrene beads decrease and

carboxyl-modified polystyrene beads increase the time of thrombus formation in small arteries, but neither of them have an impact on thrombus formation in the microcirculation

ii) DEP and TiO_2 (rutile) nanoparticles injected into healthy mice have no effect on platelet activation or thrombus formation

iii) SWNT induces activation and aggregation of platelets

iv) SWNT exerts prothrombotic effects in small arteries as well as in the microcirculation

DOI:10.14753/SE.2016.1824

VIII. Summary

The increasing technological and medical utilisation of manufactured nanoparticles necessitates the assessment of their risk to human health. Although ambient nanoparticles have been shown to exert prothrombotic effects, manufactured nanoparticles have been less well investigated in this regard. Moreover, although nanoparticles can also reach the microcirculation, prothrombotic effects of manufactured nanoparticles in the microvasculature have not been investigated yet. Thus the aim of our study was to characterize the effects of nanoparticles on platelet activation *in vitro* and on macro- and microcirculatory thrombus formation *in vivo*.

In order to carry out our study, two methods, the preparation of particle dispersions and the measurement of platelet-granulocyte complexes, were optimised. To determine the prothrombotic effect of nanoparticles *in vitro,* platelet activation was measured by flow cytometry and aggregometry. *In vivo* thrombus formation was evaluated by intravital microscopy in small mesenteric arteries and in the cremasteric microcirculation of anaesthetised mice.

Amine-modified polystyrene beads and SWNT, but not carboxyl-modified polystyrene beads, DEP, or TiO_2 (rutile) nanoparticles induce platelet activation. Amine-modified polystyrene beads decrease and carboxyl-modified polystyrene beads increase the time of thrombus formation in mesenteric arteries, but neither of them has an impact on thrombus formation in the microcirculation. DEP and TiO_2 (rutile) nanoparticles have no effect on platelet activation or thrombus formation, while SWNT induce activation and aggregation of platelets, and exert prothrombotic effects in mesenteric arteries, as well as in the microcirculation.

Our studies strongly highlight the fact that some nanoparticles are thrombogenic in the macro- as well as in the microcirculation. Since prothrombotic effects cannot be estimated from the physicochemical parameters of the nanoparticles, screening methods would be necessary.

DOI:10.14753/SE.2016.1824

IX. Összefoglalás

A mesterséges nanorészecskék növekvő technológiai és orvosi felhasználása szükségessé teszi ezen anyagok egészségügyi kockázatának felmérését. A környezeti nanorészecskék protrombotikus hatásai ismertek, ugyanakkor a mesterséges nanorészecskék ilyen hatásairól csak kevés adat áll rendelkezésre. Míg a keringésbe bekerülő nanorészecskék a mikrocirkuláció területeire is eljutnak, az itt kifejtett protrombotikus hatásokat még nem vizsgálták. Disszertációm célja ezért a mesterséges nanorészecskék vérlemezkeaktivációra, valamint a makro- és a mikrocirkulációs trombusképződésre kifejtett hatásainak vizsgálata volt.

Mindehhez először két módszertani problémát oldottunk meg: a stabil nanorészecske diszperzió előállítását fiziológiás oldatokban, és a vérlemezke-granulocita komplexek mérésének optimalizálását. A nanorészecskék *in vitro* trombocita aktivációra kifejtett hatásait áramlási citometriával és aggregometriával mértük. Az *in vivo* trombusképződést altatott egerek mesenteriális artériájában és a cremaster izom mikrocirkulációjában intravitális mikroszkópiával vizsgáltuk.

Eredményeink azt mutatják, hogy az amin-módosított polisztirol nanogyöngyök és az egyfalú szén nanocsövek fokozzák a trombociták aktivitását, míg a karboxil-módosított polisztirol nanogyöngyöknek, a dízelpornak és a titán-dioxid (rutil) nanorészecskéknek nincs ilyen hatása. A polisztirol nanogyöngyök amin módosítása csökkenti, míg a karboxil módosítás növeli a trombotikus elzáródás idejét a mesenteriális arteriákban, egyik módosítás sem befolyásolja azonban a mikrocirkulációs trombusképződést. A dízelpornak és a titán-dioxid (rutile) nanorészecskéknek nincs hatása a trombociták aktiválódására és a trombusképződésre, míg az egyfalú szén nanocsövek aktiválják és aggregálják a trombocitákat, valamint fokozzák a trombusképződést a mesenteriális arteriákban és a mikrocirkulációban is.

Vizsgálataink ezek alapján felhívják a figyelmet arra, hogy egyes nanorészecskék mind a makro-, mind a mikrocirkulációban protrombotikus hatással rendelkeznek. Mivel ezek a hatások a nanorészecskék fizikokémiai paramétereiből nem kikövetkeztethetőek, szükség van e hatások szűrésére.

X. References

Andersen ZJ, Olsen TS, Andersen KK, Loft S, Ketzel M, Raaschou-Nielsen O. (2010) Association between short-term exposure to ultrafine particles and hospital admissions for stroke in Copenhagen, Denmark. Eur Heart J, 31(16): 2034-2040.

Andre P, Delaney SM, LaRocca T, Vincent D, DeGuzman F, Jurek M, Koller B, Phillips DR, Conley PB. (2003) P2Y12 regulates platelet adhesion/activation, thrombus growth, and thrombus stability in injured arteries. J Clin Invest, 112(3): 398-406.

Baccarelli A, Martinelli I, Pegoraro V, Melly S, Grillo P, Zanobetti A, Hou L, Bertazzi PA, Mannucci PM, Schwartz J. (2009) Living near major traffic roads and risk of deep vein thrombosis. Circulation, 119(24): 3118-3124.

Baccarelli A, Zanobetti A, Martinelli I, Grillo P, Hou L, Giacomini S, Bonzini M, Lanzani G, Mannucci PM, Bertazzi PA, Schwartz J. (2007) Effects of exposure to air pollution on blood coagulation. J Thromb Haemost, 5(2): 252-260.

Baez S. (1973) An open cremaster muscle preparation for the study of blood vessels by in vivo microscopy. Microvasc Res, 5(3): 384-394.

Barani H, Montazer M. (2008) A review on applications of liposomes in textile processing. J Liposome Res, 18(3): 249-262.

Benz K, Amann K. (2010) Thrombotic microangiopathy: new insights. Current Opinion in Nephrology and Hypertension, 19(3): 242-247.

Bertram JP, Williams CA, Robinson R, Segal SS, Flynn NT, Lavik EB. (2009) Intravenous hemostat: nanotechnology to halt bleeding. Sci Transl Med, 1(11): 11ra22.

Bigert C, Alderling M, Svartengren M, Plato N, de Faire U, Gustavsson P. (2008) Blood markers of inflammation and coagulation and exposure to airborne particles in employees in the Stockholm underground. Occup Environ Med, 65(10): 655-658.

Bihari P, Fent J, Hamar J, Furesz J, Lakatos S. (2008a) An easy-to-use practical method to measure coincidence in the flow cytometer--the case of platelet-granulocyte complex determination. J Biochem Biophys Methods, 70(6): 1080-1085.

Bihari P, Holzer M, Praetner M, Fent J, Lerchenberger M, Reichel CA, Rehberg M, Lakatos S, Krombach F. (2010) Single-walled carbon nanotubes activate

platelets and accelerate thrombus formation in the microcirculation. Toxicology, 269(2-3): 148-154.

Bihari P, Vippola M, Schultes S, Praetner M, Khandoga AG, Reichel CA, Coester C, Tuomi T, Rehberg M, Krombach F. (2008b) Optimized dispersion of nanoparticles for biological in vitro and in vivo studies. Part Fibre Toxicol, 5: 14.

Biju V, Itoh T, Anas A, Sujith A, Ishikawa M. (2008) Semiconductor quantum dots and metal nanoparticles: syntheses, optical properties, and biological applications. Anal Bioanal Chem, 391(7): 2469-2495.

Bonomini M, Sirolli V, Stuard S, Settefrati N. (1999) Interactions between platelets and leukocytes during hemodialysis. Artif Organs, 23(1): 23-28.

Borm PJ, Robbins D, Haubold S, Kuhlbusch T, Fissan H, Donaldson K, Schins R, Stone V, Kreyling W, Lademann J, Krutmann J, Warheit D, Oberdorster E. (2006) The potential risks of nanomaterials: a review carried out for ECETOC. Part Fibre Toxicol, 3: 11.

Brook RD, Franklin B, Cascio W, Hong Y, Howard G, Lipsett M, Luepker R, Mittleman M, Samet J, Smith SC, Jr., Tager I. (2004) Air pollution and cardiovascular disease: a statement for healthcare professionals from the Expert Panel on Population and Prevention Science of the American Heart Association. Circulation, 109(21): 2655-2671.

Brook RD, Rajagopalan S, Pope CA, 3rd, Brook JR, Bhatnagar A, Diez-Roux AV, Holguin F, Hong Y, Luepker RV, Mittleman MA, Peters A, Siscovick D, Smith SC, Jr., Whitsel L, Kaufman JD. (2010) Particulate matter air pollution and cardiovascular disease: An update to the scientific statement from the American Heart Association. Circulation, 121(21): 2331-2378.

Broos K, De Meyer SF, Feys HB, Vanhoorelbeke K, Deckmyn H. (2012) Blood platelet biochemistry. Thromb Res, 129(3): 245-249.

Brouwer D. (2010) Exposure to manufactured nanoparticles in different workplaces. Toxicology, 269(2-3): 120-127.

Budinger GR, McKell JL, Urich D, Foiles N, Weiss I, Chiarella SE, Gonzalez A, Soberanes S, Ghio AJ, Nigdelioglu R, Mutlu EA, Radigan KA, Green D, Kwaan HC, Mutlu GM. (2011) Particulate matter-induced lung inflammation increases

systemic levels of PAI-1 and activates coagulation through distinct mechanisms. PLoS One, 6(4): e18525.

Buford MC, Hamilton RF, Jr., Holian A. (2007) A comparison of dispersing media for various engineered carbon nanoparticles. Part Fibre Toxicol, 4: 6.

Bunescu A, Widman J, Lenkei R, Menyes P, Levin K, Egberg N. (2002) Increases in circulating levels of monocyte-platelet and neutrophil-platelet complexes following hip arthroplasty. Clin Sci (Lond), 102(3): 279-286.

Burda C, Chen X, Narayanan R, El-Sayed MA. (2005) Chemistry and properties of nanocrystals of different shapes. Chem Rev, 105(4): 1025-1102.

Cedervall T, Lynch I, Foy M, Berggard T, Donnelly SC, Cagney G, Linse S, Dawson KA. (2007a) Detailed identification of plasma proteins adsorbed on copolymer nanoparticles. Angew Chem Int Ed Engl, 46(30): 5754-5756.

Cedervall T, Lynch I, Lindman S, Berggard T, Thulin E, Nilsson H, Dawson KA, Linse S. (2007b) Understanding the nanoparticle-protein corona using methods to quantify exchange rates and affinities of proteins for nanoparticles. Proc Natl Acad Sci U S A, 104(7): 2050-2055.

Cerletti C, Tamburrelli C, Izzi B, Gianfagna F, de Gaetano G. (2012) Platelet-leukocyte interactions in thrombosis. Thromb Res, 129(3): 263-266.

Chen Y, Liang H. (2014) Applications of quantum dots with upconverting luminescence in bioimaging. Journal of Photochemistry and Photobiology. B, Biology, 135: 23-32.

Choi HS, Liu W, Misra P, Tanaka E, Zimmer JP, Ipe BI, Bawendi MG, Frangioni JV. (2007) Renal Clearance of Nanoparticles. Nature Biotechnology, 25(10): 1165-1170.

Chuang KJ, Chan CC, Su TC, Lee CT, Tang CS. (2007) The effect of urban air pollution on inflammation, oxidative stress, coagulation, and autonomic dysfunction in young adults. Am J Respir Crit Care Med, 176(4): 370-376.

Clemetson KJ. (2012) Platelets and primary haemostasis. Thromb Res, 129(3): 220-224.

Colvin VL, Kulinowski KM. (2007) Nanoparticles as catalysts for protein fibrillation. Proc Natl Acad Sci U S A, 104(21): 8679-8680.

Conhaim RL, Eaton A, Staub NC, Heath TD. (1988) Equivalent pore estimate for the alveolar-airway barrier in isolated dog lung. J Appl Physiol, 64(3): 1134-1142.

Conner SD, Schmid SL. (2003) Regulated portals of entry into the cell. Nature, 422(6927): 37-44.

Davis ME, Chen ZG, Shin DM. (2008) Nanoparticle therapeutics: an emerging treatment modality for cancer. Nat Rev Drug Discov, 7(9): 771-782.

De Volder MF, Tawfick SH, Baughman RH, Hart AJ. (2013) Carbon nanotubes: present and future commercial applications. Science, 339(6119): 535-539.

Deb S, Patra HK, Lahiri P, Dasgupta AK, Chakrabarti K, Chaudhuri U. (2011) Multistability in platelets and their response to gold nanoparticles. Nanomedicine, 7(4): 376-384.

Deguchi S, Yamazaki T, Mukai SA, Usami R, Horikoshi K. (2007) Stabilization of C60 nanoparticles by protein adsorption and its implications for toxicity studies. Chem Res Toxicol, 20(6): 854-858.

Delfino RJ, Staimer N, Tjoa T, Polidori A, Arhami M, Gillen DL, Kleinman MT, Vaziri ND, Longhurst J, Zaldivar F, Sioutas C. (2008) Circulating biomarkers of inflammation, antioxidant activity, and platelet activation are associated with primary combustion aerosols in subjects with coronary artery disease. Environ Health Perspect, 116(7): 898-906.

Dobrovolskaia MA, McNeil SE. (2007) Immunological properties of engineered nanomaterials. Nat Nanotechnol, 2(8): 469-478.

Dobrovolskaia MA, Patri AK, Zheng J, Clogston JD, Ayub N, Aggarwal P, Neun BW, Hall JB, McNeil SE. (2009) Interaction of colloidal gold nanoparticles with human blood: effects on particle size and analysis of plasma protein binding profiles. Nanomedicine, 5(2): 106-117.

Dockery DW, Pope CA, 3rd, Xu X, Spengler JD, Ware JH, Fay ME, Ferris BG, Jr., Speizer FE. (1993) An association between air pollution and mortality in six U.S. cities. N Engl J Med, 329(24): 1753-1759.

Douglas T, Young M. (2006) Viruses: making friends with old foes. Science, 312(5775): 873-875.

Ekdahl KN, Lambris JD, Elwing H, Ricklin D, Nilsson PH, Teramura Y, Nicholls IA, Nilsson B. (2011) Innate immunity activation on biomaterial surfaces: a

mechanistic model and coping strategies. Adv Drug Deliv Rev, 63(12): 1042-1050.

Elder A, Gelein R, Silva V, Feikert T, Opanashuk L, Carter J, Potter R, Maynard A, Ito Y, Finkelstein J, Oberdorster G. (2006) Translocation of inhaled ultrafine manganese oxide particles to the central nervous system. Environ Health Perspect, 114(8): 1172-1178.

Emmerechts J, Hoylaerts MF. (2012) The effect of air pollution on haemostasis. Hamostaseologie, 32(1): 5-13.

Esmon CT, Esmon NL. (2011) The link between vascular features and thrombosis. Annual Review of Physiology, 73: 503-514.

Fent J, Bihari P, Furesz J, Hamar J, Lakatos S. (2008) Impact of coincidence on granulocyte-platelet complex determination by flow cytometry is evaluated by a novel computer simulation model of coincidence. J Biochem Biophys Methods, 70(6): 1086-1090.

Foley JH, Kim PY, Mutch NJ, Gils A. (2013) Insights into thrombin activatable fibrinolysis inhibitor function and regulation. J Thromb Haemost, 11 Suppl 1: 306-315.

Forestier M, Al-Tamimi M, Gardiner EE, Hermann C, Meyer SC, Beer JH. (2012) Diesel exhaust particles impair platelet response to collagen and are associated with GPIbalpha shedding. Toxicol In Vitro, 26(6): 930-938.

Franchini M, Mannucci PM. (2012) Air pollution and cardiovascular disease. Thromb Res, 129(3): 230-234.

Fuchs TA, Brill A, Wagner DD. (2012) Neutrophil extracellular trap (NET) impact on deep vein thrombosis. Arterioscler Thromb Vasc Biol, 32(8): 1777-1783.

Gando S. (2010) Microvascular thrombosis and multiple organ dysfunction syndrome. Critical Care Medicine, 38(2 Suppl): S35-42.

Geiser M, Kreyling WG. (2010) Deposition and biokinetics of inhaled nanoparticles. Part Fibre Toxicol, 7: 2.

Geiser M, Rothen-Rutishauser B, Kapp N, Schurch S, Kreyling W, Schulz H, Semmler M, Im Hof V, Heyder J, Gehr P. (2005) Ultrafine particles cross cellular membranes by nonphagocytic mechanisms in lungs and in cultured cells. Environ Health Perspect, 113(11): 1555-1560.

Geys J, Nemmar A, Verbeken E, Smolders E, Ratoi M, Hoylaerts MF, Nemery B, Hoet PH. (2008) Acute toxicity and prothrombotic effects of quantum dots: impact of surface charge. Environ Health Perspect, 116(12): 1607-1613.

Gilmour PS, Morrison ER, Vickers MA, Ford I, Ludlam CA, Greaves M, Donaldson K, MacNee W. (2005) The procoagulant potential of environmental particles (PM10). Occup Environ Med, 62(3): 164-171.

Gonzalez L, Lison D, Kirsch-Volders M. (2008) Genotoxicity of engineered nanomaterials: A critical review. Nanotoxicology, 2(4): 252-273.

Gorbet MB, Sefton MV. (2004) Biomaterial-associated thrombosis: roles of coagulation factors, complement, platelets and leukocytes. Biomaterials, 25(26): 5681-5703.

Haberl N, Hirn S, Holzer M, Zuchtriegel G, Rehberg M, Krombach F. (2015) Effects of acute systemic administration of TiO, ZnO, SiO, and Ag nanoparticles on hemodynamics, hemostasis and leukocyte recruitment. Nanotoxicology: 1-9.

Hagberg IA, Lyberg T. (2000) Evaluation of circulating platelet-leukocyte conjugates: a sensitive flow cytometric assay well suited for clinical studies. Platelets, 11(3): 151-160.

Hagens WI, Oomen AG, de Jong WH, Cassee FR, Sips AJ. (2007) What do we (need to) know about the kinetic properties of nanoparticles in the body? Regul Toxicol Pharmacol, 49(3): 217-229.

Hamburger SA, McEver RP. (1990) GMP-140 mediates adhesion of stimulated platelets to neutrophils. Blood, 75(3): 550-554.

Hardman R. (2006) A toxicologic review of quantum dots: toxicity depends on physicochemical and environmental factors. Environ Health Perspect, 114(2): 165-172.

He H, Pham-Huy LA, Dramou P, Xiao D, Zuo P, Pham-Huy C. (2013) Carbon nanotubes: applications in pharmacy and medicine. Biomed Res Int, 2013: 578290.

He X, Zhang H, Ma Y, Bai W, Zhang Z, Lu K, Ding Y, Zhao Y, Chai Z. (2010) Lung deposition and extrapulmonary translocation of nano-ceria after intratracheal instillation. Nanotechnology, 21(28): 285103.

Hermans C, Bernard A. (1999) Lung epithelium-specific proteins: characteristics and potential applications as markers. Am J Respir Crit Care Med, 159(2): 646-678.

Hilscher T (2005). Ultrasonic production of nano-size dispersions and emulsions. Dans European Nano Systems Worshop – ENS 2005. Paris, France.

Hu YL, Gao JQ. (2010) Potential neurotoxicity of nanoparticles. Int J Pharm, 394(1-2): 115-121.

Hudson SP, Padera RF, Langer R, Kohane DS. (2008) The biocompatibility of mesoporous silicates. Biomaterials, 29(30): 4045-4055.

Ito A, Shinkai M, Honda H, Kobayashi T. (2005) Medical application of functionalized magnetic nanoparticles. J Biosci Bioeng, 100(1): 1-11.

Ittrich H, Peldschus K, Raabe N, Kaul M, Adam G. (2013) Superparamagnetic iron oxide nanoparticles in biomedicine: applications and developments in diagnostics and therapy. Rofo, 185(12): 1149-1166.

Jackson SP. (2007) The growing complexity of platelet aggregation. Blood, 109(12): 5087-5095.

Jackson SP, Mistry N, Yuan Y. (2000) Platelets and the injured vessel wall-- "rolling into action": focus on glycoprotein Ib/V/IX and the platelet cytoskeleton. Trends in Cardiovascular Medicine, 10(5): 192-197.

Jani P, Halbert GW, Langridge J, Florence AT. (1990) Nanoparticle uptake by the rat gastrointestinal mucosa: quantitation and particle size dependency. J Pharm Pharmacol, 42(12): 821-826.

Jensen MK, de Nully Brown P, Lund BV, Nielsen OJ, Hasselbalch HC. (2001) Increased circulating platelet-leukocyte aggregates in myeloproliferative disorders is correlated to previous thrombosis, platelet activation and platelet count. Eur J Haematol, 66(3): 143-151.

Jokerst JV, Lobovkina T, Zare RN, Gambhir SS. (2011) Nanoparticle PEGylation for imaging and therapy. Nanomedicine (Lond), 6(4): 715-728.

Juzenas P, Chen W, Sun YP, Coelho MA, Generalov R, Generalova N, Christensen IL. (2008) Quantum dots and nanoparticles for photodynamic and radiation therapies of cancer. Adv Drug Deliv Rev, 60(15): 1600-1614.

Keij JF, van Rotterdam A, Groenewegen AC, Stokdijk W, Visser JW. (1991) Coincidence in high-speed flow cytometry: models and measurements. Cytometry, 12(5): 398-404.

Khandoga A, Stampfl A, Takenaka S, Schulz H, Radykewicz R, Kreyling W, Krombach F. (2004) Ultrafine particles exert prothrombotic but not inflammatory effects on the hepatic microcirculation in healthy mice in vivo. Circulation, 109(10): 1320-1325.

Khandoga A, Stoeger T, Khandoga AG, Bihari P, Karg E, Ettehadieh D, Lakatos S, Fent J, Schulz H, Krombach F. (2010) Platelet adhesion and fibrinogen deposition in murine microvessels upon inhalation of nanosized carbon particles. J Thromb Haemost, 8(7): 1632-1640.

Kilinc E, Van Oerle R, Borissoff JI, Oschatz C, Gerlofs-Nijland ME, Janssen NA, Cassee FR, Sandstrom T, Renne T, Ten Cate H, Spronk HM. (2011) Factor XII activation is essential to sustain the procoagulant effects of particulate matter. J Thromb Haemost, 9(7): 1359-1367.

Kim H, Oh SJ, Kwak HC, Kim JK, Lim CH, Yang JS, Park K, Kim SK, Lee MY. (2012) The impact of intratracheally instilled carbon black on the cardiovascular system of rats: elevation of blood homocysteine and hyperactivity of platelets. J Toxicol Environ Health A, 75(24): 1471-1483.

Kis A, Zettl A. (2008) Nanomechanics of carbon nanotubes. Philosophical Transactions of the Royal Society A: Mathematical, Physical and Engineering Sciences, 366(1870): 1591-1611.

Kreuter J. (2001) Nanoparticulate systems for brain delivery of drugs. Adv Drug Deliv Rev, 47(1): 65-81.

Kreyling WG, Semmler M, Erbe F, Mayer P, Takenaka S, Schulz H, Oberdorster G, Ziesenis A. (2002) Translocation of ultrafine insoluble iridium particles from lung epithelium to extrapulmonary organs is size dependent but very low. J Toxicol Environ Health A, 65(20): 1513-1530.

Landsiedel R, Fabian E, Ma-Hock L, van Ravenzwaay B, Wohlleben W, Wiench K, Oesch F. (2012) Toxico-/biokinetics of nanomaterials. Archives of Toxicology, 86(7): 1021-1060.

Lewinski N, Colvin V, Drezek R. (2008) Cytotoxicity of nanoparticles. Small, 4(1): 26-49.

Ley K. The Microcirculation in Inflammation, Comprehensive Physiology. John Wiley & Sons, Inc., 2011.

Li N, Goodall AH, Hjemdahl P. (1999) Efficient flow cytometric assay for platelet-leukocyte aggregates in whole blood using fluorescence signal triggering. Cytometry, 35(2): 154-161.

Li N, Xia T, Nel AE. (2008) The role of oxidative stress in ambient particulate matter-induced lung diseases and its implications in the toxicity of engineered nanoparticles. Free Radic Biol Med, 44(9): 1689-1699.

Li Z, Delaney MK, O'Brien KA, Du X. (2010) Signaling during platelet adhesion and activation. Arterioscler Thromb Vasc Biol, 30(12): 2341-2349.

Lindman S, Lynch I, Thulin E, Nilsson H, Dawson KA, Linse S. (2007) Systematic investigation of the thermodynamics of HSA adsorption to N-iso-propylacrylamide/N-tert-butylacrylamide copolymer nanoparticles. Effects of particle size and hydrophobicity. Nano Lett, 7(4): 914-920.

Linse S, Cabaleiro-Lago C, Xue WF, Lynch I, Lindman S, Thulin E, Radford SE, Dawson KA. (2007) Nucleation of protein fibrillation by nanoparticles. Proc Natl Acad Sci U S A, 104(21): 8691-8696.

Lipka J, Semmler-Behnke M, Sperling RA, Wenk A, Takenaka S, Schleh C, Kissel T, Parak WJ, Kreyling WG. (2010) Biodistribution of PEG-modified gold nanoparticles following intratracheal instillation and intravenous injection. Biomaterials, 31(25): 6574-6581.

Lomer MC, Thompson RP, Powell JJ. (2002) Fine and ultrafine particles of the diet: influence on the mucosal immune response and association with Crohn's disease. Proc Nutr Soc, 61(1): 123-130.

Longmire M, Choyke PL, Kobayashi H. (2008) Clearance properties of nano-sized particles and molecules as imaging agents: considerations and caveats. Nanomedicine (Lond), 3(5): 703-717.

Lu AH, Salabas EL, Schuth F. (2007) Magnetic nanoparticles: synthesis, protection, functionalization, and application. Angew Chem Int Ed Engl, 46(8): 1222-1244.

Lucking AJ, Lundback M, Mills NL, Faratian D, Barath SL, Pourazar J, Cassee FR, Donaldson K, Boon NA, Badimon JJ, Sandstrom T, Blomberg A, Newby DE. (2008) Diesel exhaust inhalation increases thrombus formation in man. Eur Heart J, 29(24): 3043-3051.

Lundqvist M, Stigler J, Elia G, Lynch I, Cedervall T, Dawson KA. (2008) Nanoparticle size and surface properties determine the protein corona with possible implications for biological impacts. Proc Natl Acad Sci U S A, 105(38): 14265-14270.

Lynch I, Dawson KA. (2008) Protein-nanoparticle interactions. Nano Today, 3(1): 40-47.

Lynch I, Salvati A, Dawson KA. (2009) Protein-nanoparticle interactions: What does the cell see? Nat Nanotechnol, 4(9): 546-547.

Maas C, Renne T. (2012) Regulatory mechanisms of the plasma contact system. Thromb Res, 129 Suppl 2: S73-76.

Machovich R. A véralvadási-fibrinolitikus rendszer. In: Boda Z (Editor), Thrombosis és vérzékenység. Medicina, Budapest, 2006: 1-23.

Maehara T, Eda Y, Mitani K, Matsuzawa S. (1990) Glycidyl methacrylate-styrene copolymer latex particles for immunologic agglutination tests. Biomaterials, 11(2): 122-126.

Mandzy N, Grulke E, Druffel T. (2005) Breakage of TiO2 agglomerates in electrostatically stabilized aqueous dispersions. Powder Technology, 160(2): 121-126.

Markiewski MM, Nilsson B, Ekdahl KN, Mollnes TE, Lambris JD. (2007) Complement and coagulation: strangers or partners in crime? Trends Immunol, 28(4): 184-192.

May AE, Langer H, Seizer P, Bigalke B, Lindemann S, Gawaz M. (2007) Platelet-leukocyte interactions in inflammation and atherothrombosis. Seminars in Thrombosis and Hemostasis, 33(2): 123-127.

Mayer A, Vadon M, Rinner B, Novak A, Wintersteiger R, Frohlich E. (2009) The role of nanoparticle size in hemocompatibility. Toxicology, 258(2-3): 139-147.

Maynard A, Rejeski D. (2009) Too small to overlook. Nature, 460(7252): 174.

Maynard AD, Aitken RJ, Butz T, Colvin V, Donaldson K, Oberdorster G, Philbert MA, Ryan J, Seaton A, Stone V, Tinkle SS, Tran L, Walker NJ, Warheit DB. (2006) Safe handling of nanotechnology. Nature, 444(7117): 267-269.

Maynard AD, Baron PA, Foley M, Shvedova AA, Kisin ER, Castranova V. (2004) Exposure to carbon nanotube material: aerosol release during the handling of

unrefined single-walled carbon nanotube material. J Toxicol Environ Health A, 67(1): 87-107.

McGuinnes C, Duffin R, Brown S, N LM, Megson IL, Macnee W, Johnston S, Lu SL, Tran L, Li R, Wang X, Newby DE, Donaldson K. (2011) Surface derivatization state of polystyrene latex nanoparticles determines both their potency and their mechanism of causing human platelet aggregation in vitro. Toxicol Sci, 119(2): 359-368.

Meng J, Kong H, Xu HY, Song L, Wang CY, Xie SS. (2005) Improving the blood compatibility of polyurethane using carbon nanotubes as fillers and its implications to cardiovascular surgery. J Biomed Mater Res A, 74(2): 208-214.

Mickelson JK, Lakkis NM, Villarreal-Levy G, Hughes BJ, Smith CW. (1996) Leukocyte activation with platelet adhesion after coronary angioplasty: a mechanism for recurrent disease? J Am Coll Cardiol, 28(2): 345-353.

Miller VM, Hunter LW, Chu K, Kaul V, Squillace PD, Lieske JC, Jayachandran M. (2009) Biologic nanoparticles and platelet reactivity. Nanomedicine (Lond), 4(7): 725-733.

Mills NL, Donaldson K, Hadoke PW, Boon NA, MacNee W, Cassee FR, Sandstrom T, Blomberg A, Newby DE. (2009) Adverse cardiovascular effects of air pollution. Nat Clin Pract Cardiovasc Med, 6(1): 36-44.

Mills NL, Tornqvist H, Gonzalez MC, Vink E, Robinson SD, Soderberg S, Boon NA, Donaldson K, Sandstrom T, Blomberg A, Newby DE. (2007) Ischemic and thrombotic effects of dilute diesel-exhaust inhalation in men with coronary heart disease. N Engl J Med, 357(11): 1075-1082.

Mills NL, Tornqvist H, Robinson SD, Gonzalez M, Darnley K, MacNee W, Boon NA, Donaldson K, Blomberg A, Sandstrom T, Newby DE. (2005) Diesel exhaust inhalation causes vascular dysfunction and impaired endogenous fibrinolysis. Circulation, 112(25): 3930-3936.

Mortensen LJ, Oberdorster G, Pentland AP, Delouise LA. (2008) In vivo skin penetration of quantum dot nanoparticles in the murine model: the effect of UVR. Nano Lett, 8(9): 2779-2787.

Mota LC, Urena-Benavides EE, Yoon Y, Son A. (2013) Quantitative detection of single walled carbon nanotube in water using DNA and magnetic fluorescent spheres. Environ Sci Technol, 47(1): 493-501.

Müller RH. Zetapotential und Partikelladung in der Laborpraxis, 1996.

Murdock RC, Braydich-Stolle L, Schrand AM, Schlager JJ, Hussain SM. (2008) Characterization of nanomaterial dispersion in solution prior to in vitro exposure using dynamic light scattering technique. Toxicol Sci, 101(2): 239-253.

Mutlu GM, Green D, Bellmeyer A, Baker CM, Burgess Z, Rajamannan N, Christman JW, Foiles N, Kamp DW, Ghio AJ, Chandel NS, Dean DA, Sznajder JI, Budinger GR. (2007) Ambient particulate matter accelerates coagulation via an IL-6-dependent pathway. J Clin Invest, 117(10): 2952-2961.

Naota M, Shimada A, Morita T, Inoue K, Takano H. (2009) Translocation pathway of the intratracheally instilled C60 fullerene from the lung into the blood circulation in the mouse: possible association of diffusion and caveolae-mediated pinocytosis. Toxicol Pathol, 37(4): 456-462.

Nel A, Xia T, Madler L, Li N. (2006) Toxic potential of materials at the nanolevel. Science, 311(5761): 622-627.

Nel AE, Madler L, Velegol D, Xia T, Hoek EM, Somasundaran P, Klaessig F, Castranova V, Thompson M. (2009) Understanding biophysicochemical interactions at the nano-bio interface. Nat Mater, 8(7): 543-557.

Nemmar A, Al-Maskari S, Ali BH, Al-Amri IS. (2007) Cardiovascular and lung inflammatory effects induced by systemically administered diesel exhaust particles in rats. Am J Physiol Lung Cell Mol Physiol, 292(3): L664-670.

Nemmar A, Al-Salam S, Zia S, Dhanasekaran S, Shudadevi M, Ali BH. (2010) Time-course effects of systemically administered diesel exhaust particles in rats. Toxicol Lett, 194(3): 58-65.

Nemmar A, Hoet PH, Dinsdale D, Vermylen J, Hoylaerts MF, Nemery B. (2003a) Diesel exhaust particles in lung acutely enhance experimental peripheral thrombosis. Circulation, 107(8): 1202-1208.

Nemmar A, Hoet PH, Vanquickenborne B, Dinsdale D, Thomeer M, Hoylaerts MF, Vanbilloen H, Mortelmans L, Nemery B. (2002a) Passage of inhaled particles into the blood circulation in humans. Circulation, 105(4): 411-414.

Nemmar A, Hoet PH, Vermylen J, Nemery B, Hoylaerts MF. (2004) Pharmacological stabilization of mast cells abrogates late thrombotic events induced by diesel exhaust particles in hamsters. Circulation, 110(12): 1670-1677.

Nemmar A, Hoylaerts MF, Hoet PH, Dinsdale D, Smith T, Xu H, Vermylen J, Nemery B. (2002b) Ultrafine particles affect experimental thrombosis in an in vivo hamster model. Am J Respir Crit Care Med, 166(7): 998-1004.

Nemmar A, Hoylaerts MF, Hoet PH, Vermylen J, Nemery B. (2003b) Size effect of intratracheally instilled particles on pulmonary inflammation and vascular thrombosis. Toxicol Appl Pharmacol, 186(1): 38-45.

Nemmar A, Melghit K, Ali BH. (2008) The acute proinflammatory and prothrombotic effects of pulmonary exposure to rutile TiO2 nanorods in rats. Exp Biol Med (Maywood), 233(5): 610-619.

Nemmar A, Nemery B, Hoet PH, Vermylen J, Hoylaerts MF. (2003c) Pulmonary inflammation and thrombogenicity caused by diesel particles in hamsters: role of histamine. Am J Respir Crit Care Med, 168(11): 1366-1372.

Nemmar A, Vanbilloen H, Hoylaerts MF, Hoet PH, Verbruggen A, Nemery B. (2001) Passage of intratracheally instilled ultrafine particles from the lung into the systemic circulation in hamster. Am J Respir Crit Care Med, 164(9): 1665-1668.

Nohynek GJ, Antignac E, Re T, Toutain H. (2010) Safety assessment of personal care products/cosmetics and their ingredients. Toxicol Appl Pharmacol, 243(2): 239-259.

Nohynek GJ, Dufour EK, Roberts MS. (2008) Nanotechnology, cosmetics and the skin: is there a health risk? Skin Pharmacol Physiol, 21(3): 136-149.

Nohynek GJ, Lademann J, Ribaud C, Roberts MS. (2007) Grey goo on the skin? Nanotechnology, cosmetic and sunscreen safety. Crit Rev Toxicol, 37(3): 251-277.

Nuyttens BP, Thijs T, Deckmyn H, Broos K. (2011) Platelet adhesion to collagen. Thromb Res, 127 Suppl 2: S26-29.

Oberdorster G. (2001) Pulmonary effects of inhaled ultrafine particles. Int Arch Occup Environ Health, 74(1): 1-8.

Oberdorster G, Maynard A, Donaldson K, Castranova V, Fitzpatrick J, Ausman K, Carter J, Karn B, Kreyling W, Lai D, Olin S, Monteiro-Riviere N, Warheit D,

Yang H. (2005a) Principles for characterizing the potential human health effects from exposure to nanomaterials: elements of a screening strategy. Part Fibre Toxicol, 2: 8.

Oberdorster G, Oberdorster E, Oberdorster J. (2005b) Nanotoxicology: an emerging discipline evolving from studies of ultrafine particles. Environ Health Perspect, 113(7): 823-839.

Pekkanen J, Brunner EJ, Anderson HR, Tiittanen P, Atkinson RW. (2000) Daily concentrations of air pollution and plasma fibrinogen in London. Occup Environ Med, 57(12): 818-822.

Peters A, Dockery DW, Muller JE, Mittleman MA. (2001) Increased particulate air pollution and the triggering of myocardial infarction. Circulation, 103(23): 2810-2815.

Peters A, von Klot S, Heier M, Trentinaglia I, Hormann A, Wichmann HE, Lowel H. (2004) Exposure to traffic and the onset of myocardial infarction. N Engl J Med, 351(17): 1721-1730.

Peters MJ, Dixon G, Kotowicz KT, Hatch DJ, Heyderman RS, Klein NJ. (1999) Circulating platelet-neutrophil complexes represent a subpopulation of activated neutrophils primed for adhesion, phagocytosis and intracellular killing. Br J Haematol, 106(2): 391-399.

Peters MJ, Heyderman RS, Hatch DJ, Klein NJ. (1997) Investigation of platelet-neutrophil interactions in whole blood by flow cytometry. J Immunol Methods, 209(2): 125-135.

Pitchford SC, Yano H, Lever R, Riffo-Vasquez Y, Ciferri S, Rose MJ, Giannini S, Momi S, Spina D, O'Connor B, Gresele P, Page CP. (2003) Platelets are essential for leukocyte recruitment in allergic inflammation. J Allergy Clin Immunol, 112(1): 109-118.

Pohl M, Hogekamp S, Hoffmann NQ, Schuchmann HP. (2004) Dispergieren und Desagglomerieren von Nanopartikeln mit Ultraschall. Chemie Ingenieur Technik, 76(4): 392-396.

Poland CA, Duffin R, Kinloch I, Maynard A, Wallace WA, Seaton A, Stone V, Brown S, Macnee W, Donaldson K. (2008) Carbon nanotubes introduced into the

abdominal cavity of mice show asbestos-like pathogenicity in a pilot study. Nat Nanotechnol, 3(7): 423-428.

Pope CA, 3rd, Burnett RT, Thun MJ, Calle EE, Krewski D, Ito K, Thurston GD. (2002) Lung cancer, cardiopulmonary mortality, and long-term exposure to fine particulate air pollution. JAMA, 287(9): 1132-1141.

Pope CA, 3rd, Burnett RT, Thurston GD, Thun MJ, Calle EE, Krewski D, Godleski JJ. (2004) Cardiovascular mortality and long-term exposure to particulate air pollution: epidemiological evidence of general pathophysiological pathways of disease. Circulation, 109(1): 71-77.

Pope CA, 3rd, Dockery DW. (2006) Health effects of fine particulate air pollution: lines that connect. J Air Waste Manag Assoc, 56(6): 709-742.

Powers KW, Brown SC, Krishna VB, Wasdo SC, Moudgil BM, Roberts SM. (2006) Research strategies for safety evaluation of nanomaterials. Part VI. Characterization of nanoscale particles for toxicological evaluation. Toxicol Sci, 90(2): 296-303.

Praetner M, Rehberg M, Bihari P, Lerchenberger M, Uhl B, Holzer M, Eichhorn ME, Furst R, Perisic T, Reichel CA, Welsch U, Krombach F. (2010) The contribution of the capillary endothelium to blood clearance and tissue deposition of anionic quantum dots in vivo. Biomaterials, 31(26): 6692-6700.

Radomski A, Jurasz P, Alonso-Escolano D, Drews M, Morandi M, Malinski T, Radomski MW. (2005) Nanoparticle-induced platelet aggregation and vascular thrombosis. Br J Pharmacol, 146(6): 882-893.

Ray MR, Mukherjee S, Roychoudhury S, Bhattacharya P, Banerjee M, Siddique S, Chakraborty S, Lahiri T. (2006) Platelet activation, upregulation of CD11b/ CD18 expression on leukocytes and increase in circulating leukocyte-platelet aggregates in Indian women chronically exposed to biomass smoke. Hum Exp Toxicol, 25(11): 627-635.

Roy SC, Paulose M, Grimes CA. (2007) The effect of TiO2 nanotubes in the enhancement of blood clotting for the control of hemorrhage. Biomaterials, 28(31): 4667-4672.

Ruckerl R, Phipps RP, Schneider A, Frampton M, Cyrys J, Oberdorster G, Wichmann HE, Peters A. (2007) Ultrafine particles and platelet activation in patients with

coronary heart disease--results from a prospective panel study. Part Fibre Toxicol, 4: 1.

Ruggeri ZM. (2002) Platelets in atherothrombosis. Nat Med, 8(11): 1227-1234.

Rumbaut RE, Bellera RV, Randhawa JK, Shrimpton CN, Dasgupta SK, Dong JF, Burns AR. (2006) Endotoxin enhances microvascular thrombosis in mouse cremaster venules via a TLR4-dependent, neutrophil-independent mechanism. Am J Physiol Heart Circ Physiol, 290(4): H1671-1679.

Sager TM, Porter DW, Robinson VA, Lindsley WG, Schwegler-Berry DE, Castranova V. (2007) Improved method to disperse nanoparticles for in vitro and in vivo investigation of toxicity. Nanotoxicology, 1(2): 118-129.

Saha K, Bajaj A, Duncan B, Rotello VM. (2011) Beauty is Skin Deep: A Surface Monolayer Perspective on Nanoparticle Interactions with Cells and Bio-macromolecules. Small, 7(14): 1903-1918.

Sahli H, Tapon-Bretaudiere J, Fischer AM, Sternberg C, Spenlehauer G, Verrecchia T, Labarre D. (1997) Interactions of poly(lactic acid) and poly(lactic acid-co-ethylene oxide) nanoparticles with the plasma factors of the coagulation system. Biomaterials, 18(4): 281-288.

Salata O. (2004) Applications of nanoparticles in biology and medicine. J Nanobiotechnology, 2(1): 3.

Samoli E, Peng R, Ramsay T, Pipikou M, Touloumi G, Dominici F, Burnett R, Cohen A, Krewski D, Samet J, Katsouyanni K. (2008) Acute effects of ambient particulate matter on mortality in Europe and North America: results from the APHENA study. Environ Health Perspect, 116(11): 1480-1486.

Schaller J, Gerber SS. (2011) The plasmin-antiplasmin system: structural and functional aspects. Cell Mol Life Sci, 68(5): 785-801.

Semberova J, De Paoli Lacerda SH, Simakova O, Holada K, Gelderman MP, Simak J. (2009) Carbon nanotubes activate blood platelets by inducing extracellular Ca2+ influx sensitive to calcium entry inhibitors. Nano Lett, 9(9): 3312-3317.

Semeraro N, Ammollo CT, Semeraro F, Colucci M. (2012) Sepsis, thrombosis and organ dysfunction. Thromb Res, 129(3): 290-295.

Shimada A, Kawamura N, Okajima M, Kaewamatawong T, Inoue H, Morita T. (2006) Translocation pathway of the intratracheally instilled ultrafine particles from the lung into the blood circulation in the mouse. Toxicol Pathol, 34(7): 949-957.

Shrivastava S, Bera T, Singh SK, Singh G, Ramachandrarao P, Dash D. (2009) Characterization of antiplatelet properties of silver nanoparticles. ACS Nano, 3(6): 1357-1364.

Shrivastava S, Singh SK, Mukhopadhyay A, Sinha AS, Mandal RK, Dash D. (2011) Negative regulation of fibrin polymerization and clot formation by nanoparticles of silver. Colloids Surf B Biointerfaces, 82(1): 241-246.

Silva VM, Corson N, Elder A, Oberdorster G. (2005) The rat ear vein model for investigating in vivo thrombogenicity of ultrafine particles (UFP). Toxicol Sci, 85(2): 983-989.

Simkhovich BZ, Kleinman MT, Kloner RA. (2008) Air pollution and cardiovascular injury epidemiology, toxicology, and mechanisms. J Am Coll Cardiol, 52(9): 719-726.

Singh N, Manshian B, Jenkins GJ, Griffiths SM, Williams PM, Maffeis TG, Wright CJ, Doak SH. (2009) NanoGenotoxicology: the DNA damaging potential of engineered nanomaterials. Biomaterials, 30(23-24): 3891-3914.

Snow C. (2004) Flow cytometer electronics. Cytometry A, 57(2): 63-69.

Stewart JC, Chalupa DC, Devlin RB, Frasier LM, Huang LS, Little EL, Lee SM, Phipps RP, Pietropaoli AP, Taubman MB, Utell MJ, Frampton MW. (2010) Vascular effects of ultrafine particles in persons with type 2 diabetes. Environ Health Perspect, 118(12): 1692-1698.

Su TC, Chan CC, Liau CS, Lin LY, Kao HL, Chuang KJ. (2006) Urban air pollution increases plasma fibrinogen and plasminogen activator inhibitor-1 levels in susceptible patients. Eur J Cardiovasc Prev Rehabil, 13(5): 849-852.

Sun Q, Yue P, Kirk RI, Wang A, Moatti D, Jin X, Lu B, Schecter AD, Lippmann M, Gordon T, Chen LC, Rajagopalan S. (2008) Ambient air particulate matter exposure and tissue factor expression in atherosclerosis. Inhal Toxicol, 20(2): 127-137.

Sun T, Tan H, Han D, Fu Q, Jiang L. (2005) No platelet can adhere--largely improved blood compatibility on nanostructured superhydrophobic surfaces. Small, 1(10): 959-963.

Tanaka KA, Key NS, Levy JH. (2009) Blood coagulation: hemostasis and thrombin regulation. Anesthesia and Analgesia, 108(5): 1433-1446.

Tavano R, Segat D, Reddi E, Kos J, Rojnik M, Kocbek P, Iratni S, Scheglmann D, Colucci M, Echevarria IM, Selvestrel F, Mancin F, Papini E. (2010) Procoagulant properties of bare and highly PEGylated vinyl-modified silica nanoparticles. Nanomedicine (Lond), 5(6): 881-896.

Totani L, Evangelista V. (2010) Platelet-leukocyte interactions in cardiovascular disease and beyond. Arterioscler Thromb Vasc Biol, 30(12): 2357-2361.

Uchida M, Klem MT, Allen M, Suci P, Flenniken M, Gillitzer E, Varpness Z, Liepold LO, Young M, Douglas T. (2007) Biological Containers: Protein Cages as Multifunctional Nanoplatforms. Advanced Materials, 19(8): 1025-1042.

Varga-Szabo D, Pleines I, Nieswandt B. (2008) Cell adhesion mechanisms in platelets. Arterioscler Thromb Vasc Biol, 28(3): 403-412.

Verma A, Stellacci F. (2010) Effect of surface properties on nanoparticle-cell interactions. Small, 6(1): 12-21.

Vogler EA, Siedlecki CA. (2009) Contact activation of blood-plasma coagulation. Biomaterials, 30(10): 1857-1869.

Wang B, Zhang L, Bae SC, Granick S. (2008) Nanoparticle-induced surface reconstruction of phospholipid membranes. Proc Natl Acad Sci U S A, 105(47): 18171-18175.

Weir A, Westerhoff P, Fabricius L, Hristovski K, von Goetz N. (2012) Titanium dioxide nanoparticles in food and personal care products. Environ Sci Technol, 46(4): 2242-2250.

Wilder JWG, Venema LC, Rinzler AG, Smalley RE, Dekker C. (1998) Electronic structure of atomically resolved carbon nanotubes. Nature, 391(6662): 59-62.

Xia T, Kovochich M, Liong M, Zink JI, Nel AE. (2008) Cationic polystyrene nanosphere toxicity depends on cell-specific endocytic and mitochondrial injury pathways. ACS Nano, 2(1): 85-96.

Yu M, Mo Y, Wan R, Chien S, Zhang X, Zhang Q. (2010) Regulation of plasminogen activator inhibitor-1 expression in endothelial cells with exposure to metal nanoparticles. Toxicol Lett, 195(1): 82-89.

Zhang L, Gu FX, Chan JM, Wang AZ, Langer RS, Farokhzad OC. (2008) Nanoparticles in medicine: therapeutic applications and developments. Clinical Pharmacology and Therapeutics, 83(5): 761-769.

Zhao F, Zhao Y, Liu Y, Chang X, Chen C. (2011) Cellular uptake, intracellular trafficking, and cytotoxicity of nanomaterials. Small, 7(10): 1322-1337.

Zhu Y, Hinds WC, Kim S, Sioutas C. (2002) Concentration and size distribution of ultrafine particles near a major highway. J Air Waste Manag Assoc, 52(9): 1032-1042.

DOI:10.14753/SE.2016.1824

XI. Publications

Publications used in the dissertation

1. **Bihari P**, Holzer M, Praetner M, Fent J, Lerchenberger M, Reichel CA, Rehberg M, Lakatos S, Krombach F. (2010) Single-walled carbon nanotubes activate platelets and accelerate thrombus formation in the microcirculation. Toxicology, 269(2-3):148-54. (IF: 3.641)
2. **Bihari P**, Vippola M, Schultes S, Praetner M, Khandoga AG, Reichel CA, Coester C, Tuomi T, Rehberg M, Krombach F. (2008) Optimized dispersion of nanoparticles for biological in vitro and in vivo studies. Part Fibre Toxicol, 5:14. (IF: no impact factor in 2008)
3. **Bihari P**, Fent J, Hamar J, Furész J, Lakatos S. (2008) An easy-to-use practical method to measure coincidence in the flow cytometer – the case of platelet-granulocyte complex determination. J Biochem Biophys Methods, 70(6):1080-5. (IF: 1.994; equal contribution with Fent J.)

Other publications

4. Holzer M, **Bihari P**, Praetner M, Uhl B, Reichel C, Fent J, Vippola M, Lakatos S, Krombach F. (2014) Carbon-based nanomaterials accelerate arteriolar thrombus formation in the murine microcirculation independently of their shape. J Appl Toxicol, 34(11):1167-76. (IF: 3.174)
5. Karatolios K, Wittek A, Nwe TH, **Bihari P**, Shelke A, Josef D, Schmitz-Rixen T, Geks J, Maisch B, Blase C, Moosdorf R, Vogt S. (2013) Method for aortic wall strain measurement with three-dimensional ultrasound speckle tracking and fitted finite element analysis. Ann Thorac Surg, 96(5):1664-71. (IF: 3.631)
6. Wittek A, Karatolios K, **Bihari P**, Schmitz-Rixen T, Moosdorf R, Vogt S, Blase C. (2013) In vivo determination of elastic properties of the human aorta based on 4D ultrasound data. J Mech Behav Biomed Mater, 27:167-83. (IF: 3.048)
7. **Bihari P**, Shelke A, Nwe TH, Mularczyk M, Nelson K, Schmandra T, Knez P, Schmitz-Rixen T. (2013) Strain measurement of abdominal aortic aneurysm

with real-time 3D ultrasound speckle tracking. Eur J Vasc Endovasc Surg, 45(4):315-23. (IF: 3.070)

8. Bubik MF, Willer EA, **Bihari P**, Jürgenliemk G, Ammer H, Krombach F, Zahler S, Vollmar AM, Fürst R. (2012) A novel approach to prevent endothelial hyperpermeability: the Crataegus extract WS® 1442 targets the cAMP/Rap1 pathway. J Mol Cell Cardiol, 52(1):196-205. (IF: 5.148)
9. Bihari I, Tornoci L, **Bihari P**. (2012) Epidemiological study on varicose veins in Budapest. Phlebology, 27(2):77-81. (IF: 1.458)
10. Rehberg M, Praetner M, Leite CF, Reichel CA, **Bihari P**, Mildner K, Duhr S, Zeuschner D, Krombach F. (2010) Quantum dots modulate leukocyte adhesion and transmigration depending on their surface modification. Nano Lett, 10(9):3656-64. (IF: 12.186)
11. Praetner M, Rehberg M, **Bihari P**, Lerchenberger M, Uhl B, Holzer M, Eichhorn ME, Fürst R, Perisic T, Reichel CA, Welsch U, Krombach F. (2010) The contribution of the capillary endothelium to blood clearance and tissue deposition of anionic quantum dots in vivo. Biomaterials, 31(26):6692-700. (IF: 7.882)
12. Khandoga A, Stoeger T, Khandoga AG, **Bihari P**, Karg E, Ettehadieh D, Lakatos S, Fent J, Schulz H, Krombach F. (2010) Platelet adhesion and fibrinogen deposition in murine microvessels upon inhalation of nanosized carbon particles. J Thromb Haemost, 8(7):1632-40. (IF: 5.439)
13. Tasnádi G, Bihari I, **Bihari P**. (2010) Peritoneo-venous shunt implantation as a therapy for chylous ascites. Phlebologie, 39: 24-27. (IF: 0.733)
14. Reichel CA, Rehberg M, Lerchenberger M, Berberich N, **Bihari P**, Khandoga AG, Zahler S, Krombach F. (2009) Ccl2 and Ccl3 mediate neutrophil recruitment via induction of protein synthesis and generation of lipid mediators. Arterioscler Thromb Vasc Biol, 29(11):1787-93. (IF: 7.235)
15. Khandoga AG, Khandoga A, Reichel CA, **Bihari P**, Rehberg M, Krombach F. (2009) In vivo imaging and quantitative analysis of leukocyte directional migration and polarization in inflamed tissue. PLoS One, 4(3):e4693. (IF: 4.351)
16. Fürst R, Bubik MF, **Bihari P**, Mayer BA, Khandoga AG, Hoffmann F, Rehberg M, Krombach F, Zahler S, Vollmar AM. (2008) Atrial natriuretic peptide

protects against histamine-induced endothelial barrier dysfunction in vivo. Mol Pharmacol, 74(1):1-8. (IF: 4.711)

17. Reichel CA, Rehberg M, **Bihari P**, Moser CM, Linder S, Khandoga A, Krombach F. (2008) Gelatinases mediate neutrophil recruitment in vivo: evidence for stimulus specificity and a critical role in collagen IV remodeling. J Leukoc Biol, 83(4):864-74. (IF: 4.605)
18. Fent J, **Bihari P**, Furész J, Hamar J, Lakatos S. (2008) Impact of coincidence on granulocyte-platelet complex determination by flow cytometry is evaluated by a novel computer simulation model of coincidence. J Biochem Biophys Methods, 70(6):1086-90. (IF: 1.994)
19. Bihari I, Muranyi A, **Bihari P**. (2005) Laser-doppler examination shows high flow in some common telangiectasias of the lower limb. Dermatol Surg, 31(4):388-90. (IF: 2.254)
20. Bihari I, Tasnádi G, **Bihari P**. (2003) Importance of subfascial collaterals in deep-vein malformations. Dermatol Surg, 29(2):146-9. (IF: 1.806)

Hungarian publications

21. Bihari I, Tornóczi L, **Bihari P**. (2002) Alsó végtagi varicositas hazai epidemiológiai felmérése. [Epidemiological study on chronic venous insufficiency in Hungary]. Érbetegségek, 2:57-62. (IF: no impact factor)

DOI:10.14753/SE.2016.1824

XII. Acknowledgements

I am indebted and very thankful to my supervisors: Prof. Dr. Fritz Krombach (Walter Brendel Centre of Experimental Medicine, Ludwig-Maximilians-Universität München, Munich, Germany), Prof. Dr. Susan Lakatos (Department of Pathophysiology, Research Institute of the Military Health Center, Budapest, Hungary), and Prof. Dr. János Hamar (National Institute of Traumatology, Budapest, Hungary) for continuous help and support throughout my dissertation. I also thank Prof. Dr. Béla Merkely (The Heart and Vascular Center of Semmelweis University, Budapest, Hungary) for being my consultant for the defence of this dissertation.

I owe sincere and earnest thanks to Dr. János Fent for his support and help in several research problems, and especially for the mathematical description of coincidence. I would like to express my gratitude to Prof. Dr. Géza Tasnádi (Heim Pal Children's Hospital, Budapest, Hungary) and to Prof. Dr. Thomas Schmitz-Rixen (Department of Vascular and Endovascular Surgery, Johann Wolfgang Goethe University, Frankfurt am Main, Germany) for supporting me in my clinical research experiments. I would like to gratefully thank Prof. Dr. Erzsébet Ligeti and Prof. Dr. Péter Enyedi for their supervision at the Department of Physiology, Semmelweis University, Budapest.

I would like to give my thanks to Martin Holzer, Alexander Khandoga, Marc Praetner, Max Lerchenberger, Christoph Reichel, Markus Rehberg, Minnamari Vippola, Stephan Schultes, Amit Shelke, and Karen Nelson for their invaluable help in the experimental work. I am very grateful to Dr. Violetta Kékesi for helping me organise my PhD defence. I would also like to thank John C. Williams for English proofreading and correction of the manuscript. I am obliged to many of my colleagues who supported me throughout my dissertation.

Last but not least, I would like to thank my family and friends for their love and support, which was essential for all this work to be completed.